

UNIVERSITY OF SOUTHERN QUEENSLAND

Faculty of Engineering and Surveying

Performance and Stability Analysis of an AC Variable Speed Drive

A dissertation submitted by

Andrew Stewart Rae

in fulfilment of the requirements of

Courses ENG4111 & ENG4112 Research Project

towards the degree of

Bachelor of Engineering (Electrical & Electronic)

Submitted: November, 2006

Abstract

In this dissertation an experimental, speed sensorless, AC variable speed drive is developed from works presented by previous researchers and the performance and stability of the drive is analysed. The experimental drive consists of a simple control algorithm that can be implemented on low cost systems and provides a performance that is superior to standard constant V/f drives.

There has been a great deal of research into AC variable speed drives and many different speed control schemes have been developed which range in complexity, performance and cost. Open-loop scalar control techniques are generally the least expensive to implement as no motor speed sensor is required. These techniques are likely to prevail in applications where instantaneous speed and position control of induction motors is not critical. Such applications may include pumps, fans and conveyors.

The experimental drive analysed in this dissertation is an open loop scalar control scheme. It utilises field orientation to control the stator voltage in the synchronously rotating frame and employs constant V/f control for basic voltage regulation. Compensation for stator resistance voltage drop and rotor slip are also employed to improve the dynamic performance and to reduce the steady state speed error.

UNIVERSITY OF SOUTHERN QUEENSLAND

Faculty of Engineering and Surveying

ENG4111 & ENG4112 Research Project

Limitations of Use

The Council of the University of Southern Queensland, its Faculty of Engineering and Surveying, and the staff of the University of Southern Queensland, do not accept any responsibility for the truth, accuracy or completeness of material contained within or associated with this dissertation.

Persons using all or any part of this material do so at their own risk, and not at the risk of the Council of the University of Southern Queensland, its Faculty of Engineering and Surveying or the staff of the University of Southern Queensland.

This dissertation reports an educational exercise and has no purpose or validity beyond this exercise. The sole purpose of the course pair entitled “Research Project” is to contribute to the overall education within the student’s chosen degree program. This document, the associated hardware, software, drawings, and other material set out in the associated appendices should not be used for any other purpose: if they are so used, it is the entirely at the risk of the user.

Professor R Smith

Dean

Faculty of Engineering and Surveying

Certification

I certify that the ideas, designs and experimental work, results, analyses and conclusions set out in this dissertation are entirely my own effort, except where otherwise indicated and acknowledged.

I further certify that the work is original and has not been previously submitted for assessment in any other course or institution, except where specifically stated.

Name: Andrew Rae

Student No: 0031210726

Signature

Date

Acknowledgments

I would like to thank my project supervisor Dr Tony Ahfock the valuable guidance and input that he provided to me in completing this project.

Table of Contents

Table of Contents	i
List of Figures	ii
List of Tables	iii
Nomenclature	iv
1. Introduction	1
1.1 Background	1
1.2 Aim and Objectives of the Project	3
1.3 Outline of Dissertation	4
2. Principles of Induction Motors	5
2.1 Construction	5
2.2 Operation	6
2.3 Dynamic Equations	7
3. 2 Phase Model of Induction Motors	11
3.1 Reference Frames	11
3.2 3 to 2 Phase Transformation	12
3.3 Development of 2 Phase Model	16
4. Implementation of IM Model in Simulink®	20
4.1 IM Simulink® Model	20
5. Verification of IM Model	25
5.1 Testing and Model Verification	25
5.2 Parameter Testing of IM	26
5.3 Verification Testing of IM	31
5.4 Verification of Model	34
6. Principles of AC VSD	39
6.1 AC VSDs	39
6.2 DC-Link VSD Construction	39
6.3 DC-Link VSD Operation	40
6.4 Constant V/f Control	42
6.5 Stator Resistance Voltage Drop Compensation	43
6.6 Slip Compensation	43
7. Experimental VSD	45
7.1 Experimental VSD Control	45
7.2 Experimental VSD Control Equations	45
8. Implementation of VSD Model in Simulink®	51
8.1 VSD Models	51
9. Stability and Performance Analysis of Drive	54
9.1 Stability and Performance Analysis Methodology	54
9.2 Linear Stability Analysis	55
9.3 Small Signal Displacement Stability Analysis	61
9.4 Performance Analysis	68
9.5 Performance and Stability Evaluation	76
10. Conclusion	78
10.1 Achievement of Project Objectives	78
10.2 Project Outcomes	79
10.3 Further Work	79
References	80

Bibliography	81
Appendix A – Project Specification	82
Appendix B – Power Measurement for Testing	83
Appendix C – Stability Analysis	85
Derivation of Closed Loop System Equations	85
Derivation of Small Signal Closed Loop System Equations	88
Appendix D – Matlab [®] Function for Linear Stability Analysis	96
Appendix E – Matlab [®] Function for Small Signal Stability Analysis	98
Appendix F – Complete Experimental Drive	101

List of Figures

Figure 2.1 Induction Motor Construction	6
Figure 2.2 Wye Induction Motor Equivalent Circuit	7
Figure 2.3 Winding Distribution	9
Figure 3.1 Reference Vectors	12
Figure 3.2 IM Field Orientation	13
Figure 4.1 Stator Direct Phase Sub-Function Block	21
Figure 4.2 Electromagnetic Torque Sub-Function Block	21
Figure 4.3 Stator Voltage 3-2 Transformation Sub-Function Block	22
Figure 4.4 Stator Current 2-3 Transformation Sub-Function Block	22
Figure 4.5 IM Simulink [®] Model	24
Figure 5.1 IM Test Bed	26
Figure 5.2 Inertia Test - Recordings	30
Figure 5.3 DOL Start Test – Stator Line Current	32
Figure 5.4 Sudden Removal of Load Test – Speed Calculated From Armature Voltage	33
Figure 5.5 Sudden Removal of Load Test - Stator Current	33
Figure 5.6 Sudden Application of Load Test – Stator Current	34
Figure 5.7 DOL Start - Simulated and Recorded Stator Current	36
Figure 5.8 Sudden Removal of Load - Recorded and Simulated Stator Current	37
Figure 5.9 Sudden Application of Load - Recorded and Simulated Stator Currents	38
Figure 6.1 DC-Link Conversion VSD	40
Figure 7.1 Experimental VSD Block Diagram	50
Figure 8.1 Constant V/f Simulink [®] Model	52
Figure 8.2 Experimental VSD Simulink [®] Model	53
Figure 9.1 Rotor Current Poles for Equal Rs Compensation and Zero Slip Compensation	58
Figure 9.2 Stator Current Poles for Equal Rs Compensation and Zero Slip Compensation	58
Figure 9.3 Stator Current Poles for Slip Compensation and Zero Rs Compensation	59
Figure 9.4 Combined Root Locus for Small Signal Stability Analysis in Table 9.2	65
Figure 9.5 3D Unstable Conditions for Small Signal Stability Analysis in Table 9.2	65
Figure 9.6 Unstable Conditions for Small Signal Stability Analysis in Table 9.2	66
Figure 9.7 Combined Root Locus for Small Signal Stability Analysis in Table 9.2 with Rsx Zero	67

Figure 9.8 Combined Locus for Small Signal stability Analysis in Table 9.2 with R _{sx} & R _{sy} Zero	67
Figure 9.9 Experimental VSD Start-up, 80% Torque, 150 rad/s	68
Figure 9.10 Simulation, Start-up, Zero Torque, 150 rad/s	70
Figure 9.11 Simulation, Start-up, 80% Rated Torque, 150 rad/s	71
Figure 9.12 Simulation, Start-up, Zero Torque, 30 rad/s	72
Figure 9.13 Simulation, Start-up, 80% Rated Torque, 30 rad/s	73
Figure 9.14 Simulation, Load Change, 0-100% Rated Torque, 150 rad/s	74
Figure 9.15 Simulation, Load Change, 0-100% Rated Torque, 30 rad/s	75

List of Tables

Table 3.1 Reference Frames	11
Table 5.1 Test Bed IM Nameplate Data	25
Table 5.2 IM Parameter Test	27
Table 5.3 IM Electrical Parameters	27
Table 5.4 Generator Friction Coefficient Test Data	29
Table 5.5 Motor-Generator Parameters	31
Table 5.6 DOL Start Test - Recordings	32
Table 5.7 Sudden Removal of Load Test - Recordings	34
Table 5.8 Sudden Application of Load Test – Recordings	34
Table 5.9 DOL Start - Simulated and Recorded Data	36
Table 5.10 Sudden Removal of Load - Simulated and Recorded Data	37
Table 5.11 Sudden Application of Load - Simulated and Recorded Data	38
Table 9.1 Motor Details for VSD Stability and Performance Evaluation	55
Table 9.2 Small Signal Stability Analysis Parameters	64
Table 9.3 Simulated Performance Criteria, Start-up, Zero Torque, 150 rad/s	70
Table 9.4 Simulated Performance Criteria, Start-up, 80% Rated Torque, 150 rad/s	71
Table 9.5 Simulated Performance Criteria, Start-up, Zero Torque, 30 rad/s	72
Table 9.6 Simulated Performance Criteria, Start-up, 80% Rated Torque, 30 rad/s	73
Table 9.7 Simulated Performance Criteria, Load Change 0-100% Rated Torque, 150 rad/s	74
Table 9.8 Simulated Performance Criteria, Load Change 0-100% Rated Torque, 30 rad/s	75
Table 9.9 Worst Performance Criteria from Performance Analysis	77

Nomenclature

Principle Symbols

a	Rotational operator, $e^{j2\pi/3}$
\vec{i}_r	Rotor current vector, A
i_a, i_b, i_c	Instantaneous rotor phase currents in rotor reference frame, A
i_{ra}, i_{rb}, i_{rc}	Instantaneous rotor phase currents in rotor reference frame, A
i_{rd}^r, i_{rq}^r	Direct and quadrature components of rotor current vector in rotor reference frame, A
i_{rd}^s, i_{rq}^s	Direct and quadrature components of rotor current vector in stator reference frame, A
$i_{rd}^{\psi_s}, i_{rq}^{\psi_s}$	Direct and quadrature components of rotor current vector in stator flux reference frame, A
i_{rx}, i_{ry}	Real and imaginary components of vector current vector in stator flux reference frame, A
I_{srated}	Stator current magnitude at rated power and speed.
\vec{i}_s	Stator current vector, A
i_A, i_B, i_C	Instantaneous stator phase currents in stator reference frame, A
i_{sA}, i_{sB}, i_{sC}	Instantaneous stator phase currents in stator reference frame, A
i_{sd}^s, i_{sq}^s	Direct and quadrature components of stator current vector in stator reference frame, A
$i_{sd}^{\psi_s}, i_{sq}^{\psi_s}$	Direct and quadrature components of stator current vector in stator flux reference frame, A
i_{sx}, i_{sy}	Real and imaginary components of stator current vector in stator flux reference frame, A
J	Mass moment of inertia, kg.m ² .
J_r	Rotor mass moment of inertia, kg.m ² .

L_m	Mutual inductance in the T equivalent circuit, H/ph
L_r	Rotor inductance in the T equivalent circuit, H/ph
L_{lr}	Rotor leakage inductance, H/ph
L_s	Stator inductance in the T equivalent circuit, H/ph
L_{ls}	Stator leakage inductance, H/ph
N_r	Number of turns in rotor winding (per phase)
N_s	Number of turns in stator winding (per phase)
p	Differentiation operator, $\frac{d}{dt}$
R_s	Stator resistance in the T equivalent circuit, Ω /ph
R_r	Rotor resistance in the T equivalent circuit, Ω /ph
S	Rotor slip
S_{rated}	Rotor slip at rated torque and speed
T_e	Electromagnetic torque, N.m
T_L	Load torque, N.m
\vec{u}_r	Rotor voltage vector, V
u_{rd}^r, u_{rq}^r	Direct and quadrature components of rotor voltage vector in rotor reference frame, V
u_{rd}^s, u_{rq}^s	Direct and quadrature components of rotor voltage vector in stator reference frame, V
$u_{rd}^{\psi_s}, u_{rq}^{\psi_s}$	Direct and quadrature components of rotor voltage vector in stator flux reference frame, V
u_{rx}, u_{ry}	Real and imaginary components of rotor voltage vector in stator flux reference frame, V
\vec{u}_s	Stator voltage vector, V
u_{sA}, u_{sB}, u_{sC}	Instantaneous stator phase voltages, V
u_{sd}^s, u_{sq}^s	Direct and quadrature components of stator voltage vector in stator reference frame, V

$u_{sd}^{\psi_s}, u_{sq}^{\psi_s}$	Direct and quadrature components of stator voltage vector in stator flux reference frame, V
u_{sx}, u_{sy}	Real and imaginary components of stator voltage vector in stator flux reference frame, V
$\vec{\psi}_r$	Rotor flux vector, Wb
ψ_{rd}^s, ψ_{rq}^s	Direct and quadrature components of rotor flux vector in stator reference frame, Wb
$\psi_{rd}^{\psi_s}, \psi_{rq}^{\psi_s}$	Direct and quadrature components of rotor flux vector in stator flux reference frame, Wb
ψ_{rx}, ψ_{ry}	Real and imaginary components of rotor flux vector in stator flux reference frame, Wb
$\vec{\psi}_s$	Stator flux vector, Wb
$\psi_{sA}, \psi_{sB}, \psi_{sC}$	Stator phase fluxes, Wb
ψ_{sd}^s, ψ_{sq}^s	Direct and quadrature components of stator flux vector in stator reference frame, Wb
$\psi_{sd}^{\psi_s}, \psi_{sq}^{\psi_s}$	Direct and quadrature components of stator flux vector in stator flux reference frame, Wb
ψ_{sx}, ψ_{sy}	Real and imaginary components of stator flux vector in stator flux reference frame, Wb
n_p	Number of pole pairs
ω_{ms}	Motor synchronous speed, rad/s
ω_r	Rotor angular speed, rad/s
σ	Leakage parameter
θ_r	Angular position of rotor, rad

Subscripts

A,B,C	Stator phase A, phase B, phase C
a,b,c	Rotor phase a, phase b, phase c
d	Direct axis

q	Quadrature axis
0	Zero sequence
x	Real axis in stator flux reference frame
y	Imaginary axis in stator flux reference frame
s	Stator
r	Rotor
L	Load

Superscripts

r	Rotor reference frame
s	Stator reference frame
ψ_r	Rotor flux reference frame
ψ_s	Stator flux reference frame

Abbreviations

AC	Alternating Current
DC	Direct Current
CSI	Current Source Inverter
FOC	Field Orientation Control
IM	Induction Motor
PWM	Pulse Width Modulation
VSD	Variable Speed Drive
VSI	Voltage Source Inverter
V/f	Volt / frequency (ratio)

1. Introduction

1.1 Background

In the past DC motors have been prominently used in variable speed drives (VSD) as the torque and flux of these motors can be easily regulated by controlling the armature and field currents of the motor with methods such as the Ward-Leonard system. With the development of semiconductor technology, variable frequency converters emerged and AC induction motor VSDs became available which are now capable of replacing DC drives in many applications.

AC induction motor VSDs have been replacing DC drives as AC induction motors provide operational benefits over DC motors. Due to the constructional aspects of DC motors they require periodic maintenance and have operational limitations such as speed and environmental considerations. AC induction motors on the other hand are more robust than DC motors, require little or no maintenance and generally overcome the operational limitations of DC motors. However, AC induction motor speed control is difficult to implement as the torque and the flux of the motor can not be directly controlled as in the DC motor variable speed drive system.

In AC induction motor drives only the stator voltages and currents can be directly controlled. Therefore a control technique is required to deduce and control the torque and flux of the induction motor. Field orientation control (FOC) as formulated by Blachke (1972) is a technique in which the flux orientation in the motor is used to deduce the torque and flux producing currents of the stator. Therefore the torque and flux of the motor can be controlled and used to control the speed of the motor. Field orientation control has only become practical since the implementation of cost effective power electronics and microprocessor controls.

There has been a great deal of research and development of field orientation control techniques and many different techniques have been developed which range in complexity and performance. Full vector control techniques provide the best operational performance but are complex and generally more expensive to implement.

Scalar control techniques are less complicated and generally less expensive to implement but their performance is generally inferior to that of full vector control.

Open-loop scalar control techniques are generally the least expensive to implement as no motor speed sensor is required. These techniques are likely to prevail in applications where instantaneous speed and position control of induction motors is not critical. Such applications may include pumps, fans and conveyors. Open loop scalar control techniques usually only require feedback of the motor stator currents and are the methods that are considered within this dissertation.

In the research and development of AC induction motor VSD technology the physical implementation of experimental AC induction motor VSDs is not always practical due to the physical resources that are required. To overcome this the operation of experimental drives can be simulated by developing and implementing a model of the VSD. These models can be implemented in programs such as Matlab[®] and Simulink[®] and allow the performance of the system to be analysed without access to physical resources.

The AC induction motor VSD control methods considered in this dissertation are stator voltage-drop compensation and slip compensation. A stator voltage-drop compensation method has been presented by Francis (1997). This method is simple to implement but it does not provide slip compensation. A stator voltage-drop and slip compensation method has been presented by Munoz-Garcia (1998) but this method is more complex and the published work does not address the stability of the system. In this dissertation, sections of these works have been combined to produce a low complexity VSD control with a performance that is superior to constant V/f drives.

1.2 Aim and Objectives of the Project

The general aim of this project is to implement a model for an AC variable speed drive for induction motors and to use this model to determine the limits of stability. The objectives of this project as defined in the project specification are:

1. Develop a state space model for the standard three phase induction motor. State variables can be either direct-axis and quadrature-axis currents or direct-axis and quadrature-axis flux linkages or a combination of currents and flux linkages.
2. Implement the model in (1) using Simulink[®] and simulate:
 - a. DOL start-up from rest.
 - b. Sudden application of mechanical load with the motor initially operating at steady-state speed on no-load.
3. Design and carry out physical tests to verify some of the predictions of step (2).
4. Develop a state-space model for an AC variable speed drive that consists of the induction motor model in (2), slip compensation and stator resistance voltage drop compensation.
5. Implement the model in (4) using Simulink[®] and analyse the performance and stability of the drive.

In setting the above objectives the focus has been on low complexity speed control schemes that provide a mid range performance and can be implemented on low cost systems.

1.3 Outline of Dissertation

In this dissertation the reader is presented with the basic theory of AC induction motors and AC variable speed drives before the experimental drive is developed and the performance and stability of the drive is analysed.

Chapters 2 to 5 cover induction motor operation and modelling. In chapter 2 the principles of the induction motor are presented before the 2-phase model of the induction motor is developed in chapter 3. In chapter 4 a Simulink[®] model of the induction motor is developed and then verified in chapter 5. The verification consists of induction motor tests and comparison of test results and simulations.

Chapters 6 to 8 cover variable speed drive operation, development of the experimental drive and modelling of the drive. In chapter 6 the principles of AC variable speed drives are presented before the experimental drive is developed in chapter 7. In chapter 8 a Simulink[®] model of the experimental drive and a constant V/f drive are developed.

In Chapter 9 the performance and stability of the experimental drive is analysed and evaluated. Chapter 10 concludes the dissertation with outcomes of the project and suggested future work. Additional support material is provided in the appendices.

2. Principles of Induction Motors

2.1 Construction

Induction motors consist of a stationary frame referred to as the stator and a rotating frame referred to as the rotor. The stator is housed in a frame onto which mounting feet are attached for securing the machine and bearing housings are attached for supporting the rotor. Both the stator and rotor carry windings which are magnetically coupled across the air gap in the machine.

The stator is an annular steel frame which carries distributed windings in slots on its inner surface. In three phase IMs the stator windings are arranged in coil groups with even spacing around the stator so that a rotating magnetic field is generated by the three phase supply.

The rotor of IMs can be of wound rotor construction or squirrel-cage construction. Wound rotor constructions consist of a cylindrical steel frame which carries distributed windings in slots on its outer surface. This type of construction usually incorporates slip rings so that external resistances can be inserted into the rotor circuit to modify the torque characteristics of the motor.

Squirrel-cage rotor constructions consist of a cylindrical steel frame with slots, in which bars are housed and shorted at the ends by short-circuiting end rings. The steel frame and the end rings form the rotor winding of the machine. A typical squirrel-cage induction motor is shown in Figure 2.1.

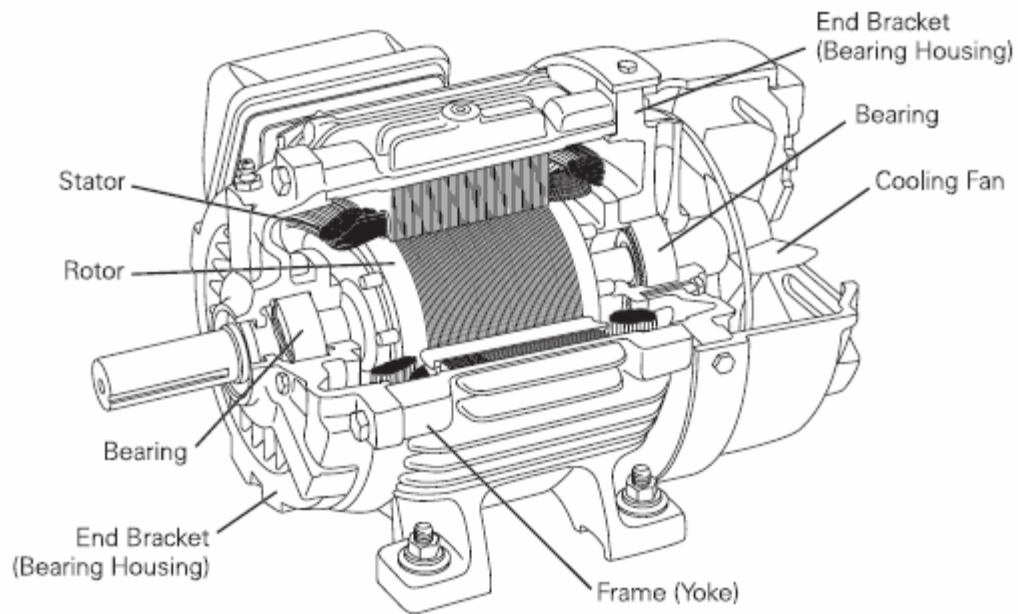


Figure 2.1 Induction Motor Construction

(source: <http://www.sea.siemens.com/step>)

2.2 Operation

The electrical operation of the IM is similar to that of an electrical transformer where the stator windings form the primary winding and the rotor windings form the secondary winding. The application of alternating currents to the 3 phase stator windings produces a rotating magnetic field through the air gap and the rotor. The speed at which this stator magnetic field rotates is referred to the synchronous speed of the motor. If the rotor is not rotating at a speed equal to synchronous speed then the stator magnetic field will produce an alternating flux in the rotor. By Faraday's law, this alternating flux will produce currents in the rotor windings and the resultant interaction between the rotor current and the flux will produce a force. As the rotor is mounted on a shaft this force will cause the rotor to rotate if friction and the torque of the load is overcome.

If the rotor is rotating at synchronous speed then the flux through the rotor will not alternate with respect to the rotor and no currents will be induced in the rotor to create a rotational torque. Therefore a difference between the synchronous and rotor speeds

must exist for a rotational torque to be produced. This difference between synchronous and rotor speeds is referred to as slip.

2.3 Dynamic Equations

In symmetrical IMs all phases are identical and distributed equally within the machine. Therefore the phase parameters across all phases are identical. If a symmetrical IM is operated from a symmetrical power supply then the magnitude of the voltage, current and flux phasors in each phase are also identical and the analysis of the symmetrical IM is greatly simplified. Each winding of an IM can be represented by a resistance and an inductance in series, which forms the circuit in Figure 2.2, when the windings are connected in Wye configuration.

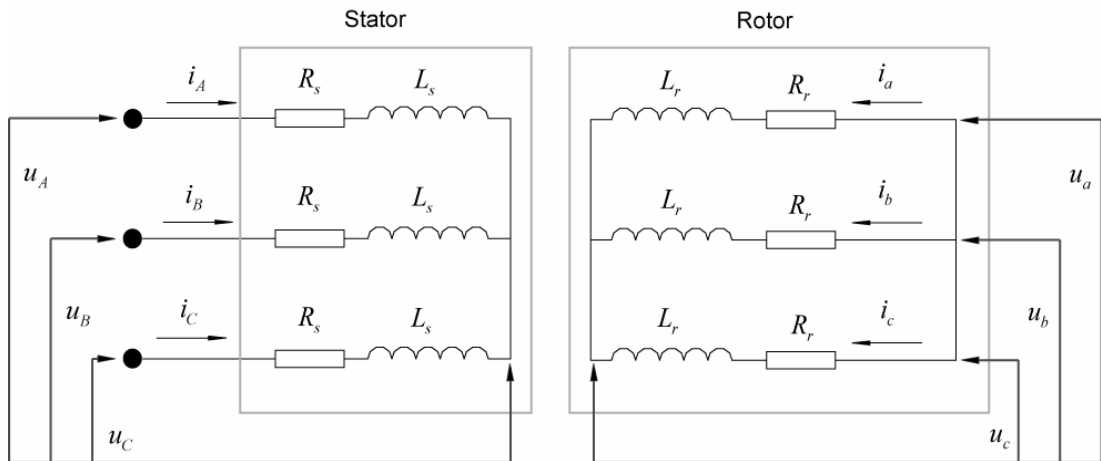


Figure 2.2 Wye Induction Motor Equivalent Circuit

The voltage across each winding in the IM can be deduced from the current, resistance and the rate of change of the magnetic flux in that winding. For the Wye connected IM represented by Figure 2.2, the winding voltages are given by (2.1) to (2.6).

$$u_A = R_s i_A + \frac{d}{dt} \psi_A \quad (2.1)$$

$$u_B = R_s i_B + \frac{d}{dt} \psi_B \quad (2.2)$$

$$u_C = R_s i_C + \frac{d}{dt} \psi_C \quad (2.3)$$

$$u_a = R_r i_a + \frac{d}{dt} \psi_a = 0 \quad (2.4)$$

$$u_b = R_r i_b + \frac{d}{dt} \psi_b = 0 \quad (2.5)$$

$$u_c = R_r i_c + \frac{d}{dt} \psi_c = 0 \quad (2.6)$$

The magnetic flux in the stator or rotor windings of the IM is a summation of magnetic fluxes produced within the winding and the mutual coupling of magnetic fluxes from the other stator and rotor windings, which is dependant upon the mutual inductances between the windings. Using the phase current and mutual inductances the magnetic flux in each winding is given by (2.7) to (2.12).

$$\psi_A = L_{AA} i_A + L_{AB} i_B + L_{AC} i_C + L_{Aa} i_a + L_{Ab} i_b + L_{Ac} i_c \quad (2.7)$$

$$\psi_B = L_{BA} i_A + L_{BB} i_B + L_{BC} i_C + L_{Ba} i_a + L_{Bb} i_b + L_{Bc} i_c \quad (2.8)$$

$$\psi_C = L_{CA} i_A + L_{CB} i_B + L_{CC} i_C + L_{Ca} i_a + L_{Cb} i_b + L_{Cc} i_c \quad (2.9)$$

$$\psi_a = L_{aa} i_a + L_{ab} i_b + L_{ac} i_c + L_{aA} i_A + L_{aB} i_B + L_{aC} i_C \quad (2.10)$$

$$\psi_b = L_{ba} i_a + L_{bb} i_b + L_{bc} i_c + L_{bA} i_A + L_{bB} i_B + L_{bC} i_C \quad (2.11)$$

$$\psi_c = L_{ca} i_a + L_{cb} i_b + L_{cc} i_c + L_{cA} i_A + L_{cB} i_B + L_{cC} i_C \quad (2.12)$$

The mutual coupling between the stator and rotor windings varies during IM operation due to the rotational variation in the spatial orientation of the rotor to the stator. For symmetrical IMs the mutual coupling between the stator and rotor varies as a function of the angular displacement between the windings as shown in Figure 2.3.

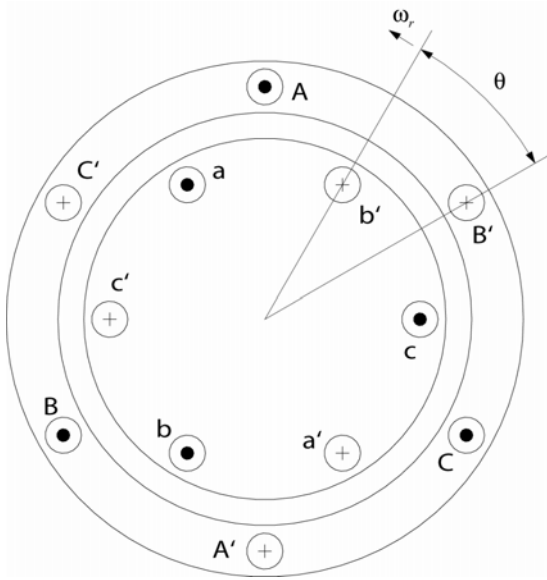


Figure 2.3 Winding Distribution

The mutual inductances in the winding flux equations of (2.7) to (2.12) can be represented by fixed inductances and inductances as functions of angular displacement as given in (2.13) to (2.19).

$$L_s = L_{AA} = L_{BB} = L_{CC} \quad (2.13)$$

$$L_r = L_{aa} = L_{bb} = L_{cc} \quad (2.14)$$

$$M_{ss} = L_{AB} = L_{AC} = L_{BC} = L_{BA} = L_{CA} = L_{CB} \quad (2.15)$$

$$M_{rr} = L_{ab} = L_{ac} = L_{bc} = L_{ba} = L_{ca} = L_{cb} \quad (2.16)$$

$$M_{sr} \cos \theta = L_{Aa} = L_{aA} = L_{Bb} = L_{bB} = L_{Cc} = L_{cC} \quad (2.17)$$

$$M_{sr} \cos(\theta + 120^\circ) = L_{Ab} = L_{bA} = L_{Bc} = L_{cB} = L_{Ca} = L_{aC} \quad (2.18)$$

$$M_{sr} \cos(\theta + 240^\circ) = L_{Ac} = L_{cA} = L_{Ba} = L_{aB} = L_{Cb} = L_{bC} \quad (2.19)$$

Applying (2.13) to (2.19) to the winding flux equations of (2.7) to (2.12) produces the reduced winding flux equations of (2.20) to (2.25).

$$\psi_A = L_s i_A + M_{ss} i_B + M_{ss} i_C + M_{sr} (\cos(\theta) i_a + \cos(\theta + 120^\circ) i_b + \cos(\theta + 240^\circ) i_c) \quad (2.20)$$

$$\psi_B = M_{ss} i_A + L_s i_B + M_{ss} i_C + M_{sr} (\cos(\theta + 240^\circ) i_a + \cos(\theta) i_b + \cos(\theta + 120^\circ) i_c) \quad (2.21)$$

$$\psi_C = M_{ss} i_A + M_{ss} i_B + L_s i_C + M_{sr} (\cos(\theta + 120^\circ) i_a + \cos(\theta + 240^\circ) i_b + \cos(\theta) i_c) \quad (2.22)$$

$$\psi_a = L_r i_a + M_{rr} i_b + M_{rr} i_c + M_{sr} (\cos(\theta) i_A + \cos(\theta + 120^\circ) i_B + \cos(\theta + 240^\circ) i_C) \quad (2.23)$$

$$\psi_b = M_{rr} i_a + L_r i_b + M_{rr} i_c + M_{sr} (\cos(\theta + 240^\circ) i_A + \cos(\theta) i_B + \cos(\theta + 120^\circ) i_C) \quad (2.24)$$

$$\psi_c = M_{rr} i_a + M_{rr} i_b + L_r i_c + M_{sr} (\cos(\theta + 120^\circ) i_A + \cos(\theta + 240^\circ) i_B + \cos(\theta) i_C) \quad (2.25)$$

3. 2 Phase Model of Induction Motors

3.1 Reference Frames

Reference frames of IMs are the spatial orientations that are used as a reference for defining quantities. For example the induction motor dynamic equations in chapter 2.3 had stator and rotor quantities referenced to the physical location of the windings within the stator and rotor. Therefore cosine terms were required to transform the rotor quantities to the stator and vice-versa.

IM references frames are defined with respect to rotational references, which vary in rotational speed. In this dissertation the reference frame is denoted by the superscript applied to quantities. The four common reference frames used in IMs are given in Table 3.1.

Table 3.1 Reference Frames

Frame	Reference	Superscript
Stator (Stationary)	Stator	S
Stator flux (Synchronous)	Stator flux vector	ψ_s
Rotor	Rotor	R
Rotor flux	Rotor flux vector	ψ_r

Reference frames can be visually illustrated by considering the space vectors of the stator and rotor currents as shown in Figure 3.1. Both these current vectors have constant magnitudes during steady state operation and rotate around a common axis.

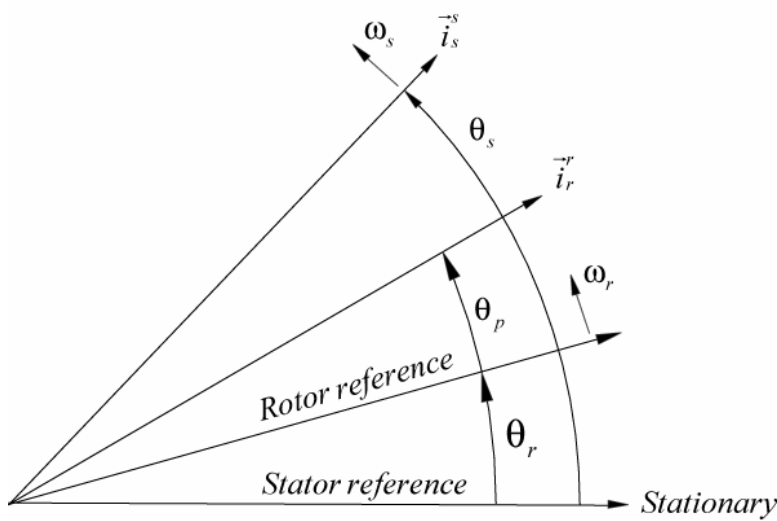


Figure 3.1 Reference Vectors

The space vectors can be transformed between reference frames by using the rotational operator $e^{j\theta_r}$ and the turns ratio of the stator to rotor windings. The transformation of the rotor currents from the rotor to the stator reference frames is given in (3.1).

$$\vec{i}_r^s = \frac{e^{j\theta_r}}{v} \vec{i}_r^r \quad (3.1)$$

where:

$$v = \frac{N_s}{N_r}$$

3.2 3 to 2 Phase Transformation

3 to 2 phase transformations are used to transform quantities in 3 phase machines to equivalent quantities in a two phase machine. These transformations are useful in IM models as the models can be formulated with two phases which reduces the complexity of the model and aids with analysis and control.

The transformations are achieved by resolving the space vectors of 3 phase quantities into orthogonal components. The space vector of three phase quantities is obtained by

using a rotational operator to sum the instantaneous 3 phase quantities. The space vector is then resolved into real and imaginary parts to obtain two orthogonal quantities as shown in Figure 3.2 for the stator voltage.

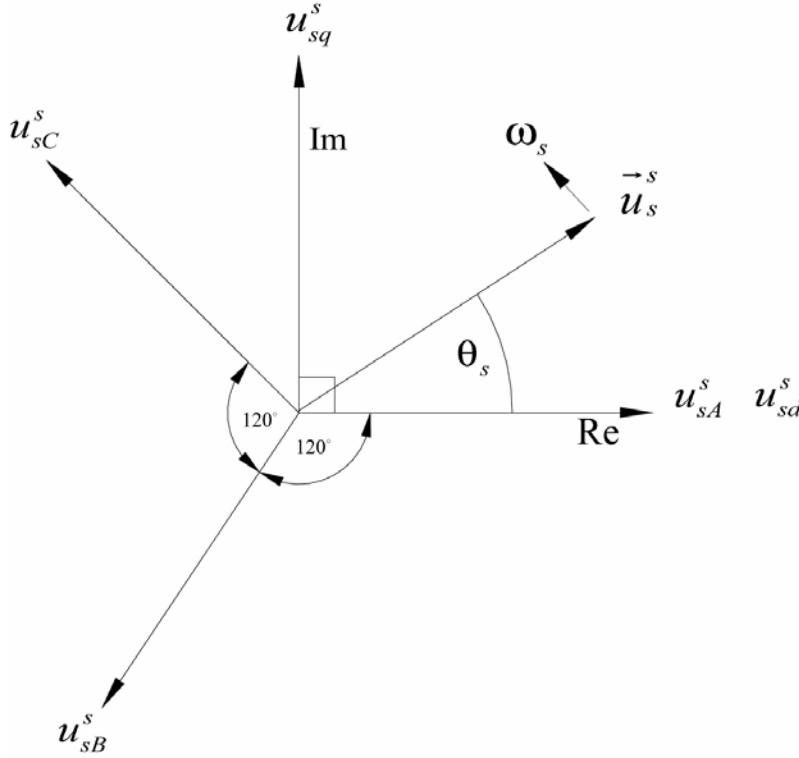


Figure 3.2 IM Field Orientation

The 3 to 2 phase transformation of stator voltages are demonstrated in the following and is the same process for currents and fluxes. The space vector of the stator voltage is obtained from the 3 phase voltages using (3.2). The space vector is then resolved into real and imaginary components as in (3.3). The voltage component on the real axis is referred to as the direct axis voltage and component on the imaginary axis is referred to as the quadrature component.

$$\vec{u}_s^s = u_{sA}^s + a u_{sB}^s + a^2 u_{sC}^s \quad (3.2)$$

where:

$$a = e^{j\frac{2\pi}{3}}$$

$$\vec{u}_s^s = u_{sd}^s + ju_{sq}^s \quad (3.3)$$

where:

$u_{sd}^s = \text{direct axis voltage}$

$u_{sq}^s = \text{quadrature axis voltage}$

The two phase components can be directly obtained from the 3 phase components by using (3.4) and (3.5).

$$\begin{aligned} u_{sd}^s &= \text{Re}(u_{sA(1)} + au_{sA(2)} + a^2u_{sA(0)}) \\ &= u_{sA}^s + u_{sB}^s \cos(120^\circ) + u_{sC}^s \cos(240^\circ) \\ &= u_{sA}^s - u_{sB}^s \frac{1}{2} - u_{sC}^s \frac{1}{2} \end{aligned} \quad (3.4)$$

$$\begin{aligned} u_{sq}^s &= \text{Im}(u_{sA(1)} + au_{sA(2)} + a^2u_{sA(0)}) \\ &= u_{sB}^s \sin(120^\circ) + u_{sC}^s \sin(240^\circ) \\ &= u_{sB}^s \frac{\sqrt{3}}{2} - u_{sC}^s \frac{\sqrt{3}}{2} \end{aligned} \quad (3.5)$$

From (3.4) and (3.5), the 3-2 phase transformation matrix is formed. The zero sequence voltage, u_{s0}^s is also included in this matrix to form a square matrix so that the inverse transformation matrix can be obtained from direct inversion of the transformation matrix. For balanced three phase operation of a symmetrical machine the sum of the stator voltage phasors is equal to zero, so u_{s0}^s is equal to zero and has no affect on the 3-2 phase transformations. The 3-2 phase and 2-3 phase transformations are given in (3.6) and (3.7). Q is the 3-2 transformation matrix and Q^{-1} is the 2-3 transformation matrix.

$$\begin{bmatrix} u_{sd}^s \\ u_{sq}^s \\ u_{s0}^s \end{bmatrix} = Q \begin{bmatrix} u_{sA}^s \\ u_{sB}^s \\ u_{sC}^s \end{bmatrix} \quad (3.6)$$

$$\begin{bmatrix} u_{sA}^s \\ u_{sB}^s \\ u_{sC}^s \end{bmatrix} = Q^{-1} \begin{bmatrix} u_{sd}^s \\ u_{sq}^s \\ u_{s0}^s \end{bmatrix} \quad (3.7)$$

where:

$$Q = \begin{bmatrix} 1 & -\frac{1}{2} & -\frac{1}{2} \\ 0 & \frac{\sqrt{3}}{2} & -\frac{\sqrt{3}}{2} \\ 1 & 1 & 1 \end{bmatrix} \quad Q^{-1} = \begin{bmatrix} \frac{2}{3} & 0 & \frac{1}{3} \\ -\frac{1}{3} & \frac{1}{\sqrt{3}} & \frac{1}{3} \\ -\frac{1}{3} & -\frac{1}{\sqrt{3}} & \frac{1}{3} \end{bmatrix}$$

The product of the 2 phase currents and voltages is proportional to the product of the 3 phase currents and voltages by a factor of 2/3 as given in (3.8). Therefore the power in the 3 phase motor is 2/3 the power in the 2 phase motor as given by (3.9).

$$u_{sABC}^S T i_{sABC}^S = [Q^{-1} u_{sdq}^s]^T Q i_{sdq}^s = \frac{2}{3} u_{sdq}^S T i_{sdq}^S \quad (3.8)$$

where:

$$[Q^{-1} u_{sdq}^s]^T = [u_{sdq}^s]^T [Q^{-1}]^T$$

$$P_{ABC} = \frac{2}{3} P_{dq} \quad (3.9)$$

3.3 Development of 2 Phase Model

The 2 phase model of the induction motor is developed from the dynamic equations of the induction motor in chapter 2.3. Using vector quantities, the stator and rotor voltages are given by the dynamic equations (3.10) and (3.11).

$$\vec{u}_s^s = R_s^s \vec{i}_s^s + \frac{d\vec{\psi}_s^s}{dt} \quad (3.10)$$

$$\vec{u}_r^r = R_r^r \vec{i}_r^r + \frac{d\vec{\psi}_r^r}{dt} \quad (3.11)$$

(3.10) is referenced to the stator reference frame and (3.11) is referenced to the rotor reference frame. (3.11) can be transformed to the stator reference using a rotational operator as in (3.12). The dynamic equation of the rotor voltage referenced to the stator is then (3.13).

$$\frac{e^{-j\theta_0}}{v} \vec{u}_r^s = \frac{e^{-j\theta_0}}{v} R_r^s \vec{i}_r^s + \frac{d}{dt} \left(\frac{e^{-j\theta_0}}{v} \vec{\psi}_r^s \right) \quad (3.12)$$

$$\vec{u}_r^s = R_r^s \vec{i}_r^s + \frac{d\vec{\psi}_r^s}{dt} - j\omega_r^s \vec{\psi}_r^s \quad (3.13)$$

where:

$v = \frac{N_s}{N_r}$, turns ratio of stator and rotor windings

$e^{j\theta_0}$, rotational operator

The voltage equations in the stator reference frame are then given by (3.14) and (3.15).

$$\vec{u}_s^s = R_s^s \vec{i}_s^s + p\vec{\psi}_s^s \quad (3.14)$$

$$\vec{u}_r^s = R_r^s \vec{i}_r^s + (p - j\omega_r^s) \vec{\psi}_r^s \quad (3.15)$$

where:

$$p = \frac{d}{dt}, \text{ differential operator}$$

The flux linkages in the stationary stator reference frame can be expressed by the flux linkage equation (3.16).

$$\begin{bmatrix} \vec{\psi}_s^s \\ \vec{\psi}_r^s \end{bmatrix} = \begin{bmatrix} L_s & L_m \\ L_m & L_r \end{bmatrix} \begin{bmatrix} \vec{i}_s^s \\ \vec{i}_r^s \end{bmatrix} \quad (3.16)$$

Combining the flux linkage equation (3.16) and the voltage equations (3.14) and (3.15) forms the matrix equation (3.17) for the voltages in the stationary stator reference frame.

$$\begin{bmatrix} \vec{u}_s^s \\ \vec{u}_r^s \end{bmatrix} = \begin{bmatrix} R_s + pL_s & pL_m \\ (p - j\omega_r^s)L_m & R_r + (p - j\omega_r^s)L_r \end{bmatrix} \begin{bmatrix} \vec{i}_s^s \\ \vec{i}_r^s \end{bmatrix} \quad (3.17)$$

By breaking the voltage and current vectors into to the orthogonal components ‘d’ and ‘q’, equation (3.17) can be written as (3.18). After isolating the derivatives (3.18) can be written as (3.19). Note all the parameters are referred to the stator reference frame so the superscript ‘s’ has been omitted for the remaining model development.

$$\begin{bmatrix} u_{sd} \\ u_{sq} \\ u_{rd} \\ u_{rq} \end{bmatrix} = \begin{bmatrix} R_s + pL_s & 0 & pL_m & 0 \\ 0 & R_s + pL_s & 0 & pL_m \\ pL_m & \omega_r L_m & R_r + pL_r & \omega_r L_r \\ -\omega_r L_m & pL_m & -\omega_r L_r & R_r + pL_r \end{bmatrix} \begin{bmatrix} i_{sd} \\ i_{sq} \\ i_{rd} \\ i_{rq} \end{bmatrix} \quad (3.18)$$

$$\begin{bmatrix} u_{sd} \\ u_{sq} \\ u_{rd} \\ u_{rq} \end{bmatrix} = \begin{bmatrix} R_s & 0 & 0 & 0 \\ 0 & R_s & 0 & 0 \\ 0 & \omega_r L_m & R_r & \omega_r L_r \\ -\omega_r L_m & 0 & -\omega_r L_r & R_r \end{bmatrix} \begin{bmatrix} i_{sd} \\ i_{sq} \\ i_{rd} \\ i_{rq} \end{bmatrix} + \begin{bmatrix} L_s & 0 & L_m & 0 \\ 0 & L_s & 0 & L_m \\ L_m & 0 & L_r & 0 \\ 0 & L_m & 0 & L_r \end{bmatrix} \frac{d}{dt} \begin{bmatrix} i_{sd} \\ i_{sq} \\ i_{rd} \\ i_{rq} \end{bmatrix} \quad (3.19)$$

By using matrix inversion the derivatives of the currents can be isolated in (3.19). Assuming that the closed loop rotor voltages are zero the system can be arranged to produce (3.20) which is the 2 phase ‘dq’ state space model of the induction motor. This model is used in many publications.

$$\frac{d}{dt} \begin{bmatrix} i_{sd} \\ i_{sq} \\ i_{rd} \\ i_{rq} \end{bmatrix} = \begin{bmatrix} -\frac{R_s}{\sigma L_s} & \frac{\omega_r L_m^2}{L_r \sigma L_s} & \frac{L_m R_r}{L_r \sigma L_s} & \frac{\omega_r L_m}{\sigma L_s} \\ -\frac{\omega_r L_m^2}{L_r \sigma L_s} & -\frac{R_s}{\sigma L_s} & -\frac{\omega_r L_m}{\sigma L_s} & \frac{L_m R_r}{L_r \sigma L_s} \\ \frac{L_m R_s}{L_r \sigma L_s} & -\frac{\omega_r L_m}{\sigma L_r} & -\frac{R_r}{\sigma L_r} & -\frac{\omega_r}{\sigma} \\ \frac{\omega_r L_m}{\sigma L_r} & \frac{L_m R_s}{L_r \sigma L_s} & \frac{\omega_r}{\sigma} & -\frac{R_r}{\sigma L_r} \end{bmatrix} \begin{bmatrix} i_{sd} \\ i_{sq} \\ i_{rd} \\ i_{rq} \end{bmatrix} + \begin{bmatrix} \frac{1}{\sigma L_s} & 0 \\ 0 & \frac{1}{\sigma L_s} \\ -\frac{L_m}{L_r \sigma L_s} & 0 \\ 0 & -\frac{L_m}{L_r \sigma L_s} \end{bmatrix} \begin{bmatrix} u_{sd} \\ u_{sq} \end{bmatrix} \quad (3.20)$$

where:

$$\sigma = 1 - \frac{L_m^2}{L_r L_s}, \text{leakage parameter}$$

The state space model (3.20) is for a 2 pole machine ($n_p = 1$). Therefore the rotor speed, ω_r in the state space model is the speed of an equivalent two pole machine. The real and model rotor speeds are related as in (3.21).

$$\omega_r = \eta_p \omega_r(\text{real}) \quad (3.21)$$

The electromagnetic torque produced by the two phase model can be determined by considering the rotational force produced by the reaction between stator flux vector linking the rotor and the rotor current vector. When the stator flux linkage vector and the rotor current vector are perpendicular, the 2 phase electromagnetic torque is maximum and is given by the product of the stator flux linkage vector and the rotor current vector. When the displacement angle between the stator flux linkage vector and the rotor current vector is not perpendicular, the torque produced is proportional to the sine of the displacement angle. The 2 phase electromagnetic torque of a 2 pole motor is then given by (3.22).

$$T_e' = \vec{\psi}_{rs} \vec{i}_r \sin(\delta) \quad (3.22)$$

where:

δ = Angular displacement between stator and rotor reference frames

$\vec{\psi}_{rs} = L_m \vec{i}_s$, flux linking the rotor due to stator current

The sine of the angular displacement between the stator linkage flux vector and the rotor current vector is given by:

$$\begin{aligned} \sin(\delta) &= \sin(\theta_s - \theta_r) \\ &= \sin(\theta_s) \cos(\theta_r) - \cos(\theta_s) \sin(\theta_r) \\ &= \frac{1}{\vec{i}_s \vec{i}_r} (i_{sq} i_{rd} - i_{sd} i_{rq}) \end{aligned}$$

By substituting the above relationship into (3.22) the 2 phase, 2 pole electromagnetic torque can be determined from currents only. Multiplying this by the number of pole pairs gives the electromagnetic torque produced by a 2 phase, multi-pole pair motor. As the power in the 2 phase and 3 phase motors is related by a factor of 2/3 as given in (3.9), the actual 3 phase electromagnetic torque is given by (3.23).

$$T_e = n_p L_m \frac{2}{3} (i_{sq} i_{rd} - i_{sd} i_{rq}) \quad (3.23)$$

Subtracting the load and friction torque from the electromagnetic torque and dividing by the rotor moment of inertia gives the acceleration of the rotor as in (3.24).

$$\frac{d\omega_r}{dt} = \frac{1}{J} (T_e - T_L - f \omega_r) \quad (3.24)$$

4. Implementation of IM Model in Simulink®

4.1 IM Simulink® Model

The 2 phase IM model developed in chapter 3.3 has been implemented in Simulink® so that the operation of the induction motor can be simulated. The IM model has been implemented as a function block which has the stator voltages and load torque as inputs and the stator currents and rotor speed as outputs. The parameters of the IM are defined in the Simulink® model by their respective symbols and are set by assigning their numerical values in the Matlab® workspace. This allows the model to be used for the simulation of any induction motor.

The IM state space equation (3.20) is the basis for the model and is used to calculate the stator and rotor currents of an equivalent 2 phase, 2 pole motor. Each line of the IM state space model has been implemented in separate sub-function blocks. For the stator direct phase current the relevant line from the state space equation is given by (4.1) and the Simulink® sub-function block is given Figure 4.1.

$$\frac{di_{sd}}{dt} = \begin{bmatrix} -\frac{R_s}{\sigma L_s} & \frac{\omega_r L_m^2}{L_r \sigma L_s} & \frac{L_m R_r}{L_r \sigma L_s} & \frac{\omega_r L_m}{\sigma L_s} \end{bmatrix} \begin{bmatrix} i_{sd} \\ i_{sq} \\ i_{rd} \\ i_{rq} \end{bmatrix} + \begin{bmatrix} \frac{1}{\sigma L_s} & 0 \end{bmatrix} \begin{bmatrix} u_{sd} \\ u_{sq} \end{bmatrix} \quad (4.1)$$

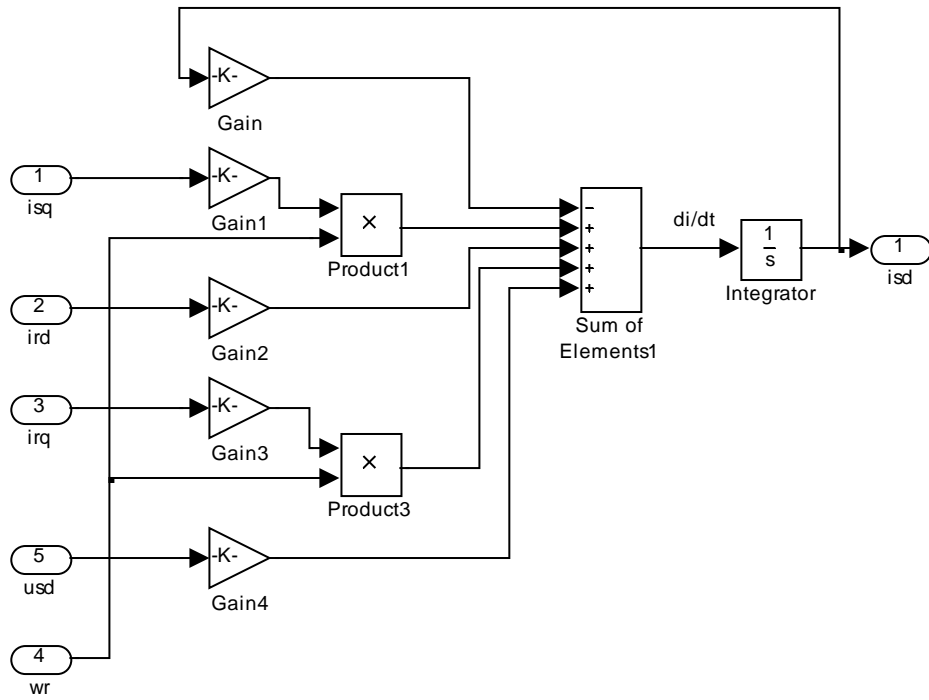


Figure 4.1 Stator Direct Phase Sub-Function Block

From the 2 phase, 2 pole stator and rotor currents the 3 phase multi-pole electromagnetic torque is calculated by implementing equation (3.23) within another sub-function block as given in Figure 4.2.

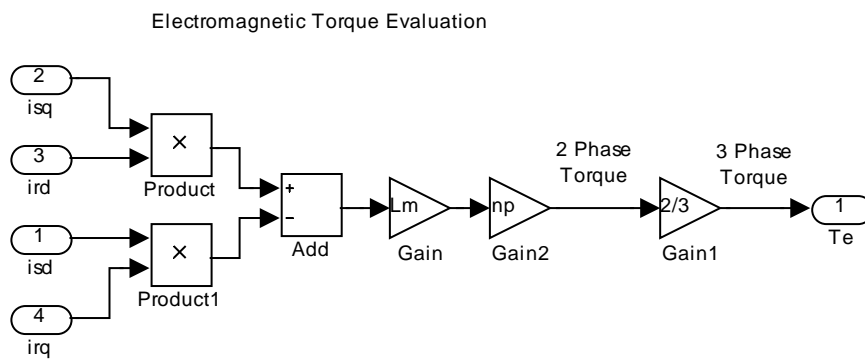


Figure 4.2 Electromagnetic Torque Sub-Function Block

The 3 phase voltage inputs to the model are transformed to 2 phase values and the stator 2 phase currents are transformed to 3 phase values using the 3-2 and 2-3 phase transformation blocks shown in Figure 4.3 and Figure 4.4. These blocks implement the 3-2 and 2-3 phase transformations defined in chapter 3.2.

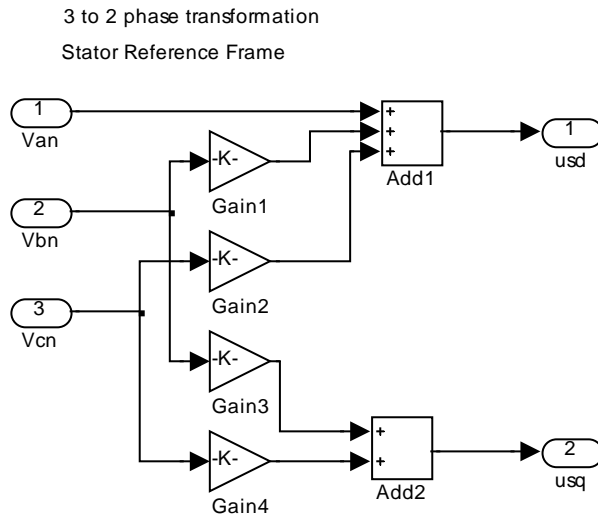


Figure 4.3 Stator Voltage 3-2 Transformation Sub-Function Block

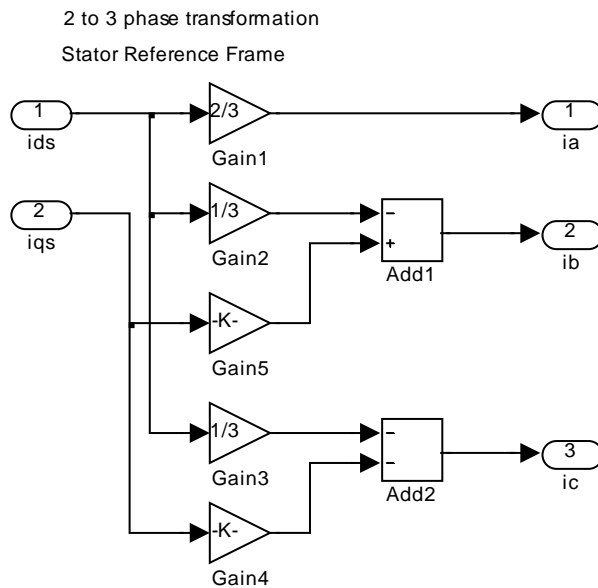


Figure 4.4 Stator Current 2-3 Transformation Sub-Function Block

In the complete model the motor acceleration torque is determined by subtracting the load and friction torque from the electromagnetic torque. Dividing the acceleration torque by the rotor moment of inertia then gives the acceleration of the rotor which is passed through an integral block to obtain the rotor speed. The rotor speed is multiplied by the number of pole pairs to obtain the equivalent 2 phase, 2 pole rotor speed which is fed back to the phase current sub-function blocks for subsequent current calculations. The complete IM Simulink[®] model is given in Figure 4.5.

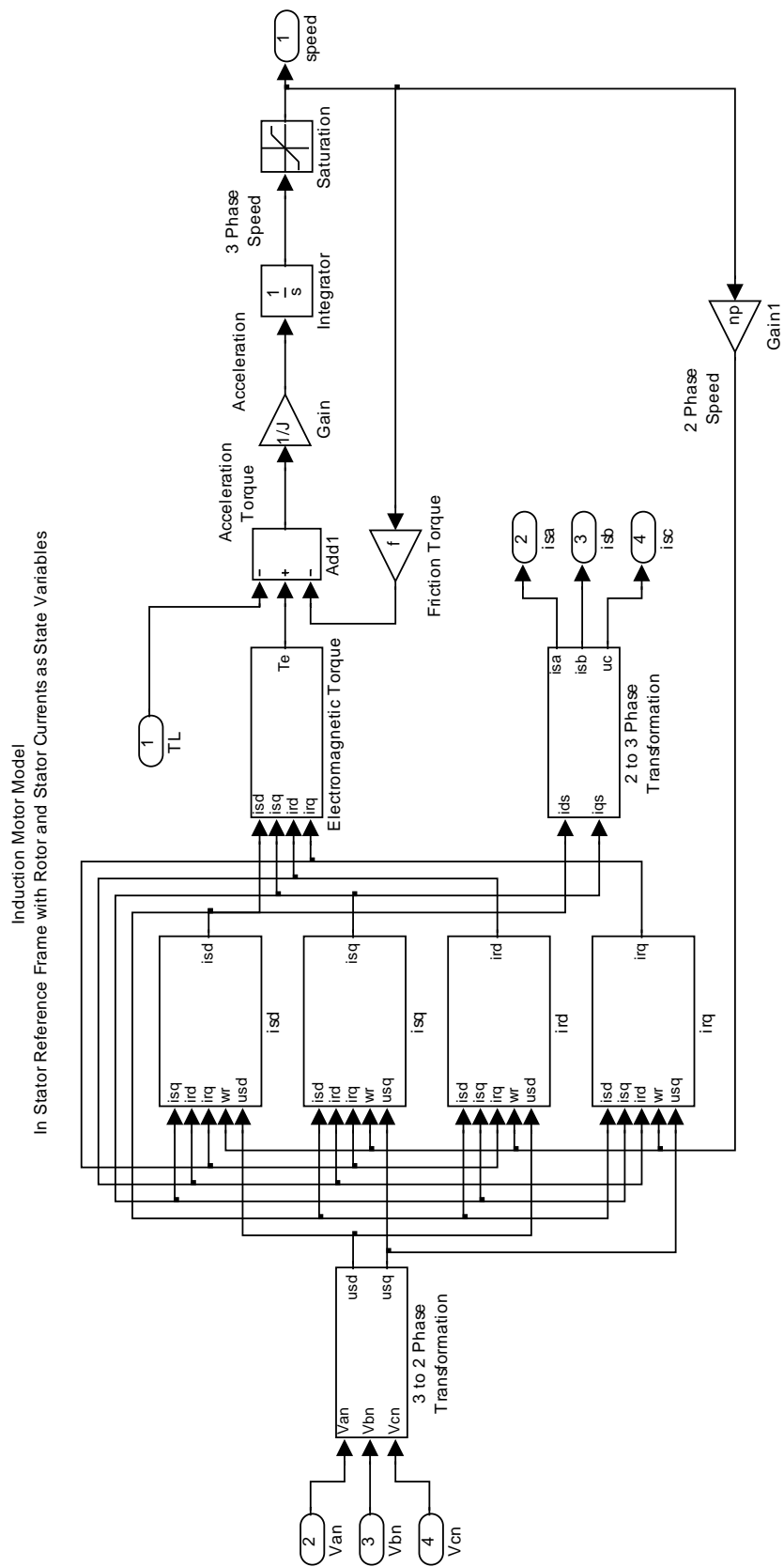


Figure 4.5 IM Simulink® Model

5. Verification of IM Model

5.1 Testing and Model Verification

The ability of the induction motor model to accurately simulate the operation of the real induction motor is required to be determined so that the validity of simulations can be verified and the reliable application of the model can be determined.

Verification of the model has been performed by comparing simulations of induction motor operation to recordings of the real induction motor operation. This has been performed for direct online starting and load variations with the motor initially operating at steady state speed.

The testing of a real induction motor was performed on a motor-generator unit with a resistive load bank. The drive motor was a 4 kW squirrel cage induction motor with coupling to the DC generator. The coupling could be disengaged so that stand alone induction motor operation could be achieved. The nameplate data of the IM in the test bed is given in Table 5.1 and the test bed is shown in Figure 5.1.

During testing voltages and currents were recorded with a 4 channel storage oscilloscope using current and voltage probes. The length of recording was limited by the maximum oscilloscope storage of 500 data entries.

Table 5.1 Test Bed IM Nameplate Data

Voltage	415 V
Frequency	50 Hz
Current	8.1 A
Power	4 KW
Speed	1420 RPM
Winding Configuration	Delta

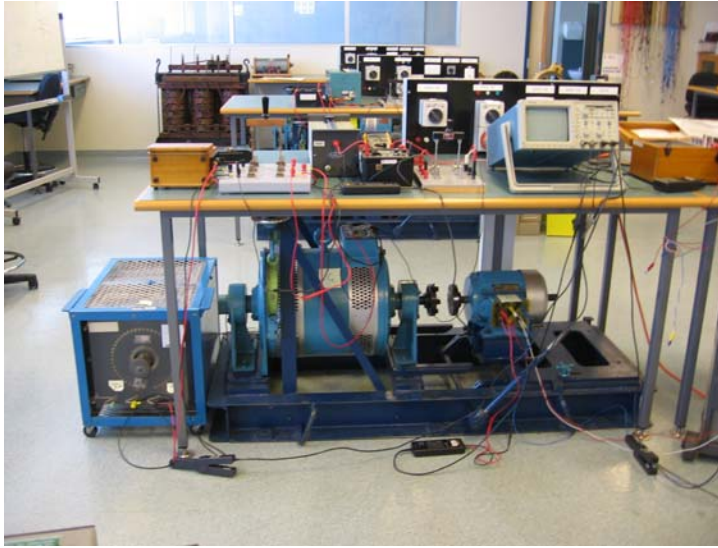


Figure 5.1 IM Test Bed

5.2 Parameter Testing of IM

Testing was performed on the motor-generator set to determine the friction coefficients and the moment of inertia of the complete unit. These are required for simulation. The induction motor electrical parameters were obtained from testing performed during previous laboratory work in practical courses.

The results of the previous induction motor parameter testing are given in Table 5.2 and the calculated induction motor electrical parameters are given in Table 5.3.

Table 5.2 IM Parameter Test

No Load Test	
Phase voltage, $V_p - V_{rms}$	227
Line current, $I_L - A_{rms}$	2.98
Input power, $P - W$	340
Input apparent power, $S - KVA \{3I_L V_p\}$	2029.38
Rotor speed - RPM / rad.s ⁻¹	1500 / 157.08
Power factor angle, θ - degrees $\{\cos^{-1}(P/S)\}$	80.36
Magnetising current, $I_m - A \{\sin(\theta)I_L\}$	2.934
Magnetising reactance, $X_m - \Omega \{V_p/I_m\}$	j77.37
Magnetising inductance, $L_m - h \{X_m/(2\pi f)\}$	0.246
Locked Rotor Test	
Phase Voltage, $V_p - V_{rms}$	49.07
Line Current, $I_L - A_{rms}$	8.1
Input power, $P - W$	648
Input apparent power, $S - KVA \{3I_L V_p\}$	1192
Power Factor Angle, θ - degrees $\{\cos^{-1}(P/S)\}$	57.07
Phase Impedance, $Z - \Omega \{V_p/I_L\}$	6.058
Resistance, $R - \Omega \{Z \cos(\theta)\}$	3.293
Reactance, $X - \Omega \{Z \sin(\theta)\}$	j5.084
Inductance, $L - H \{X/(2\pi f)\}$	0.0162
DC Stator Test	
Stator resistance, $R_s - \Omega$	1.749

Table 5.3 IM Electrical Parameters

Stator resistance, $R_s - \Omega$	1.749
Rotor resistance, $R_r - \Omega \{R - R_s\}$	1.544
Stator leakage inductance, $L_{ls} - H \{L/2\}$	0.0081
Rotor leakage inductance, $L_{lr} - H \{L/2\}$	0.0081
Mutual inductance, $L_m - H$	0.246

For an induction motor the torque relationship is described by (5.1). If the motor is operating under steady state conditions with no load then the speed is constant and the power relationship within the motor can be described by (5.2). The friction coefficient

can then be determined using (5.3) which includes all losses other than stator resistance loss as a function of rotor speed.

$$T_e = T_L + J_m \frac{d\omega_r}{dt} + f_m \omega_r \quad (5.1)$$

where:

f_m = friction coefficient of motor

$$P_{in} = f_m \omega_r^2 + P_{Loss} \quad (5.2)$$

$$f_m = \frac{P_{in} - 3I_s^2 R_s}{\omega_r^2} \quad (5.3)$$

Using the no load test data from Table 5.2 and (5.3), the friction coefficient of the induction motor was determined to be $0.012 \text{ Nm.s.rad}^{-1}$.

The torque relationship of the motor-generator set is described by (5.4). For steady state operation with no generator load the speed is constant and the power relationship within the motor can be described by (5.5).

$$T_e - J_m \frac{d\omega_r}{dt} - f_m \omega_r = J_g \frac{d\omega_r}{dt} + f_g \omega_r + \frac{P_{out}}{\omega_r} \quad (5.4)$$

$$P_{in} = (f_g + f_m) \omega_r^2 + P_{Loss} \quad (5.5)$$

If the power of the generator is zero then (5.5) can be rearranged to obtain (5.6) which solves the friction coefficient of the generator when the generator load is zero. To solve (5.6), the input power to the motor is calculated using (5.7) and data collected from the steady state operation of the motor-generator set with no load. The derivation of (5.7) is provided in Appendix B.

$$f_g = \frac{P_{in} - 3I_s^2 R_s}{\omega_r^2} - f_m \quad (5.6)$$

$$P_{in} = \sqrt{3} V_L I_L \cos \theta = \text{mean}(v_{ab} i_a) + \text{mean}(v_{ab} i_b) \quad (5.7)$$

The data used to calculate the generator friction coefficient is give in below in Table 5.4. From this data the generator friction coefficient was determined to be 0.0277 Nm.s.rad⁻¹.

Table 5.4 Generator Friction Coefficient Test Data

Power input, P_{in} - W	1040
Stator line current, I_s - A _{rms}	3.5
Rotor speed – RPM / rad.s ⁻¹	1495 / 156.6
Motor friction coefficient, f_m - Nm.s.rad ⁻¹	0.012
Generator friction coefficient, f_g - Nm.s.rad ⁻¹	0.0277
Motor - Generator friction coefficient - Nm.s.rad ⁻¹	0.0397

To obtain the moment of inertia for the complete motor-generator set, a test with speed transients was required. If the input power to the induction motor is zero then by rearranging (5.4) and integrating to remove the derivative, (5.8) is obtained. The left hand integral of (5.8) can be solved to obtain (5.9) which can be used to determine the combined moment of inertia from data recorded during the run down of the motor-generator set after supply to the induction motor is disconnected.

$$\int_{\omega_2}^{\omega_1} (J_m + J_g) d\omega_r = \int_{t_2}^{t_1} \frac{-I_a E_a}{\omega_r} - (f_m + f_g) \omega_r dt \quad (5.8)$$

$$(J_m + J_g) = \frac{1}{\omega_1 - \omega_2} \int_{t_2}^{t_1} \frac{-I_a E_a}{\omega_r} - (f_m + f_g) \omega_r dt \quad (5.9)$$

As no speed sensor was available for direct measurement of the motor speed during transients, the output voltage of the generator was measured and used to calculate the

motor speed. The output voltage of the generator is proportional to the motor speed when excitation is held constant and is described by (5.10).

$$\omega_r = \frac{V_a}{ki_f} \quad (5.10)$$

where:

V_a = generated voltage

i_f = field current

k = generator constant

To obtain the data for the inertia testing the motor-generator set was operated with a load at steady state. The power to the induction motor was then disconnected and the generator output voltage and current were recorded with the oscilloscope during the rundown of the rotor. The recorded values are plotted in Figure 5.2.

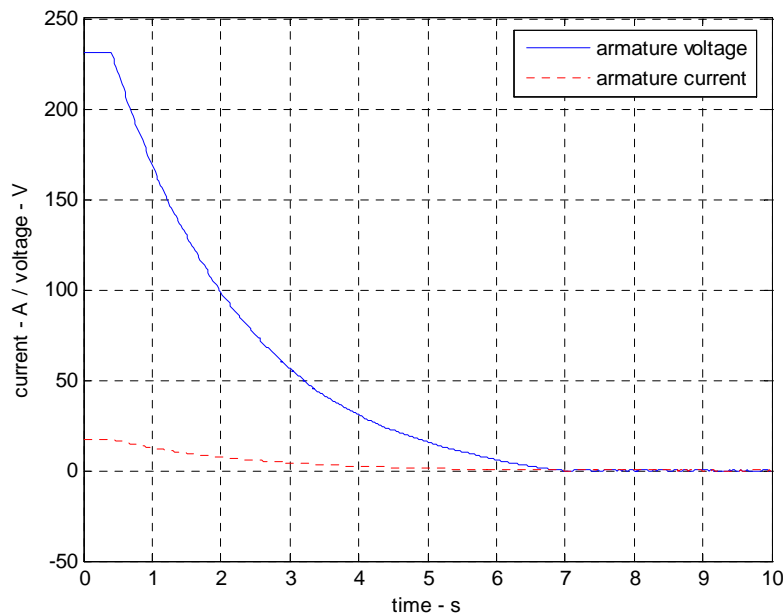


Figure 5.2 Inertia Test - Recordings

The data was then exported to Matlab[®] where the rotor speed was calculated using (5.10) and the moment of inertia was calculated by implementing (5.9) with numerical integration. The moment of inertia and the friction coefficients calculated for the motor-generator set are given in Table 5.5.

Table 5.5 Motor-Generator Parameters

Induction motor friction coefficient - Nm.s.rad^{-1}	0.012
Generator friction coefficient - Nm.s.rad^{-1}	0.0277
Motor-generator combined friction coefficient - Nm.s.rad^{-1}	0.0397
Motor-generator combined moment of inertia - kg.m^{-2}	0.3708

5.3 Verification Testing of IM

To verify the induction motor model, data from a real induction motor was required for comparison with model simulations. Tests were performed to obtain induction motor data during direct on line starting and sudden removal and sudden application of loads.

For the direct online starting, the motor was disengaged from the generator so that stand alone operation of motor was achieved. Two stator line currents and two stator line voltages were recorded during the start-up. One of the recorded stator line currents is shown in Figure 5.3 and the parameters from the test are given in Table 5.6.

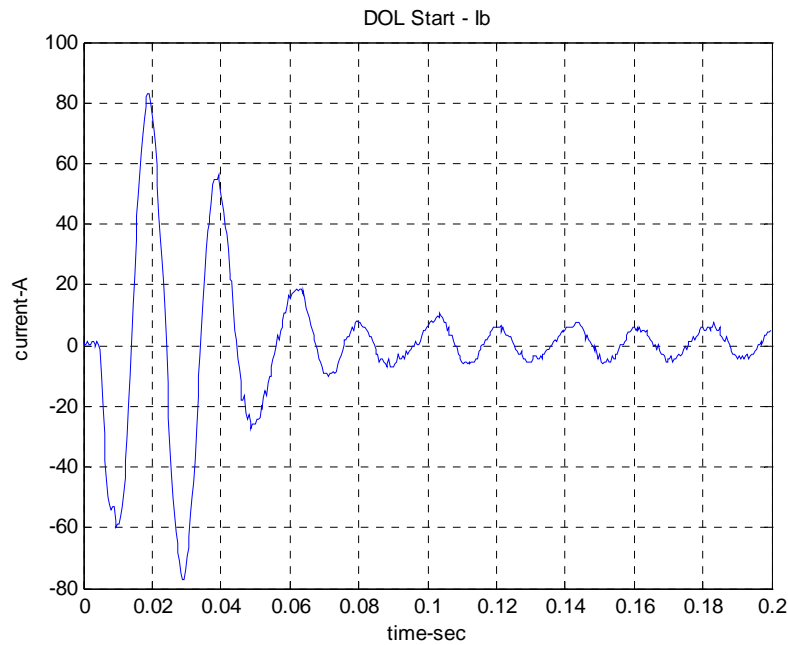


Figure 5.3 DOL Start Test – Stator Line Current

Table 5.6 DOL Start Test - Recordings

Parameter	Initial	Final
Load:	0 Nm	0 Nm
Speed:	0	157.1 rad/sec
Stator Current:	0	3 A rms

During the sudden removal and application of load to the motor, the motor was engaged to the DC generator and a resistive load was used to apply a load to the DC generator and the motor. A stator current, a stator line voltage, the generator armature voltage and the generator armature current were recorded during the test.

From the generator armature voltage the speed of the motor can be determined using (5.10) but this relationship does not hold during the switching transients in this test, due to the inductive properties of the generator. During the transient period, a speed overshoot is incorrectly indicated by the armature voltage, as shown in Figure 5.4.

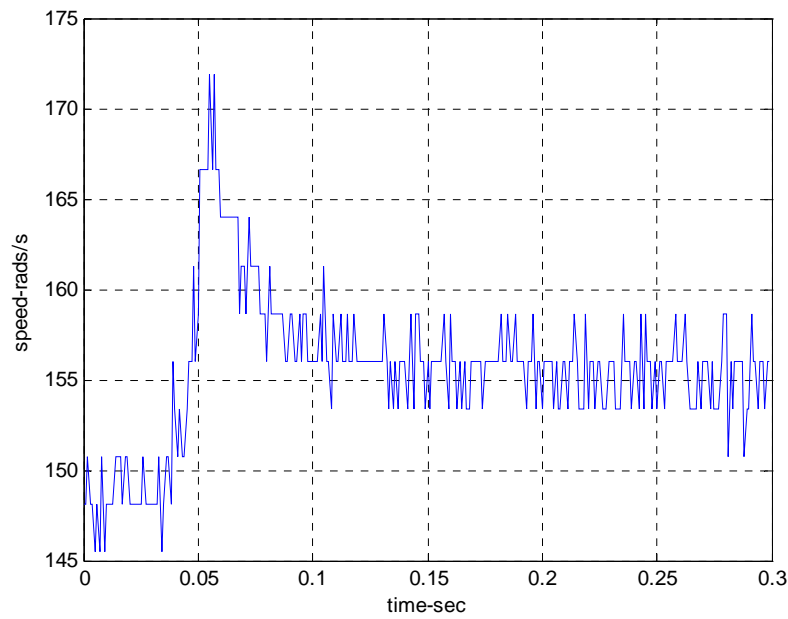


Figure 5.4 Sudden Removal of Load Test – Speed Calculated From Armature Voltage

The recorded stator line current for the sudden removal and application of load are shown in Figure 5.5 and Figure 5.6. The recorded data during these tests are given in Table 5.7 and Table 5.8.

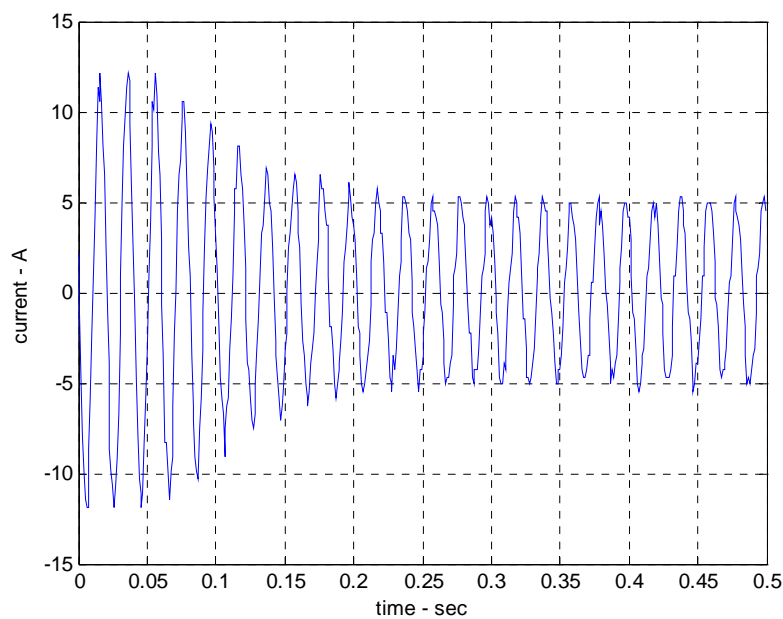
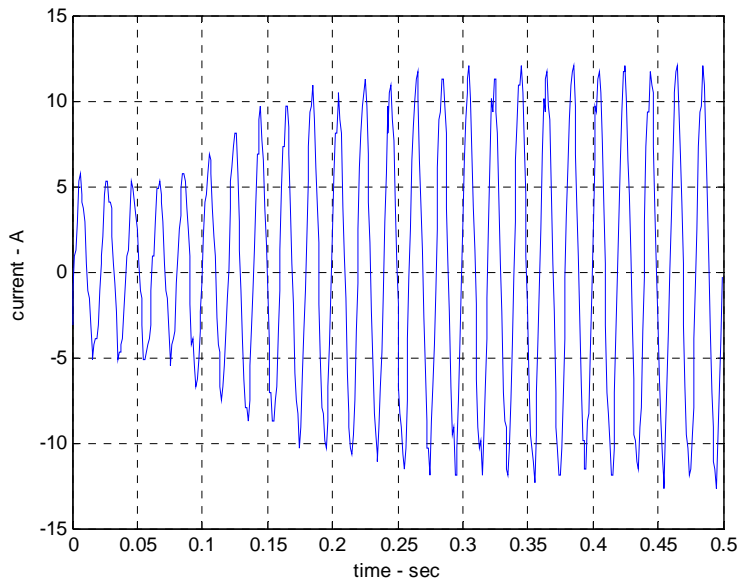


Figure 5.5 Sudden Removal of Load Test - Stator Current

Table 5.7 Sudden Removal of Load Test - Recordings

Parameter	Initial	Final
Generator Load:	3.8 KW	0 W
Speed:	148.6 rad/sec	156.6 rad/sec
Stator Current:	8.4 Arms	3.46 A rms

**Figure 5.6 Sudden Application of Load Test – Stator Current****Table 5.8 Sudden Application of Load Test – Recordings**

Parameter	Initial	Final
Resistive Load:	0 KW	3.85 KW
Speed:	156.6 rad/sec	148.5 rad/sec
Stator Current:	3.46 A rms	8.4 A rms

5.4 Verification of Model

The induction motor model has been verified by comparison of data recorded during the verification testing and simulations using the Simulink[®] induction motor model. This comparison has been performed for a direct on line (DOL) start and sudden application and removal of loads.

For the direct online start of the motor, the recorded and simulated stator currents are shown in Figure 5.7 and the recorded and simulated data is given in Table 5.9. From this figure it can be seen that the recorded and simulated currents are not the same during first 4 cycles of the stator current but they are similar after this period. During the first 4 cycles the recorded current is greater than the simulated current. This is due to the relationship between the flux and current becoming non-linear during high currents, due to magnetic flux saturation. The induction motor model is a linear model and does not accommodate this non-linear relationship at high currents.

Magnetic flux saturation within the motor occurs in the leakage and magnetising branches of the induction motor during high currents. During magnetic saturation the rate of change of flux density to the applied current decreases and the effective inductance of the relationship is reduced. Therefore a fixed inductance can only be used to model the flux and current relationship in the linear range. Magnetic saturation in the motor during motor transients is difficult to model as the level of saturation is not constant across all magnetic paths. Therefore each magnetic path needs to be considered separately which significantly increases the complexity of the model. Modelling of the saturation also requires knowledge of the physical arrangement of the motor windings to determine the flux densities.

After the first 4 cycles of the DOL start the recorded and simulated currents are similar and can be regarded as the same. From Table 5.9, the final steady state recorded currents of the motor are the same and the speeds are similar.

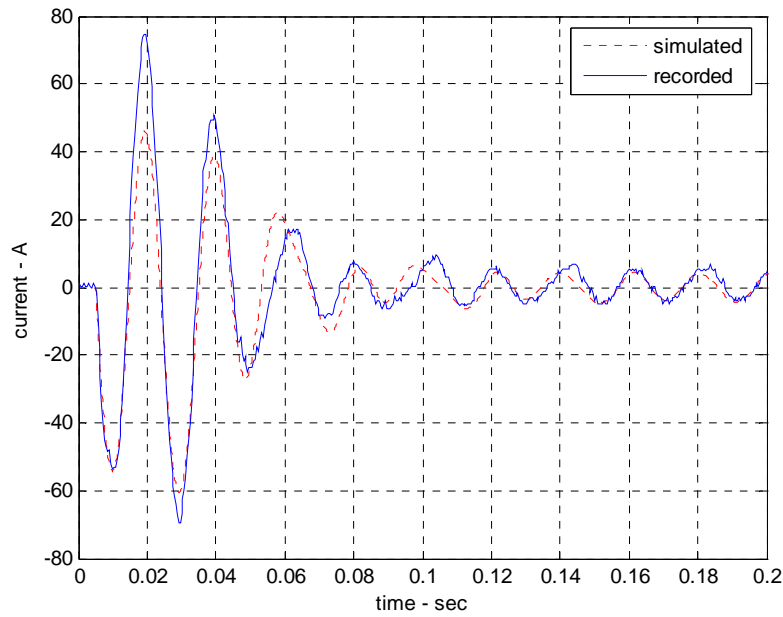


Figure 5.7 DOL Start - Simulated and Recorded Stator Current

Table 5.9 DOL Start - Simulated and Recorded Data

	Simulated	Recorded
Final speed:	156.56 rad/sec	157.1 rad/sec
Final stator current:	3 Arms	3 Arms

For the sudden removal and sudden application of load to the induction the motor, the recorded and simulated stator currents are shown in Figure 5.8 and Figure 5.9. From these figures it can be seen that the recorded and simulated stator currents are very similar and can be regarded as the same. The recorded and simulated initial and final data recordings for the tests are given in Table 5.10 and Table 5.11. This data is similar and can be regarded as the same.

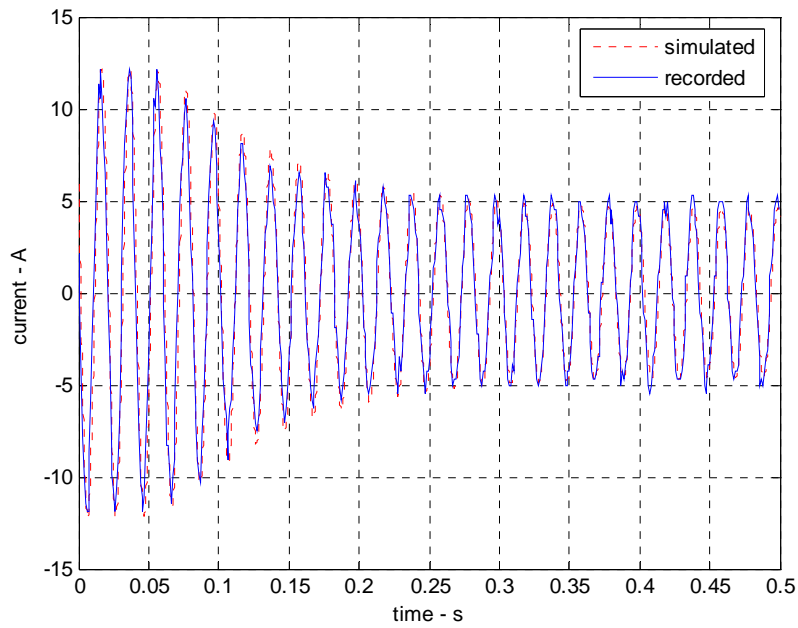


Figure 5.8 Sudden Removal of Load - Recorded and Simulated Stator Current

Table 5.10 Sudden Removal of Load - Simulated and Recorded Data

	Simulated	Recorded
Initial load:	25 Nm	3.8 Kw / 25 Nm
Final load:	0 Kw	0 Kw
Initial speed:	148 Rad/sec	148.6 rad/sec
Final speed:	155.5 rad/sec	156.6 rad/sec
Initial stator current:	8.42 A rms	8.4 A rms
Final stator current	3.3 A rms	3.46 A rms

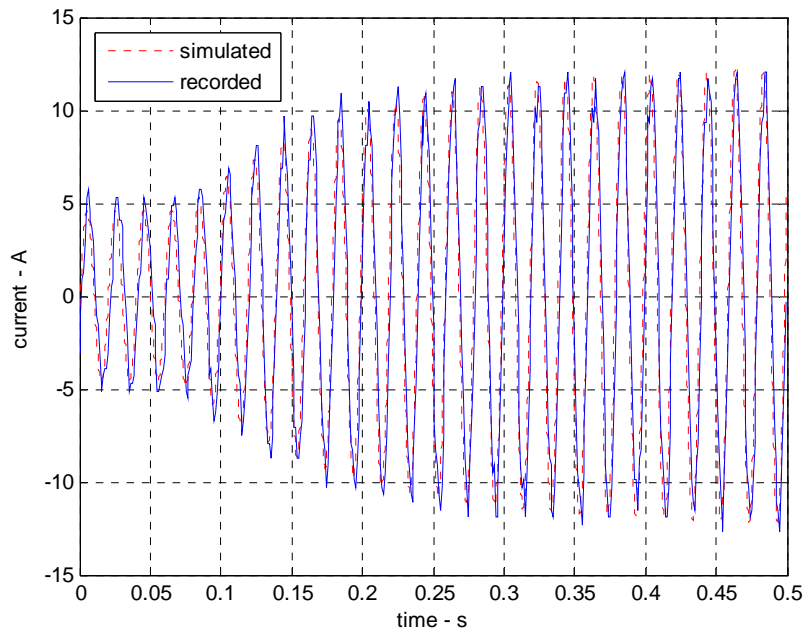


Figure 5.9 Sudden Application of Load - Recorded and Simulated Stator Currents

Table 5.11 Sudden Application of Load - Simulated and Recorded Data

	Simulated	Recorded
Initial load:	0 Nm	0 Kw / 0 Nm
Final load:	25.9 Nm	3.85 Kw / 25.9 NM
Initial speed:	155.5 rad/sec	156.6 rad/sec
Final speed:	147.8 rad/sec	148.5 rad/sec
Initial stator current:	3.3 A rms	3.46 A rms
Final stator current	8.46 A rms	8.4 A rms

From the comparison of recorded and simulated operation of the induction motor, the induction motor model can be verified for motor operation when magnetic flux saturation is not present. The model is therefore adequate for the research in this project as the focus is on the operation of variable speed drives during steady states, variations in loads within the motor capabilities and controlled variations in the speed set points. During these conditions magnetic flux saturation should not occur if the motor is adequately designed and constructed.

6. Principles of AC VSD

6.1 AC VSDs

AC variable speed drives for induction motors are generally of the variable frequency type where the frequency and power of the stator supply are controlled. Other types of variable speed drives include the reduced voltage and rotor resistance types but the variable frequency type is the only type considered in this dissertation as this provides the largest range of operating speed.

The variable frequency type of AC VSDs can be classified into DC-link converter and cycloconverter schemes. The DC-link converter scheme involves the rectification of the AC supply to a DC-link and the inversion of the DC to produce the stator supply at the required frequency and power. Cycloconverter schemes do not have a DC-link and perform direct frequency conversion of the AC supply to the stator supply. Cycloconverter VSDs are generally used in large power applications and are not considered further in this dissertation.

6.2 DC-Link VSD Construction

DC-link AC VSDs range in size and are typically enclosed in a single unit for smaller drives or in a single cabinet for larger drives. They are static power converters which use semiconductor power switches to form the converter and inverter sections as shown in Figure 6.1.

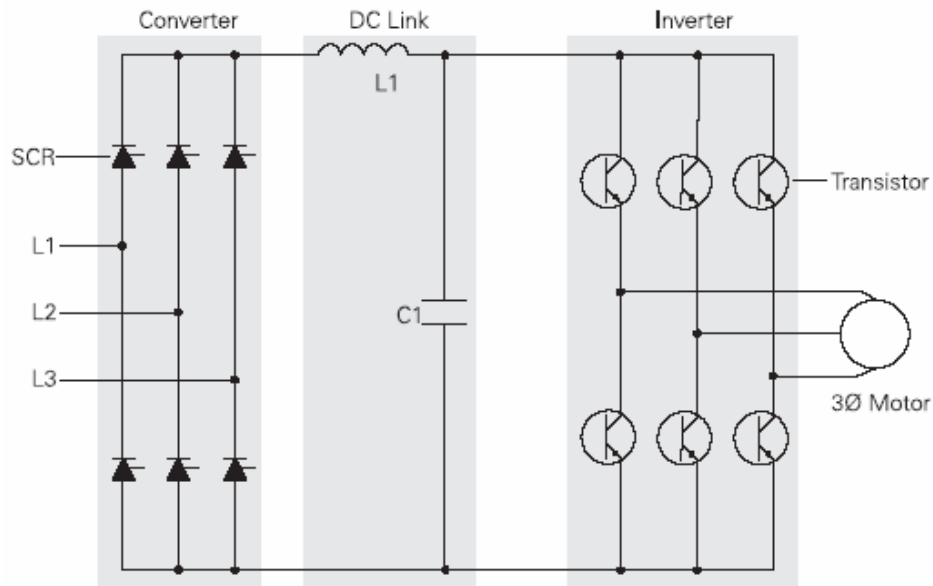


Figure 6.1 DC-Link Conversion VSD

(source: <http://www.sea.siemens.com/step>)

The semiconductor switches are installed on heat sinks which are usually cooled by forced air flow or by liquid in some high power units. The units can be installed remotely to the drive motor and require only a 3 phase connection to the drive motor in sensorless control schemes.

Microprocessors are generally installed in modern variable speed drives for controlling the semiconductor switching and user interfaces are usually installed to allow setup and control. Depending upon the control scheme, all controls for the drive may be contained within the variable speed drive unit or external controls such as distributed control systems may be connected for external control and monitoring.

6.3 DC-Link VSD Operation

DC-Link VSDs are classified according to the method used to control the power of the 3 phase supply delivered to the drive motor. The three types of classification are:

1. *Voltage Source Inverter (VSI)*. The stator voltage magnitude is the control variable which is controlled by regulating the DC-Link voltage supplied to the inverter. The inverter is a square wave inverter.
2. *Current Source Inverter (CSI)*. The stator current magnitude is the control variable which is controlled by regulating the DC-Link current supplied to the inverter. The inverter is square wave inverter.
3. *Pulse Width Modulation (PWM)*. The stator voltage magnitude is the control variable which is regulated by the inverter using PWM of the output inverter waveform.

Regulation of the DC-Link voltage or current is achieved by using a controlled rectifier. The conduction of the semiconductors in the controlled rectifier are controlled by the VSD control circuitry which senses the DC-Link voltage or current. In VSI systems the DC-Link contains a series inductance and shunt capacitor which forms a LC filter and maintains a stable voltage at the inverter. In CSI systems the DC-Link contains only a series inductance which maintains a stable DC current to the inverter.

VSI and CSI VSDs employ a square wave inverter to produce the 3 phase stator supply at the required frequency. The conduction of the inverter semiconductors is controlled by the VSD control circuitry to produce line voltages or currents that have a square waveform with a period of the required frequency. Each stator line is connected to the DC-Link via semiconductor switches which are controlled so that the stator line is connected to the positive DC rail for half the period of the required frequency and connected to the negative DC rail for the remaining half of the period. The timing of this switching is displaced by 120° for each stator line and each semiconductor performs one switching operation during each cycle of the stator waveform.

In PWM systems an uncontrolled rectifier can be used produce a constant DC-Link voltage. The conduction of the inverter semiconductors is controlled so that the magnitude of the stator voltage is regulated. The regulation is achieved by employing a multiple of switching pulses during each cycle to connect the stator line to the DC-Link. The total duration of the switching pulses in each cycle will determine the average of the stator waveform. Therefore control of the total duration of the switching pulses is used to control the magnitude of the stator voltage. The duration of each switching pulse in each cycle is also varied so that a more sinusoidal waveform is produced.

6.4 Constant V/f Control

Constant V/f induction motor speed control is a control technique which attempts to maintain the flux of the machine constant, independently of speed. If the flux of the induction motor is maintained constant, then the torque of the motor depends only on the slip of the motor and for constant torque operation the slip will remain constant. For this operation, the motor speed becomes a linear function of synchronous speed and the motor speed can be controlled by setting the synchronous speed only.

If the stator resistance of an induction motor is neglected then the stator voltage of the motor is dependant only of the synchronous frequency and the stator flux as given by (6.1).

$$\vec{u}_s^{\psi_s} = \omega_{ms} \vec{\psi}_s^{\psi_s} \quad (6.1)$$

By rearranging (6.1), (6.2) is obtained which defines the stator flux as a function of the stator voltage and the synchronous frequency. If the ratio of the stator voltage to synchronous frequency is maintained, then the stator flux will be maintained. This is referred to as constant V/f operation.

$$\vec{\psi}_s^{\psi_s} = \frac{1}{2\pi} \frac{\vec{u}_s^{\psi_s}}{f_{ms}} \quad (6.2)$$

For constant flux operation the torque of the induction motor will be dependant only on the slip of the motor. Therefore for constant torque operation the rotor slip remains constant and the motor speed becomes a linear function of the synchronous frequency as given in (6.3).

$$\omega_r = 2\pi f_s - \omega_{slip} \quad (6.3)$$

The constant V/f control described has assumed that the stator resistance is zero and that the load remains constant. In practice variations in the load will affect the motor torque

and the stator resistance will have a significant impact on the stator flux and torque production at low speeds. These changes in torque will change the rotor slip and will impact on the linear relationship between the synchronous speed and the rotor speed. The impact of these issues can be compensated for with stator resistance voltage-drop compensation and slip compensation.

6.5 Stator Resistance Voltage Drop Compensation

Stator resistance voltage drop compensation is a control technique in which the stator voltage is boosted to compensate for the affect of the stator resistance. In constant V/f control techniques this will allow a constant V/f ratio to be maintained across the stator inductance so that the flux of the motor is maintained.

At lower speeds the affect of the stator resistance voltage-drop is more significant as the magnitude of the voltage drop is larger in comparison to the voltage across the stator inductance. The required voltage across the stator inductance will be significantly less than required and the flux of the motor will drop significantly. Therefore stator resistance voltage-drop compensation greatly improves the low speed performance of AC variable speed drives. Maintaining a constant flux will also improve the dynamic performance of the drive.

6.6 Slip Compensation

Slip compensation is a control technique in which the difference between synchronous and rotor speeds are compensated for by boosting the synchronous speed above the speed set point by an amount equal to the slip. Therefore the rotor speed will be equal to the speed set point.

Slip compensation is usually determined by estimating the torque produced by the motor. In the operational range of the induction motor, the relationship between slip and torque is approximately linear and the slip compensation can be approximated. The

slip determined from the torque of the motor can then be added to the speed set point to obtain the required synchronous speed as given by (6.4).

$$\omega_{ms} = \omega_r + \omega_{slip} \quad (6.4)$$

7. Experimental VSD

7.1 Experimental VSD Control

The experimental AC VSD is a constant V/f VSD with slip compensation and stator resistance voltage drop compensation. The performance of the VSD is not as good as that of more complicated drives but the cost of implementing the drive will be less as the control algorithm is relatively simple and is able to be implemented on simpler systems. The drive is therefore a compromise between performance and cost.

A major advantage of this VSD is that only motor nameplate data and the stator resistance are required for control. Therefore setup and self commissioning is simplified. During setup the installer only needs to enter the motor name plate data and a short self commissioning program can determine the stator resistance with current injection to the stator.

The constant V/f control technique is the basis of this drive and enables a simple and low cost variable speed drive to be produced. The slip compensation reduces the steady state error of the drive and the stator voltage drop compensation improves the low speed and dynamic performance of the drive.

7.2 Experimental VSD Control Equations

Using a rotational operator the two phase dynamic equation of the stator voltage can be transformed into values in the general reference frame denoted by ‘g’ as shown in (7.1). The stator voltage in the general reference frame is given by (7.2).

$$\vec{u}_s^s = e^{j\theta_g} \vec{u}_s^g = e^{j\theta_g} R_s \vec{i}_s^g + \frac{d}{dt} \left(e^{j\theta_g} \vec{\psi}_s^g \right) \quad (7.1)$$

where:

$e^{j\theta_g}$, rotational operator

$$\vec{u}_s^g = R_s \vec{i}_s^g + \frac{d}{dt}(\vec{\psi}_s^g) + j\omega_g \vec{\psi}_s^g \quad (7.2)$$

From (7.2) the stator voltage in the stator flux reference frame is given by replacing ‘g’ with ‘ ψ_s ’ to obtain (7.3).

$$\vec{u}_s^{\psi_s} = R_s \vec{i}_s^{\psi_s} + \frac{d}{dt}(\vec{\psi}_s^{\psi_s}) + j\omega_{\psi_s} \vec{\psi}_s^{\psi_s} \quad (7.3)$$

With constant V/f control the flux in the motor is maintained constant so the derivative of the stator flux in (7.3) is zero. Therefore the stator voltage equation (7.3) reduces to (7.4).

$$\vec{u}_s^{\psi_s} = R_s \vec{i}_s^{\psi_s} + j\omega_{\psi_s} \vec{\psi}_s^{\psi_s} \quad (7.4)$$

By composing the stator voltage and current into direct and quadrature components, the stator voltage (7.3) can split into (7.5) and (7.6) which define the voltages in the two axis model.

$$u_{sd}^{\psi_s} = i_{sd}^{\psi_s} R_s \quad (7.5)$$

$$u_{sq}^{\psi_s} = i_{sq}^{\psi_s} R_s + \omega_{ms} \psi_s \quad (7.6)$$

where:

$$\omega_{ms} = \omega_{\psi_s}$$

To aid with analysis the reference frames will be denoted with a subscript ‘x’ to designate the direct axis in the stator flux reference frame and the subscript ‘y’ to designate the quadrature axis in the stator flux reference frame. The stator voltage equations are then given by (7.7) and (7.8).

$$u_{sx} = i_{sx} R_s \quad (7.7)$$

$$u_{sy} = i_{sy} R_s + \omega_{ms} \psi_s \quad (7.8)$$

The stator voltage defined by (7.7) and (7.8) are the control equations used by Francis (1997) to provide stator resistance voltage drop compensation for an AC VSD. In this control scheme the user sets the synchronous speed, the flux and the stator resistance. The quantity $\omega_{ms} \psi_s$ is the voltage across the stator inductance in the IM model. This value is proportional to the set point speed when the flux is held constant. In this control scheme the user needs to enter the value of stator flux linkage during set up. This is undesirable as this information is not readily available from motor name plates.

Munoz-Garcia (1998) developed a stator resistance voltage-drop control scheme in which the voltage across the stator flux was defined by a fixed voltage V_{so} and the ratio of the set speed point to the rated speed as given by (7.9). The advantage of this scheme is the rated speed is available from the motor name plate and V_{so} can be calculated during the VSD self commissioning routine from the name plate rated voltage, rated current and measured stator resistance using (7.10).

$$\omega_{ms} \psi_s = \frac{V_{so}}{\omega_{rated}} \omega_{ms} \quad (7.9)$$

$$V_{so} = V_{rated} - I_{rated} R_s \quad (7.10)$$

By using (7.9) the control equations (7.7) and (7.8) become (7.11) and (7.12) which are referred to as the conventional V/f control method by Jung (2004).

$$u_{sx} = i_{sx} R_s \quad (7.11)$$

$$u_{sy} = i_{sy} R_s + \frac{V_{so}}{\omega_{rated}} \omega_{ms} \quad (7.12)$$

These control equations will maintain the flux constant in the motor but the synchronous speed is required to be boosted to compensate for slip which is required for the development of torque. The ‘x’ axis in the control equations is aligned with the stator flux so the torque of the motor is only dependent on the ‘y’ axis current and stator flux. Therefore the torque of the motor is given by (7.13).

$$T_e = K_T i_{sy} \psi_s \quad (7.13)$$

where:

$$K_T = \text{constant}$$

From (7.13) it can be seen that the torque is proportional to the ‘y’ axis current when flux is held constant. Therefore slip is also proportional to the ‘y’ axis current when flux is held constant and slip will be equal to the rated slip when the motor current is equal to the rated current. The rated slip, rated current and the measured ‘y’ axis currents are used in (7.14) to determine the required slip compensation to be added to the set point speed. This is linear slip estimation which approximates the actual slip.

$$\omega_k = i_{sy} \frac{S_{rated}}{I_{s rated}} \omega_{ms} \quad (7.14)$$

Linear slip estimation using rated slip, rated torque and motor torque has been used for linear slip compensation by Xue (1990) and Koga (1990) and for the linear slip component of compensation by Munoz-Garcia (1998). Linear slip estimation using currents as in (7.14) has been used for slip compensation by Holtz (2002).

The rated stator current has been used in the denominator of the (7.14) rather than the rated ‘y’ axis current as the rated ‘y’ axis current is unknown but its magnitude is similar to the rated stator current. Therefore any error in the slip estimation from (7.14) is small and has been neglected.

The control equations for the complete experimental drive are given by (7.15) and (7.16). In these equations the stator resistance compensation in each axis is considered individually to allow adjustment of the system for stability and performance. These

control equations are an approximated vector implementation of the scalar control scheme developed by Munoz-Garcia (1998) without nonlinear components of slip compensation.

$$u_{sx} = i_{sx} \tilde{R}_{sx} \quad (7.15)$$

$$u_{sy} = i_{sy} \tilde{R}_{sy} + \frac{V_{so}}{\omega_{rated}} \omega_{ms} \left(1 + i_{sy} \frac{S_{rated}}{I_{s rated}}\right) \quad (7.16)$$

where:

$\tilde{R}_{sx} = R_s$ compensation in 'x' axis

$\tilde{R}_{sy} = R_s$ compensation in 'y' axis

The control equations (7.15) and (7.16) are for a two phase motor in the stator flux reference frame. Therefore transformations are required to transform stator voltages and currents between 3 and 2 phase quantities and between the stator and stator flux reference frames. The transformation between 3 and 2 phase quantities is performed in the stator reference frame using the transformations defined in chapter 3.2 by (3.6) and (3.7). The transformation between the stator and stator flux reference frames are performed using (7.17) to (7.20). In these transforms the sine and cosine of the stator flux angular position are used to project the variables directly between the reference frames.

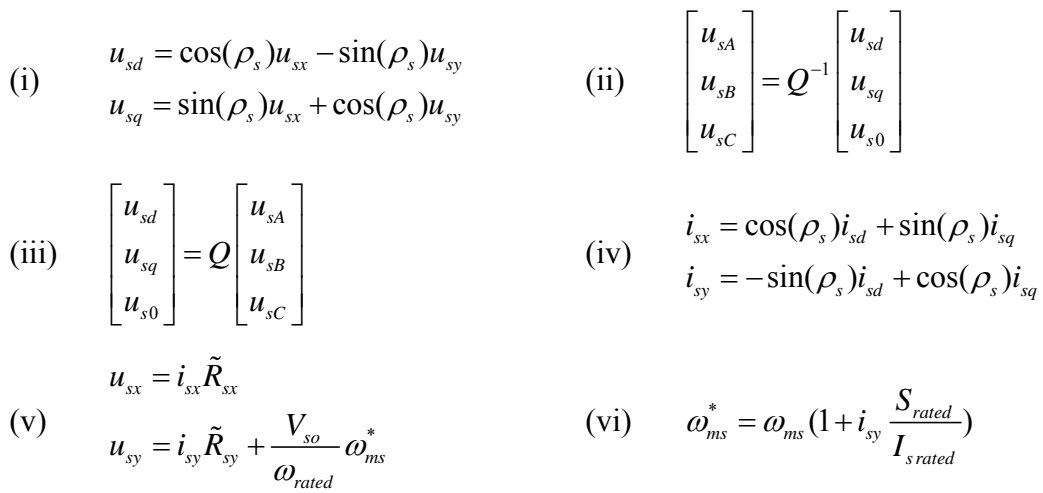
$$i_{sx} = \cos(\rho_s) i_{sd} + \sin(\rho_s) i_{sq} \quad (7.17)$$

$$i_{sy} = -\sin(\rho_s) i_{sd} + \cos(\rho_s) i_{sq} \quad (7.18)$$

$$u_{sd} = \cos(\rho_s) u_{sx} - \sin(\rho_s) u_{sy} \quad (7.19)$$

$$u_{sq} = \sin(\rho_s) u_{sx} + \cos(\rho_s) u_{sy} \quad (7.20)$$

The complete block diagram and the control equations of the experimental VSD are given in Figure 7.1. With the removal of the slip compensation block the experimental VSD is effectively the same as the drive developed by Francis (1997).



8. Implementation of VSD Model in Simulink[®]

8.1 VSD Models

VSD models for a constant V/f VSD and the experimental VSD have been implemented in Simulink[®] so that the operation of both VSDs can be simulated. This allows the performance of the experimental drive to be quantified against the constant V/f VSD which is a standard drive. The experimental VSD Simulink[®] model is also valuable for verifying the stability limits determined from the stability analysis of the system.

The Simulink[®] models of the VSDs implement the controls of the drives and neglect the operational characteristics of the real system such as small lags in the control system and non-sinusoidal stator waveforms. The IM Simulink[®] model developed in chapter 4 forms a sub-function block in the VSD Simulink[®] models and replicates a 3 phase IM.

The Simulink[®] models of the drives are given in Figure 8.1 and Figure 8.2.

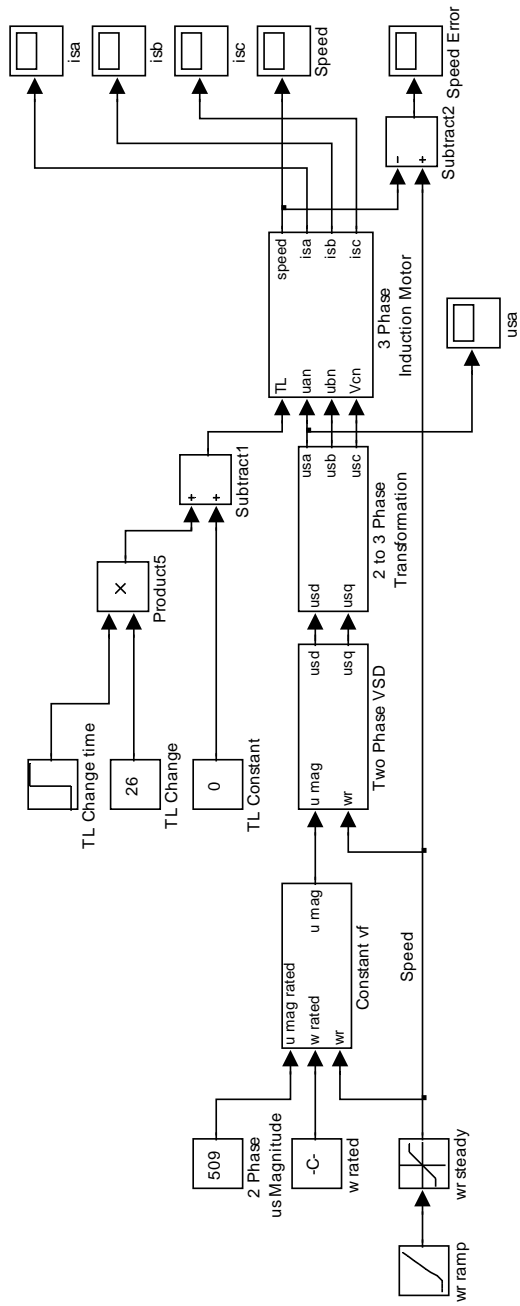


Figure 8.1 Constant V/f Simulink® Model

9. Stability and Performance Analysis of Drive

9.1 Stability and Performance Analysis Methodology

The stability and performance of the experimental VSD has been analysed so that the capability of the drive can be determined. This analysis has been performed for an induction motor with the parameters listed in Table 9.1.

The stability of the system has been analysed using linear and linear approximation analysis. The linear stability analysis is performed for constant rotor speed while the linear approximation is performed for dynamic rotor speed using small signal displacements. Stability in both analyses is assessed by determining the root locus pole locations.

The linear stability analysis has been performed as it is simpler and requires less computing than the linear approximation analysis. As the stability limits determined from this linear analysis apply to the small signal approximation the computing required for the stability analysis is reduced as linear approximation is used only to access the electrodynamics of the system.

The performance of the system has been analysed by comparing simulations of the speed response and calculated performance criteria. The following performance criteria have been used to quantify the performance.

1. *Settling time.* Time required for the transient oscillations of rotor speed to decay to within $\pm 2\%$ of steady state rotor speed.
2. *Overshoot.* Amount that the rotor speed overshoots the steady state value.
3. *Stead state error.* Difference between the speed reference and the rotor speed at steady state.
4. *ITAE.* Time integral of absolute error between the speed reference and the rotor speed for the duration of the simulation.
5. *Speed regulation.* The change in rotor speed during load changes.

Table 9.1 Motor Details for VSD Stability and Performance Evaluation

Name Plate Details	
Rated Line Voltage: V	415
Rated Frequency: Hz	50
Rated Line Current: A	8.1
Rated Power: KW	4
Rated Speed: RPM	1420
Winding Configuration:	Delta
Measured Parameters	
Stator resistance, $R_s : \Omega$	1.749
Rotor resistance, $R_r : \Omega$	1.544
Magnetising inductance, $L_m : H$	0.246
Stator leakage inductance, $L_{ls} : H$	0.0081
Rotor leakage inductance, $L_{lr} : H$	0.0081
Motor friction coefficient, $f_m : \text{Nm.s.rad}^{-1}$	0.012
Motor-load combined moment of inertia: kg.m^{-2}	0.3708

9.2 Linear Stability Analysis

Linear stability analysis of the experimental VSD has been used to access stability of the complete system for constant speed operation where the stator and rotor currents are the only state variables. This analysis does not consider the moment of inertia of the rotor and therefore greatly simplifies the stability analysis of the VSD as the system is linear and can be analysed directly using linear system control theory. Francis (1997) used this method of analysis to access the stability of stator resistance voltage drop compensation.

The state space model of the IM was developed in chapter 3.3 and is given by (3.20). In this state space model the currents are the state variables and the state matrix remains constant for constant rotor speed. Therefore determining the poles of the closed loop state space model for the experimental VSD will give the poles of the VSD for constant operating speed. Full derivation of the closed loop state space equation in this chapter is given in Appendix C.

The induction motor state space equation can be represented by (9.1) and the VSD control equations can be represented by (9.2).

$$\dot{X} = AX + BU \quad (9.1)$$

$$\begin{bmatrix} u_{sx} \\ u_{sy} \end{bmatrix} = \begin{bmatrix} i_{sx} \tilde{R}_{sx} \\ i_{sy} (\tilde{R}_{sy} + \beta \omega_{ms}) + \alpha \omega_{ms} \end{bmatrix} \quad (9.2)$$

where:

$$\alpha = \frac{V_{so}}{\omega_{rated}} \quad \beta = \frac{S_{rated}}{I_{srated}} \frac{V_{so}}{\omega_{rated}}$$

To simplify analysis of the closed loop system the stator flux angular position is set to zero so that the stator and stator flux axes align. The control equation (9.2) after rearranging is now (9.3) which can be represented by state space representation of (9.4).

$$\begin{bmatrix} u_{sd} \\ u_{sq} \end{bmatrix} = \begin{bmatrix} \tilde{R}_{sx} & 0 & 0 & 0 \\ 0 & (\tilde{R}_{sy} + \beta \omega_{ms}) & 0 & 0 \end{bmatrix} \begin{bmatrix} i_{sd} \\ i_{sq} \\ i_{rd} \\ i_{rq} \end{bmatrix} + \begin{bmatrix} 0 \\ \alpha \omega_{ms} \end{bmatrix} \quad (9.3)$$

$$U = KX + U_{ref} \quad (9.4)$$

where:

$$K = \begin{bmatrix} \tilde{R}_{sx} & 0 & 0 & 0 \\ 0 & (\tilde{R}_{sy} + \beta \omega_{ms}) & 0 & 0 \end{bmatrix}$$

The complete closed loop state space model of the experimental VSD is now obtained by combining (9.1) and (9.4) to obtain (9.5).

$$\begin{aligned} \dot{X} &= AX + B(KX + U_{ref}) \\ &= A_c X + B_c U_{ref} \end{aligned} \quad (9.5)$$

where:

$$A_c = A + BK$$

A_c is the closed loop state matrix for the drive which is:

$$A_c = \begin{bmatrix} \frac{\tilde{R}_{sx} - R_s}{\sigma L_s} & \frac{\omega_r L_m^2}{L_r \sigma L_s} & \frac{L_m R_r}{L_r \sigma L_s} & \frac{\omega_r L_m}{\sigma L_s} \\ -\frac{\omega_r L_m^2}{L_r \sigma L_s} & \frac{\tilde{R}_{sy} - R_s + \beta \omega_{ms}}{\sigma L_s} & -\frac{\omega_r L_m}{\sigma L_s} & \frac{L_m R_r}{L_r \sigma L_s} \\ \frac{L_m (R_s - \tilde{R}_{sx})}{L_r \sigma L_s} & -\frac{\omega_r L_m}{\sigma L_r} & -\frac{R_r}{\sigma L_r} & -\frac{\omega_r}{\sigma} \\ \frac{\omega_r L_m}{\sigma L_r} & \frac{L_m (R_s - \tilde{R}_{sy} - \beta \omega_{ms})}{L_r \sigma L_s} & \frac{\omega_r}{\sigma} & -\frac{R_r}{\sigma L_r} \end{bmatrix}$$

From the closed loop system it can be seen that the compensation terms \tilde{R}_{sx} , \tilde{R}_{sy} and β appear in the entries of A_c containing R_s . \tilde{R}_{sx} and \tilde{R}_{sy} act to remove R_s from A_c while β acts to increase i_{sy} and i_{ry} which increases the electromagnetic torque.

The stability of the complete closed loop state space model of the experimental VSD can be determined directly from A_c for static rotor speeds. For static rotor speeds the terms in A_c containing ω_r or ω_{ms} are constant and linear control system theory can be applied to the system. The poles of the closed loop system are the eigenvalue solutions for:

$$\det(\lambda I - A_c) = 0 \quad (9.6)$$

The poles of the closed loop system have been solved with Matlab[®] using the Matlab[®] function listed in Appendix D. The poles of the system are plotted in Figure 9.1 and Figure 9.2 for slip compensation of zero and stator resistance compensation equal for both axis. In these figures the rotor current poles move away from the zero imaginary axis as speed increases and are stable for all speeds and values of compensation. The stator current poles move away from the origin as speed increases and are positioned in the positive real plane for stator resistant compensation of 1.0 or greater. The system is therefore unstable for stator resistance compensation of 1.0 or greater when slip compensation is zero.

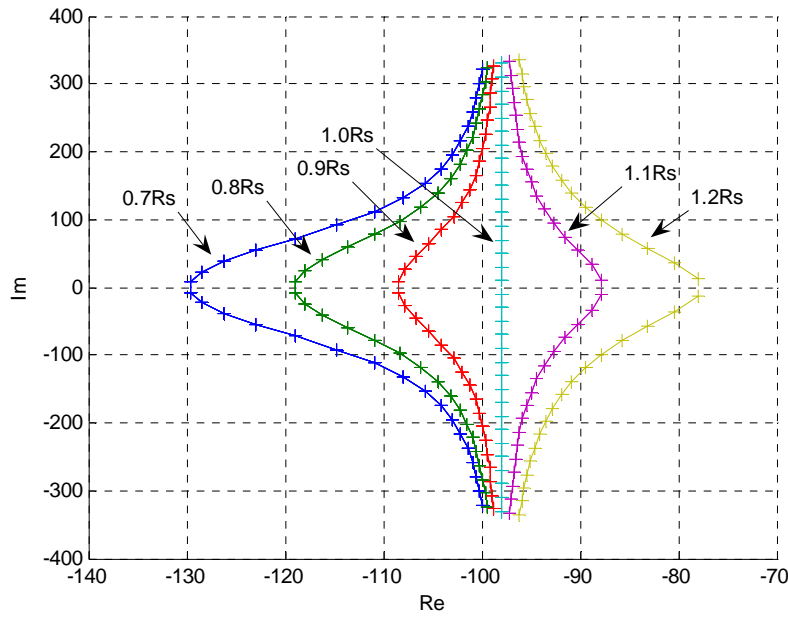


Figure 9.1 Rotor Current Poles for Equal R_s Compensation and Zero Slip Compensation

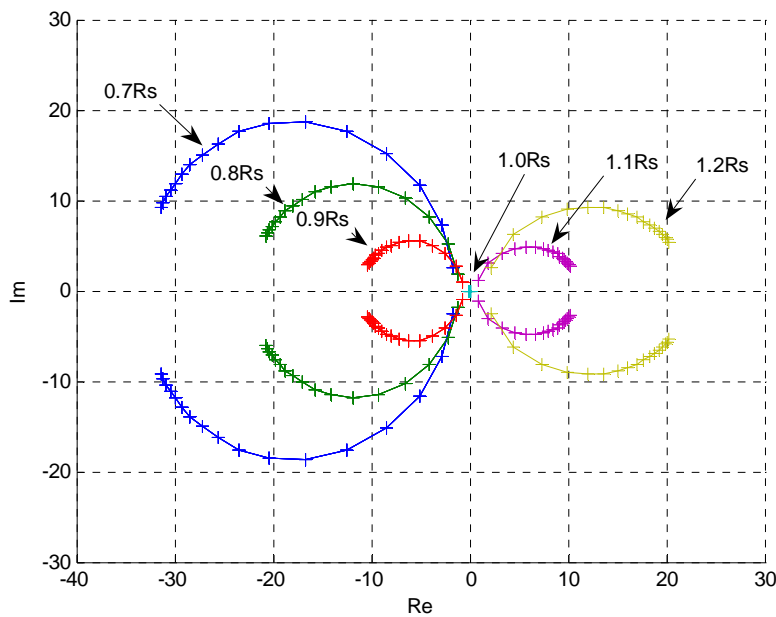


Figure 9.2 Stator Current Poles for Equal R_s Compensation and Zero Slip Compensation

For slip compensation with zero stator resistance compensation the rotor current poles of the system are all in the negative real plane. However the stator current poles cross in to the positive plane as speed increases. The stator current poles are plotted in Figure

9.3. The poles of this system cross into the positive plane when the value of the slip compensation causes β to become greater than the stator resistance.

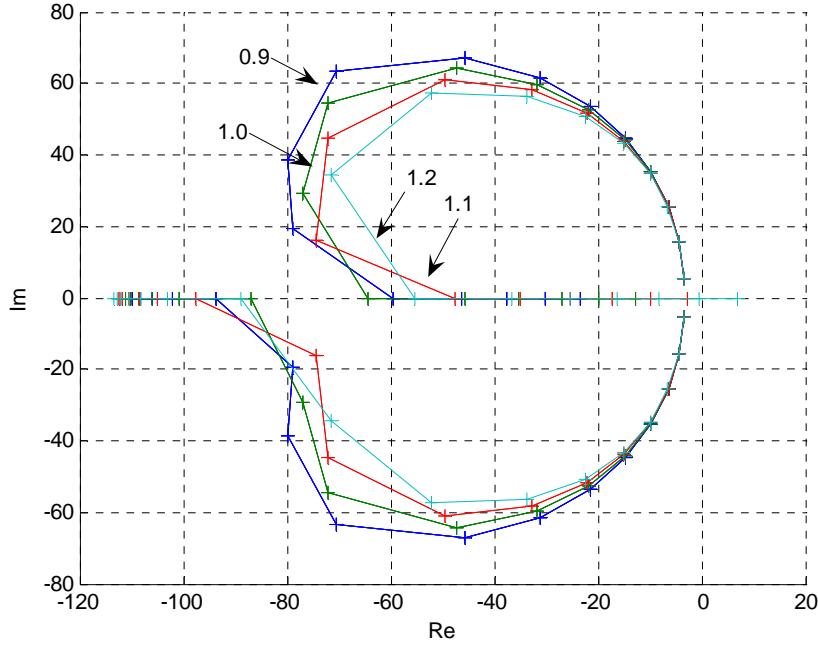


Figure 9.3 Stator Current Poles for Slip Compensation and Zero R_s Compensation

For any combination of stator resistance and slip compensation, instability of the closed loop system occurs when the entries of A_c containing R_s become zero or change sign. Therefore the combined stator resistance compensation and slip compensation must maintain the following inequalities for the system to be stable.

$$\tilde{R}_{sx} < R_s \quad (9.7)$$

$$(\tilde{R}_{sy} + \beta\omega_{ms}) < R_s \quad (9.8)$$

The above conditions can be confirmed by considering the conditions that yield a zero determinant. A zero determinant of a matrix occurs when two rows of the matrix are linearly dependant. If \tilde{R}_{sx} is equal to R_s then the 1st and 3rd rows of the eigenvalue matrix in (9.11) become linearly dependent when λ is zero. Therefore the stator current poles will be positioned at the origin on the root locus and the system is

marginally stable. If the sum of \tilde{R}_{sy} and $\beta\omega_{ms}$ is equal to R_s then the 2nd and 4th rows of the matrix become linearly dependant when λ is zero and stator current poles will be positioned at the origin of the root locus. The system is once again marginally stable. Therefore the following conditions are the stability limits for compensation in the system.

$$\tilde{R}_{sx} = R_s \quad \text{1st and 3rd rows linearly dependant} \quad (9.9)$$

$$(\tilde{R}_{sy} + \beta\omega_{ms}) = R_s \quad \text{2nd and 4th rows linearly dependant} \quad (9.10)$$

$$\det(\lambda I - A_c) = \begin{vmatrix} \lambda I - \frac{\tilde{R}_{sx} - R_s}{\sigma L_s} & -\frac{\omega_r L_m^2}{L_r \sigma L_s} & -\frac{L_m R_r}{L_r \sigma L_s} & -\frac{\omega_r L_m}{\sigma L_s} \\ \frac{\omega_r L_m^2}{L_r \sigma L_s} & \lambda I - \frac{\tilde{R}_{sy} - R_s + \beta\omega_{ms}}{\sigma L_s} & \frac{\omega_r L_m}{\sigma L_s} & -\frac{L_m R_r}{L_r \sigma L_s} \\ -\frac{L_m (R_s - \tilde{R}_{sx})}{L_r \sigma L_s} & \frac{\omega_r L_m}{\sigma L_r} & \lambda I + \frac{R_r}{\sigma L_r} & \frac{\omega_r}{\sigma} \\ -\frac{\omega_r L_m}{\sigma L_r} & -\frac{L_m (R_s - \tilde{R}_{sy} - \beta\omega_{ms})}{L_r \sigma L_s} & -\frac{\omega_r}{\sigma} & \lambda I + \frac{R_r}{\sigma L_r} \end{vmatrix} \quad (9.11)$$

The above stability limits have been confirmed with Simulink[®] simulations of the system for equal R_{sx} and R_{sy} compensation. For compensation beyond the stability limits the simulated rotor speed will not respond and will remain at zero.

9.3 Small Signal Displacement Stability Analysis

Small signal stability analysis of the experimental VSD has been used to access the stability of the complete system for dynamic operation where the stator and rotor currents and the rotor speed are the state variables. This analysis accesses the electrodynamic stability of the system.

The electrodynamics of the VSD and IM can be described by a 5th order nonlinear state space equation which is formed from the closed loop VSD state space equation (9.5), the IM torque equation (3.23) and the IM rotor speed equation (3.24). This combination expands the VSD state space equation to include the rotor speed as a state variable and a 5th row which describes the rotor speed. The resultant state space equation is:

$$\frac{d}{dt} \begin{bmatrix} i_{sd} \\ i_{sq} \\ i_{rd} \\ i_{rq} \\ \omega_r \end{bmatrix} = \begin{bmatrix} \frac{\tilde{R}_s - R_s}{\sigma L_s} & \frac{\omega_r L_m^2}{L_r \sigma L_s} & \frac{L_m R_r}{L_r \sigma L_s} & \frac{\omega_r L_m}{\sigma L_s} & 0 \\ -\frac{\omega_r L_m^2}{L_r \sigma L_s} & \frac{\tilde{R}_s - R_s + \beta \omega_{ms}}{\sigma L_s} & -\frac{\omega_r L_m}{\sigma L_s} & \frac{L_m R_r}{L_r \sigma L_s} & 0 \\ \frac{L_m (R_s - \tilde{R}_s)}{L_r \sigma L_s} & -\frac{\omega_r L_m}{\sigma L_r} & -\frac{R_r}{\sigma L_r} & -\frac{\omega_r}{\sigma} & 0 \\ \frac{\omega_r L_m}{\sigma L_r} & \frac{L_m (R_s - \tilde{R}_s - \beta \omega_{ms})}{L_r \sigma L_s} & \frac{\omega_r}{\sigma} & -\frac{R_r}{\sigma L_r} & 0 \\ 0 & 0 & \frac{2n_p^2 L_m i_{sq}}{3J} & -\frac{2n_p^2 L_m i_{sd}}{3J} & -\frac{f}{J} \end{bmatrix} \begin{bmatrix} i_{sd} \\ i_{sq} \\ i_{rd} \\ i_{rq} \\ \omega_r \end{bmatrix} + \begin{bmatrix} \frac{1}{\sigma L_s} & 0 & 0 \\ 0 & \frac{1}{\sigma L_s} & 0 \\ -\frac{L_m}{L_r \sigma L_s} & 0 & 0 \\ 0 & -\frac{L_m}{L_r \sigma L_s} & 0 \\ 0 & 0 & -\frac{n_p}{J} \end{bmatrix} \begin{bmatrix} 0 \\ \alpha \omega_{ms} \\ T_L \end{bmatrix} \quad (9.12)$$

The above 5th order state space equation is non-linear and the stability of the system can not be easily accessed. However the system can approximated as a linear system for small signal displacement about a steady state condition. Linear system control theory can then be applied to analyse the stability of the small signal linear approximation. Stability of the small signal linear approximation implies a region of stability of the non-linear system. Application of small signal displacements to the state space equation produces the state space equation (9.13).

$$\begin{aligned}
\frac{d}{dt} \begin{bmatrix} *i_{sd} + \Delta i_{sd} \\ *i_{sq} + \Delta i_{sq} \\ *i_{rd} + \Delta i_{rd} \\ *i_{rq} + \Delta i_{rq} \\ *\omega_r + \Delta \omega_r \end{bmatrix} &= \begin{bmatrix} \frac{\tilde{R}_s - R_s}{\sigma L_s} & \frac{(*\omega_r + \Delta \omega_r) L_m^2}{L_r \sigma L_s} & \frac{L_m R_r}{L_r \sigma L_s} & \frac{(*\omega_r + \Delta \omega_r) L_m}{\sigma L_s} & 0 \\ -\frac{(*\omega_r + \Delta \omega_r) L_m^2}{L_r \sigma L_s} & \frac{\tilde{R}_s - R_s + \beta(*\omega_{ms} + \Delta \omega_{ms})}{\sigma L_s} & -\frac{(*\omega_r + \Delta \omega_r) L_m}{\sigma L_s} & \frac{L_m R_r}{L_r \sigma L_s} & 0 \\ \frac{L_m (R_s - \tilde{R}_s)}{L_r \sigma L_s} & -\frac{(*\omega_r + \Delta \omega_r) L_m}{\sigma L_r} & -\frac{R_r}{\sigma L_r} & -\frac{(*\omega_r + \Delta \omega_r)}{\sigma} & 0 \\ \frac{(*\omega_r + \Delta \omega_r) L_m}{\sigma L_r} & \frac{L_m (R_s - \tilde{R}_s - \beta(*\omega_{ms} + \Delta \omega_{ms}))}{L_r \sigma L_s} & \frac{(*\omega_r + \Delta \omega_r)}{\sigma} & -\frac{R_r}{\sigma L_r} & 0 \\ 0 & 0 & \frac{2n_p^2 L_m (*i_{sq} + \Delta i_{sq})}{3J} & -\frac{2n_p^2 L_m (*i_{sd} + \Delta i_{sd})}{3J} & -\frac{f}{J} \end{bmatrix} \begin{bmatrix} *i_{sd} + \Delta i_{sd} \\ *i_{sq} + \Delta i_{sq} \\ *i_{rd} + \Delta i_{rd} \\ *i_{rq} + \Delta i_{rq} \\ *\omega_r + \Delta \omega_r \end{bmatrix} \\
&+ \begin{bmatrix} \frac{1}{\sigma L_s} & 0 & 0 \\ 0 & \frac{1}{\sigma L_s} & 0 \\ -\frac{L_m}{L_r \sigma L_s} & 0 & 0 \\ 0 & -\frac{L_m}{L_r \sigma L_s} & 0 \\ 0 & 0 & -\frac{n_p}{J} \end{bmatrix} \begin{bmatrix} 0 \\ \alpha(*\omega_{ms} + \Delta \omega_{ms}) \\ *T_L + \Delta T_L \end{bmatrix} \quad (9.13)
\end{aligned}$$

The above state space equation can be developed into a state space equation where the small signal state variables are only present within the state variable matrix. In this rearrangement products of small signals are neglected and the constant terms are eliminated. Full derivation of the small signal state space equation is given in Appendix C. The resultant small signal state space equations are given by (9.14) to (9.16).

$$\begin{aligned}
\frac{d}{dt} \begin{bmatrix} \Delta i_{sd} \\ \Delta i_{sq} \\ \Delta i_{rd} \\ \Delta i_{rq} \\ \Delta \omega_r \end{bmatrix} &= \begin{bmatrix} \frac{\tilde{R}_{sx} - R_s}{\sigma L_s} & \frac{*\omega_r L_m^2}{L_r \sigma L_s} & \frac{L_m R_r}{L_r \sigma L_s} & \frac{*\omega_r L_m}{\sigma L_s} & \frac{*\omega_r L_m^2}{L_r \sigma L_s} + \frac{*\omega_r L_m}{\sigma L_s} \\ -\frac{*\omega_r L_m^2}{L_r \sigma L_s} & \frac{\tilde{R}_{sy} - R_s + \beta*\omega_{ms}}{\sigma L_s} & -\frac{*\omega_r L_m}{\sigma L_s} & \frac{L_m R_r}{L_r \sigma L_s} & -\frac{*\omega_r L_m^2}{L_r \sigma L_s} - \frac{*\omega_r L_m}{\sigma L_s} \\ \frac{L_m (R_s - \tilde{R}_{sx})}{L_r \sigma L_s} & -\frac{*\omega_r L_m}{\sigma L_r} & -\frac{R_r}{\sigma L_r} & -\frac{*\omega_r}{\sigma} & -\frac{*\omega_r L_m}{\sigma L_r} - \frac{*\omega_r}{\sigma} \\ \frac{*\omega_r L_m}{\sigma L_r} & \frac{L_m (R_s - \tilde{R}_{sy} - \beta*\omega_{ms})}{L_r \sigma L_s} & \frac{*\omega_r}{\sigma} & -\frac{R_r}{\sigma L_r} & \frac{*\omega_r L_m}{\sigma L_r} + \frac{*\omega_r}{\sigma} \\ -\frac{*\omega_r 2n_p^2 L_m}{3J} & \frac{*\omega_r 2n_p^2 L_m}{3J} & \frac{*\omega_r 2n_p^2 L_m}{3J} & -\frac{*\omega_r 2n_p^2 L_m}{3J} & -\frac{f}{J} \end{bmatrix} \begin{bmatrix} \Delta i_{sd} \\ \Delta i_{sq} \\ \Delta i_{rd} \\ \Delta i_{rq} \\ \Delta \omega_r \end{bmatrix} \\
&+ \begin{bmatrix} 0 & 0 \\ \frac{\alpha}{\sigma L_s} + \frac{*\omega_r \alpha}{L_r \sigma L_s} & 0 \\ 0 & 0 \\ -\frac{\alpha L_m}{L_r \sigma L_s} - \frac{*\omega_r L_m \alpha}{L_r \sigma L_s} & 0 \\ 0 & -\frac{n_p}{J} \end{bmatrix} \begin{bmatrix} \Delta \omega_{ms} \\ \Delta T_L \end{bmatrix} \quad (9.14)
\end{aligned}$$

$$\dot{X}_{\Delta} = A_{c\Delta} X_{\Delta} + B_{c\Delta} U_{ref\Delta} \quad (9.15)$$

$$\Delta\omega_r = Y_{\Delta} = C_{\Delta} X_{\Delta} \quad (9.16)$$

By setting one of the small signal inputs to zero a transfer function of two variables can be achieved as given below. These equations allow the effects of changes in speed set point and load torque on rotor speed to be analysed.

for: $\Delta T_L = 0$

$$\frac{\Delta\omega_r}{\Delta\omega_{ms}} = C_{\Delta} (sI - A_{c\Delta})^{-1} B_{c\Delta} \quad (9.17)$$

for: $\Delta\omega_{ms} = 0$

$$\frac{\Delta\omega_r}{\Delta T_L} = C_{\Delta} (sI - A_{c\Delta})^{-1} B_{c\Delta} \quad (9.18)$$

As the small signal system is now approximated by a regular linear state space system and transfer functions, the stability of the system can be accessed by using linear control system theory. The poles of the two transfer functions approximate the poles of the system and are the eigenvalue solutions for:

$$\det(sI - A_{c\Delta}) = 0 \quad (9.19)$$

As for the linear stability analysis the linear dependence between rows in $A_{c\Delta}$ occurs as listed below.

$$\tilde{R}_{sx} = R_s \quad \text{1st and 3rd rows linearly dependant} \quad (9.20)$$

$$(\tilde{R}_{sy} + \beta\omega_{ms}) = R_s \quad \text{2nd and 4th rows linearly dependant} \quad (9.21)$$

When either of the above conditions are satisfied the poles of the system occur at the origin of the root locus and the system is marginally stable. Therefore as for the linear analysis the following inequalities must be maintained to keep the current poles stable.

$$\tilde{R}_{sx} < R_s \quad (9.22)$$

$$(\tilde{R}_{sy} + \beta\omega_{ms}) < R_s \quad (9.23)$$

The conditions that produce unstable rotor speed poles can not be easily determined from relationships within in the matrix $A_{c\Delta}$. Therefore the Matlab[®] function listed in Appendix E has been written to solve the system poles. This function calculates the operational steady state conditions for set speeds and load torques and then determines the poles of the system by solving the eignenvvalues of $A_{c\Delta}$. This function has been used to solve the poles of the system for the range of parameters and operation as listed in Table 9.2. In this analysis the combination of \tilde{R}_{sy} and $\beta\omega_{ms}$ was limited to maintain stability as defined above. The combined root locus, 3D unstable pole location and 2D unstable pole location plots are given in Figure 9.4, Figure 9.5 and Figure 9.6. These figures are for the full range of parameters and operation as listed in Table 9.2.

Table 9.2 Small Signal Stability Analysis Parameters

\tilde{R}_{sx}	$0.95R_s$
\tilde{R}_{sy}	$0.95R_s$
Slip gain	1.0
ω_{ms}	5 – 355 rad.m ⁻¹
J	0.1 – 1 kg.m ⁻²
T_l	0 – 30 N.m

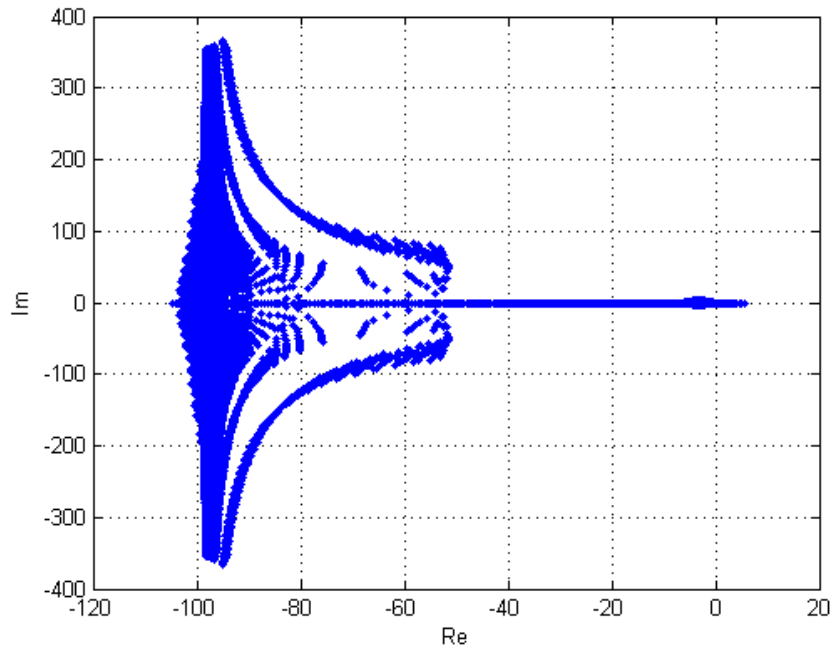


Figure 9.4 Combined Root Locus for Small Signal Stability Analysis in Table 9.2

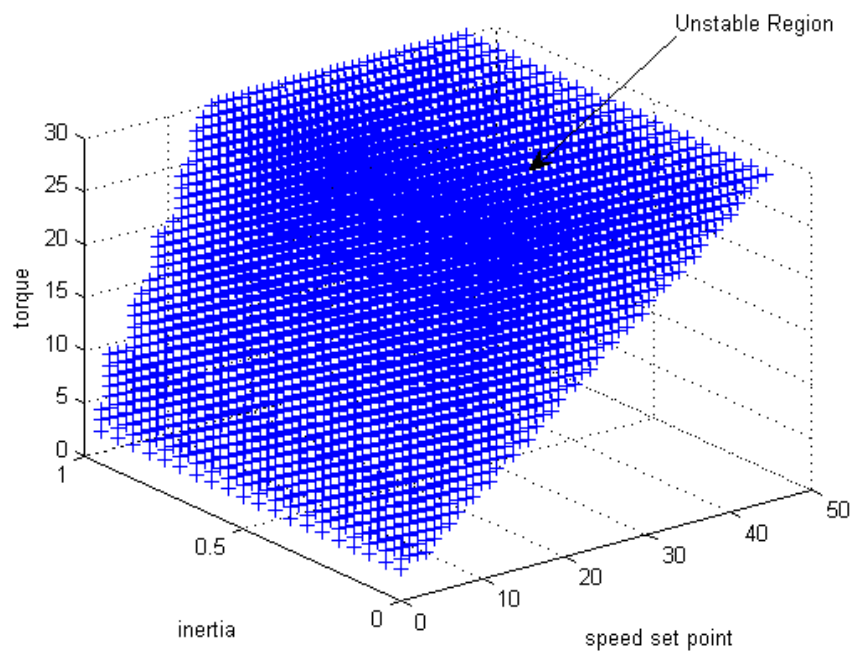


Figure 9.5 3D Unstable Conditions for Small Signal Stability Analysis in Table 9.2

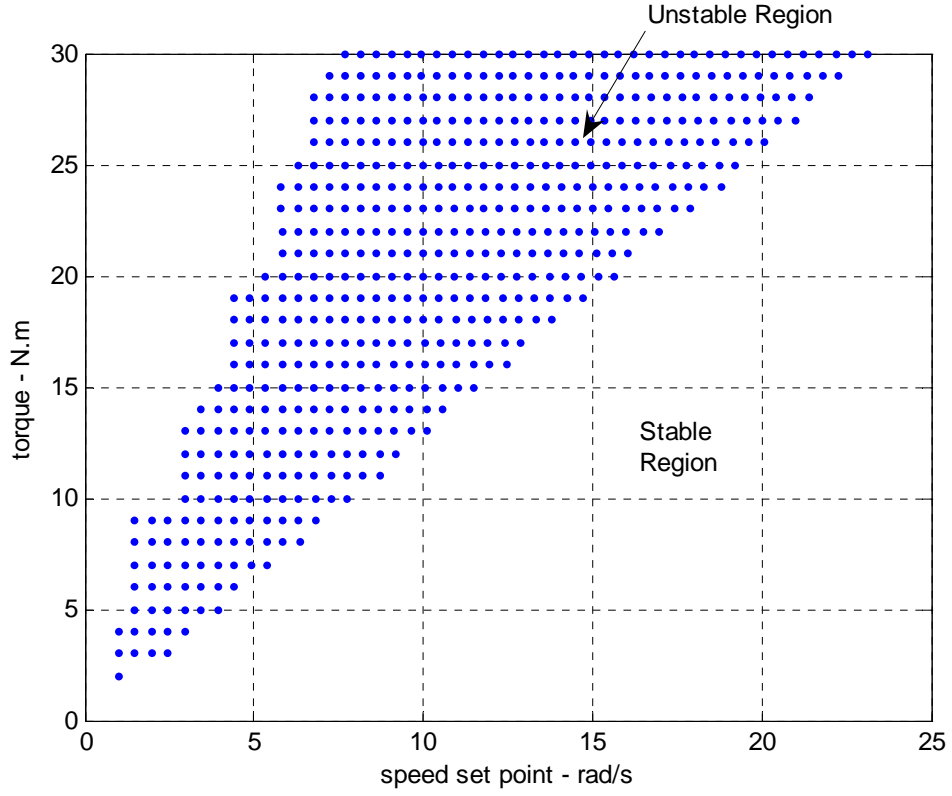


Figure 9.6 Unstable Conditions for Small Signal Stability Analysis in Table 9.2

For the above stability analysis the stability of the system is unaffected by the moment of inertia as depicted in Figure 9.6. Therefore the stability is only dependant on the speed set point and the load torque as is shown in Figure 9.6 and has been verified with simulations. With a load torque in the unstable area in Figure 9.6 the drive fails to respond and the rotor speed remains at zero. With the load torque outside of the unstable area, instability also occurs if the electromagnetic torque is within the unstable area. Torque limitation will prevent this instability and can be achieved by limiting i_{sy} as this is the torque producing current. Therefore the following i_{sy} limitation is the stability limit for torque production in the drive.

$$i_{syMax} = i_{sRated} \frac{\omega_{ms}}{25} \quad (9.24)$$

Variations in values of resistance compensation and slip compensation have a very small affect the unstable rotor speed pole locations but the root locus locations of stator

and rotor current poles are affected as shown in the combined root locus plots in Figure 9.7 and Figure 9.8.

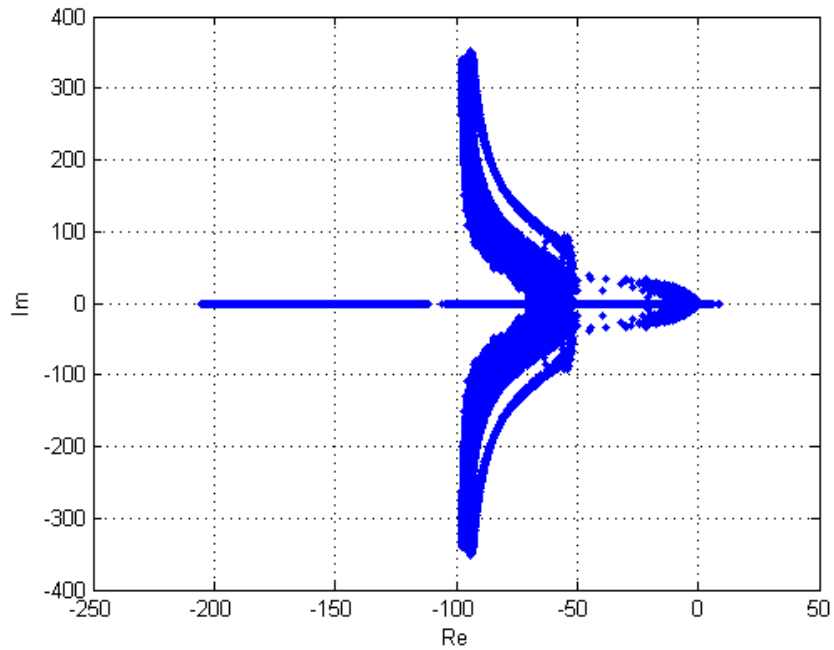


Figure 9.7 Combined Root Locus for Small Signal Stability Analysis in Table 9.2 with R_{sx} Zero

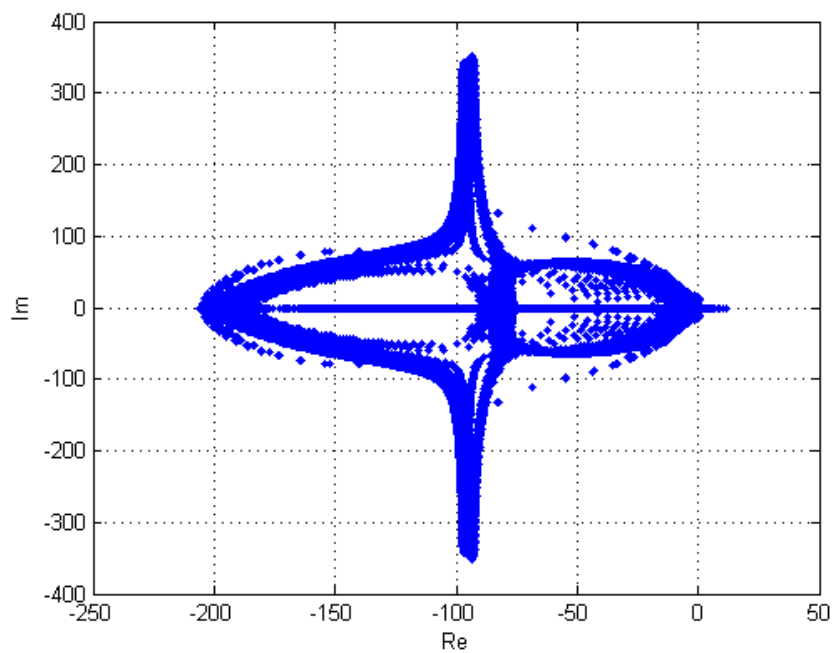


Figure 9.8 Combined Locus for Small Signal stability Analysis in Table 9.2 with R_{sx} & R_{sy} Zero

9.4 Performance Analysis

The performance of the experimental VSD has been analysed by performing simulations of the VSD in Simulink[®]. Comparison of the VSD speed responses for combinations of resistance compensation and slip compensation has been performed to identify the appropriate combination of compensation in the experimental VSD. For this combination the experimental VSD performance has been benchmarked against a constant V/f VSD.

In the experimental VSD levels of compensation can be set for \tilde{R}_{sx} , \tilde{R}_{sy} and slip. The speed response of the VSD has been simulated for these combinations while maintaining the compensation stability limits as previously defined. The simulated speed responses of the experimental VSD for several combinations of compensation are plotted in Figure 9.9.

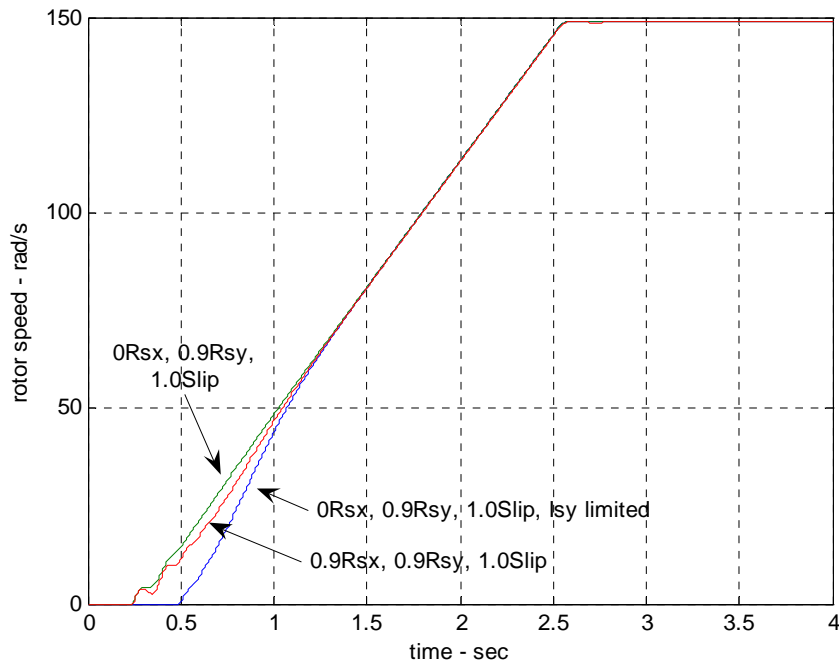


Figure 9.9 Experimental VSD Start-up, 80% Torque, 150 rad/s

Simulations of the speed response with \tilde{R}_{sx} compensation showed oscillations in the speed response during start-up for all values of \tilde{R}_{sy} and slip compensation and a long settling time for full slip compensation. This is due to small variations in the x-axis voltage having a large impact on the stator flux and therefore a large impact on the torque and speed of the motor. These oscillations during start-up and settling time are greatly reduced by reducing the \tilde{R}_{sx} compensation to zero. The oscillations during start-up can be further reduced by imposing a limiter on the i_{sy} feedback for the \tilde{R}_{sy} compensation. This limiter reduces the torque produced by the motor at low speeds so that electromagnetic torque remains within the stable area of operation as defined by the small signal displacement stability analysis. The i_{sy} limitation is defined by:

$$i_{syMax} = I_{s rated} \frac{\omega_{ms}}{25} \quad (9.25)$$

The experimental VSD gives the best performance with zero \tilde{R}_{sx} compensation, 90% \tilde{R}_{sy} compensation, full slip compensation and i_{sy} limitation. For these levels of compensation and control the performance of the experimental VSD has been benchmarked against a standard constant V/f VSD by performing simulations for each drive in Simulink[®] and calculating the performance criteria as previously defined. The simulated responses and the calculated performance are given in the following figures and tables.

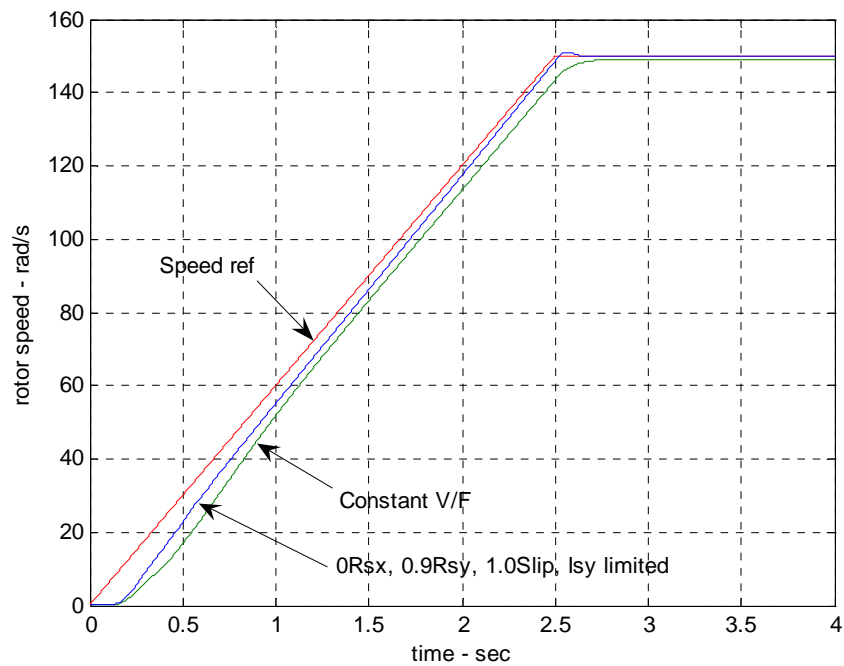


Figure 9.10 Simulation, Start-up, Zero Torque, 150 rad/s

Table 9.3 Simulated Performance Criteria, Start-up, Zero Torque, 150 rad/s

Simulation details							
Simulation time:		4 sec					
Speed reference:		Ramp 0–150 rad/s, acceleration of 60 rad/s ² .					
Load torque:		Constant at 0 Nm					
Drive Performance							
Drive	Compensation Gain			Performance Criteria			
	R_{sx}	R_{sy}	Slip	Settling time S	Overshoot %	Steady State Error %	ITAE
Constant V/f	N/A	N/A	N/A	2.559	0.00	0.521	22.196
Experimental VSD with i_{sy} limiter	0	0.9	1.0	2.475	0.752	0.043	11.54

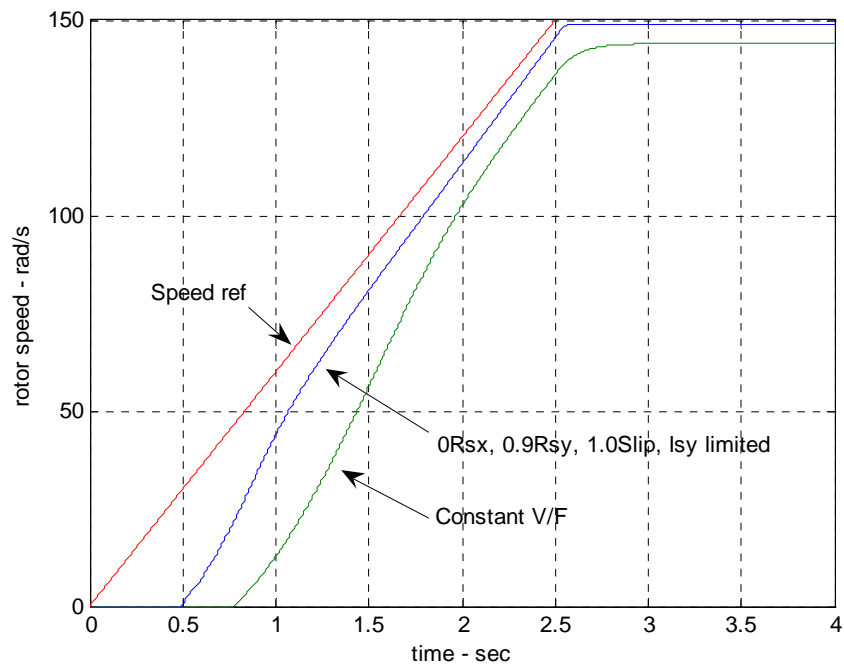


Figure 9.11 Simulation, Start-up, 80% Rated Torque, 150 rad/s

Table 9.4 Simulated Performance Criteria, Start-up, 80% Rated Torque, 150 rad/s

Simulation details							
Simulation time:		4 sec					
Speed reference:		Ramp 0–150 rad/s, acceleration of 60 rad/s ²					
Load torque:		Constant at 20 Nm					
Drive Performance							
Drive	Compensation Gain			Performance Criteria			
	R_{sx}	R_{sy}	Slip	Settling time S	Overshoot %	Steady State Error %	ITAE
Constant V/f	N/A	N/A	N/A	2.613	0.0	4.01	79.228
Experimental VSD with i_{sy} limiter	0	0.9	1.0	2.505	0.211	0.80	34.095

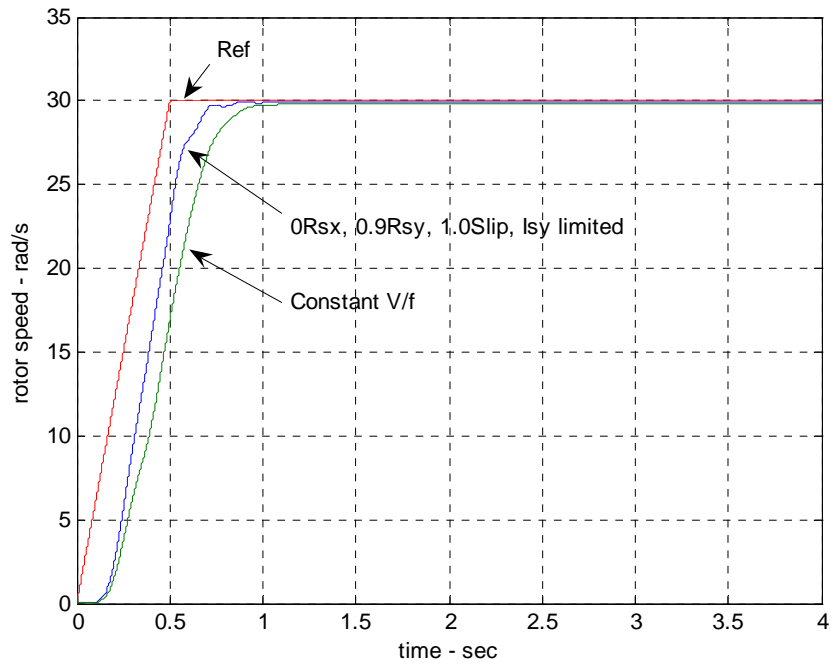


Figure 9.12 Simulation, Start-up, Zero Torque, 30 rad/s

Table 9.5 Simulated Performance Criteria, Start-up, Zero Torque, 30 rad/s

Simulation details							
Simulation time:		4 sec					
Speed reference:		Ramp 0–30 rad/s, acceleration of 60 rad/s ²					
Load torque:		Constant at 0 Nm					
Drive Performance							
Drive	Compensation Gain			Performance Criteria			
	R_{sx}	R_{sy}	Slip	Settling time S	Overshoot %	Steady State Error %	ITAE
Constant V/f	N/A	N/A	N/A	0.867	0.018	0.527	7.25
Experimental VSD with i_{sy} limiter	0	0.9	1.0	0.688	0.106	0.271	4.542

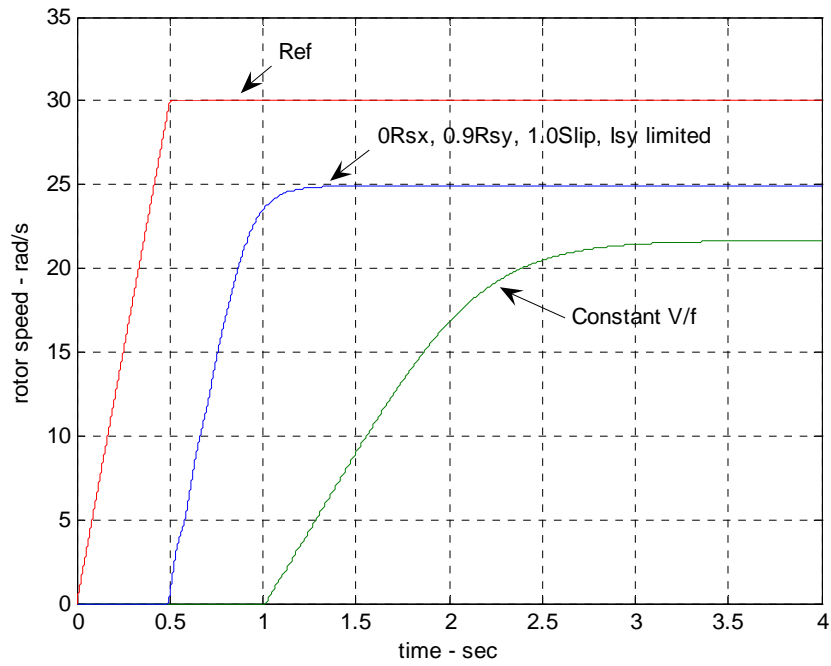


Figure 9.13 Simulation, Start-up, 80% Rated Torque, 30 rad/s

Table 9.6 Simulated Performance Criteria, Start-up, 80% Rated Torque, 30 rad/s

Simulation details							
Simulation time:		4 sec					
Speed reference:		Ramp 0–30 rad/s, acceleration of 60 rad/s ²					
Load torque:		Constant at 20 Nm					
Drive Performance							
Drive	Compensation Gain			Performance Criteria			
	R_{sx}	R_{sy}	Slip	Settling time S	Overshoot %	Steady State Error %	ITAE
Constant V/f	N/A	N/A	N/A	2.73	0.00	27.83	62.14
Experimental VSD with i_{sy} limiter	0	0.9	1.0	1.04	0.001	16.9	30.95

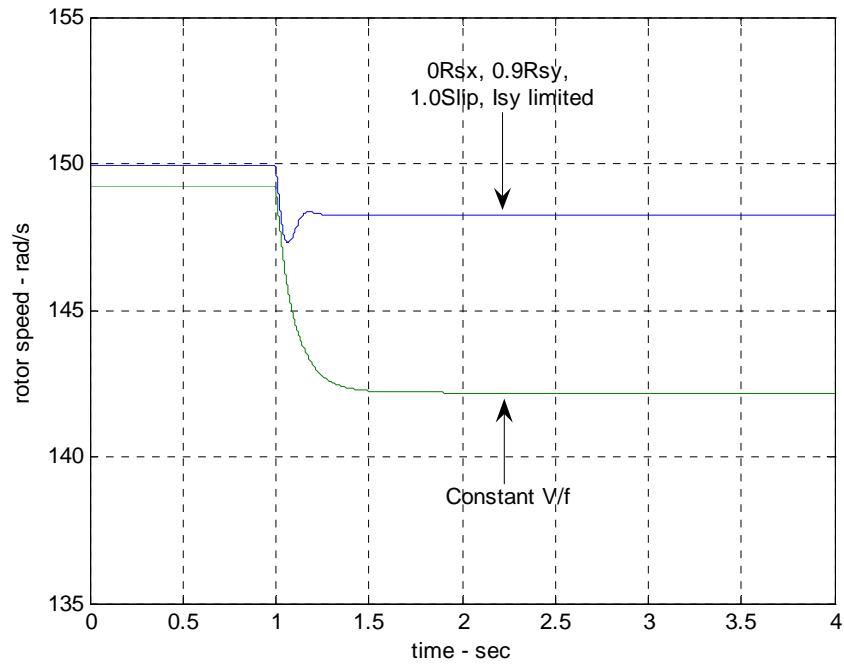


Figure 9.14 Simulation, Load Change, 0-100% Rated Torque, 150 rad/s

Table 9.7 Simulated Performance Criteria, Load Change 0-100% Rated Torque, 150 rad/s

Simulation details							
Simulation time:		4 sec					
Speed reference:		Constant 150 rad/s					
Load torque:		0 Nm initial, 26 Nm at t = 1					
Drive Performance							
Drive	Compensation Gain			Performance Criteria			
	R_{sx}	R_{sy}	Slip	Speed Change %	Overshoot %	Steady State Error %	ITAE
Constant V/f	N/A	N/A	N/A	4.71	0.00	5.21	23.517
Experimental VSD with i_{sy} limiter	0	0.9	1.0	1.12	0.66	1.16	5.32

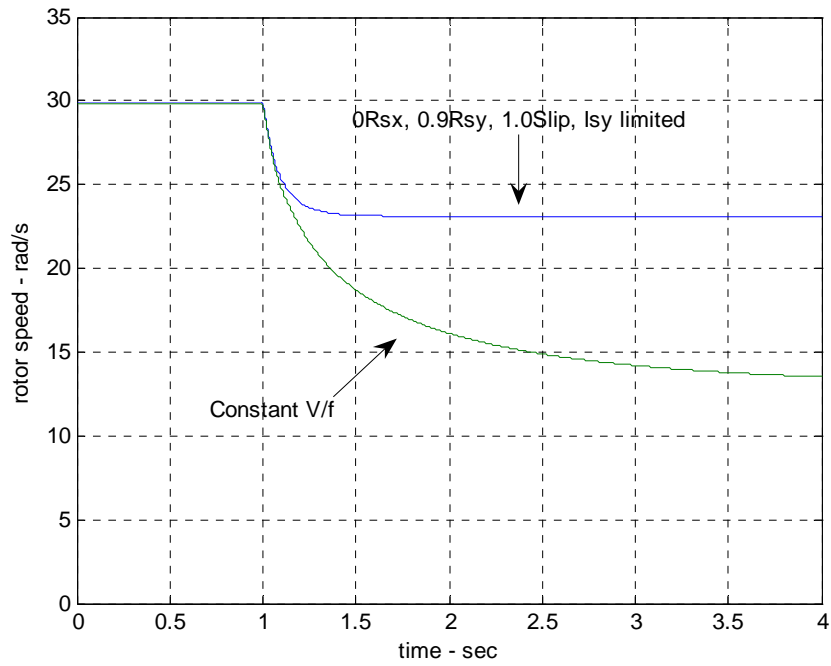


Figure 9.15 Simulation, Load Change, 0-100% Rated Torque, 30 rad/s

Table 9.8 Simulated Performance Criteria, Load Change 0-100% Rated Torque, 30 rad/s

Simulation details							
Simulation time:		4 sec					
Speed reference:		Constant 30 rad/s					
Load torque:		0 Nm initial, 26 Nm at t = 1					
Drive Performance							
Drive	Compensation Gain			Performance Criteria			
	R_{sx}	R_{sy}	Slip	Speed Change %	Overshoot %	Steady State Error %	ITAE
Constant V/f	N/A	N/A	N/A	54.69	0.00	54.9	41.59
Experimental VSD with i_{sy} limiter	0	0.9	1.0	22.7	0.00	22.9	20.1

9.5 Performance and Stability Evaluation

In the previous sections the theoretical stability limits of the experimental VSD have been determined and the performance of the VSD has been benchmarked against a standard constant V/f VSD for Simulink[®] simulations.

The stability limits determined in the previous sections are:

$$\tilde{R}_{sx} < R_s$$

$$\tilde{R}_{sy} < R_s - \beta\omega_{ms}$$

$$i_{syMax} = i_{sRated} \frac{\omega_{ms}}{\gamma}$$

where:

$$\gamma = \text{constant}$$

The above stability limits are theoretical limits and may change in a practical system even though simulations have verified them. In previous research performed by Fancis (1997) stator resistance voltage drop compensation had a theoretical limit of $1.0R_s$ but implementation of the system and testing indicated that the practical stability limit was $0.9R_s$. This practical limit was however achieved with equal compensation for R_{sx} and R_{sy} and did not consider torque limitation. Simulations for only R_{sy} compensation indicate that the stability limit is $1.5R_s$ with no i_{sy} limitation. With i_{sy} limitation this stability limit is $3R_s$ but a satisfactory performance is only obtained with compensation less than $1.7R_s$. Therefore it can be assumed that for only R_{sy} compensation the theoretical stability limit will guarantee stability and the system stability is less sensitive to R_s parameter setting. Practical testing is necessary to verify this.

Simulations for slip compensation with the theoretical stability limits indicate that slip compensation gain of 1.2 is the limit for satisfactory performance but the stability limit is a gain of 3.5. Therefore a maximum slip compensation gain of 1.0 will ensure stability and will provide a buffer for performance sensitivity to parameter setting.

The simulated performance of the experimental VSD is greatly improved on the standard constant V/f VSD as the speed error, speed regulation and settling times are greatly reduced. The operational speed range of the experimental VSD is also greater than the standard constant V/f VSD. The worst simulated performance criteria for the two VSDs are listed below in Table 9.9.

Table 9.9 Worst Performance Criteria from Performance Analysis

Performance criteria	Experimental VSD		Constant V/f VSD	
	Value	Condition	Value	Condition
Speed regulation	22.7 %	Load change 0-100% rated torque, 30 rad/s	54.69 %	Load change 0-100% rated torque, 30 rad/s
Speed error	22.9 %	Load change 0-100% rated torque, 30 rad/s	54.9 %	Load change 0-100% rated torque, 30 rad/s
Overshoot	0.752 %	Start-up, zero torque, 150rad/s	0.018 %	Start-up, zero torque, 30rad/s

As for the stability limits, the performance of the experimental VSD may vary from the simulated performance for a practical system. This variance is difficult to quantify but for a variance of 10% the performance of the experimental drive is still far greater than the standard constant V/f VSD.

From the performance simulations the experimental VSD would be suitable for applications where speed regulation is not critical but is desirable. Such applications may include pumps, fans and transport systems. For instance it is desirable to maintain the speed of human escalators constant so that comfort is maintained and entry and exit to the escalator is not cumbersome. In this application the experimental VSD could regulate speed with a maximum error of 1.16% about the rated motor speed for variations in loading on the escalator.

10. Conclusion

10.1 Achievement of Project Objectives

The aim and all of the specific objectives defined in the project specification have been achieved as described in the following.

A state space model for the standard three phase induction motor has been developed in chapter 3 with the state variables being the direct-axis and quadrature-axis currents. The state space equations of the model consist of 2 phase quantities that can represent a 3 phase induction motor with 3-2 phase transformations.

The state space model of the induction motor has been implemented in Simulink[®] in chapter 4. In this model all parameters are able to be set and variations in speed and load torque during operation can be simulated. This allows DOL start-up from rest and sudden application and removal of load to be simulated.

Verification of the Simulink[®] induction motor model was performed with physical testing as described in chapter 5. In this testing motor currents and rotor speeds were recorded for an induction motor which drives a DC generator. Recordings were performed for DOL start-up from rest and sudden application and removal of load with the motor initially operating at steady-state. The recordings were compared with simulations to verify the induction motor model.

An experimental AC variable speed drive that consists of stator resistance voltage drop compensation and slip compensation was developed in chapter 7 and implemented in Simulink[®] in chapter 8. The Simulink[®] model of the drive utilises the induction motor model as a function block to represent a 3 phase motor.

The theoretical stability limits of the experimental VSD are determined in chapter 9 for compensation and a wide range of operation. The effects of practical implementation and the practical stability limits are discussed.

10.2 Project Outcomes

The aim of this project is to implement a model for an AC variable speed drive for induction motors and to use this model to determine the limits of stability. This has been achieved and the performance of the drive has been benchmarked against a standard constant V/f VSD.

The experimental drive algorithm developed in this project is simple and can be implemented on low cost systems. It provides a simulated performance that has a better transient response and steady state error than standard constant V/f VSDs. The only parameters required for control are motor nameplate data and stator resistance. Therefore the drive could be easily commissioned by inexperienced persons as setup data is easily obtained from the motor and stator resistance can be measured using an initialisation program that uses DC injection to the stator.

In the stability and performance analysis of the experimental drive the effect of stator resistance compensation in each axis and slip compensation have been explored. It was discovered that stator resistance compensation in only the quadrature axis in the stator flux reference frame provided the best performance and reduced the sensitivity of stability to parameters. Stator resistance compensation limitation and torque limitation have also been developed which prevent instability and improve the performance of the drive.

10.3 Further Work

The operation of the experimental drive when implemented in a practical system will be affected by many factors that have not been considered in this project. Such factors are non-sinusoidal waveforms from inverters, discrete controls and current sensor lags. The effect of these factors is difficult to quantify and to analyse. Implementation of the experimental VSD on a test bench system is therefore required so that the accuracy of the stability limits and performance criteria in this project can be determined.

References

1. Francis C.J., & Zelaya De La Parra H., 1997, 'Stator Resistance Voltage-Drop Compensation for Open-Loop AC Drives', IEE Proc.-Electr.Power Appl., Vol.144, No.1, January 1997, pp. 21-26.
2. Munoz-Garcia A., Lipo T.A. & Novotny D.W., 1998, 'A New Induction Motor V/F Control Method Capable of High-Performance Regulation at Low Speed', IEEE Trans.Ind.Appl., vol.34. No.4, July/August 1998, pp 813-821
3. Blaschke F., 'The Principle of Field-Orientation as Applied to the New Transvektor Closed-Loop Control System for Rotating-Field Machines,' Siemens Review, No.34, 1972, pp 217-220
4. Xue Y., Xu X., Habetler T.G. & Divan D.M., 'A Low Cost Stator Orientated Voltage Source Variable Speed Drive', Conf. Rec IEEE-IAS Annu. Meeting. 1990, pp. 410-415
5. Koga K., Ueda R., & Sonoda T., 'Constitution of V/f Control for Reducing the Steady State Error to Zero in Induction Motor Drive System', Conf. Rec. IEEE- IAS Aunnu. Meeting, 1990, pp. 639-646
6. Jung J., Jeong G. & Kwon B., 'Stability Improvement of V/f Controlled Induction Motor Drive Systems by a Dynamic Current Compensator', IEEE Trans. Industrial Electronics, vol.51. No.4, August 2004, pp 930-933
7. Holtz J., 'Sensorless Control of Induction Motor Drives', Proceedings of the IEEE, vol.90. No.8, August 2002, pp1359-1394

Bibliography

1. Chiasson J., 'Modeling and High-Performance Control of Electric Machines', 2005, John Wiley & Sons, Inc, Hoboken, New Jersey.
2. Trzynadlowski A.M., 'The Field Orientation Principle in Control of Induction Motors', 1994, Kluwer Academic Publishers, USA.
3. Vas P., 'Vector Control of AC Machines', 1990, Oxford University Press, New York, USA.
4. Bose B., 'Power Electronics and AC Drives', 1986, Prentice-Hall, New Jersey, USA.
5. Lipo T.A. & Krause P.C., 1969, 'Stability Analysis of a Rectifier-Inverter Induction Motor Drive', IEEE Trans.Power.App.Syst, vol.PAS-88, January 1969, pp 55-66
6. 'Basics of AC Motors', n.d., Siemens Technical Training Program, Siemens Energy and Automation, USA, viewed 20 July 2006, <<http://www.sea.siemens.com/step>>

Appendix A – Project Specification

University of Southern Queensland

FACULTY OF ENGINEERING AND SURVEYING

ENG 4111/4112 Research Project **PROJECT SPECIFICATION**

FOR: **Andrew Rae**

TOPIC: Performance and Stability Analysis of an AC Variable Speed Drive

SUPERVISORS: Dr. Tony Ahfock

ENROLMENT: ENG4111 – S1, ONC, 2006
ENG4112 – S2, ONC, 2006

PROJECT AIM: This project seeks to implement a model for an AC variable speed drive for induction motors and to use this model to analyse the performance and stability of the drive.

PROGRAMME: Issue B, 6 September 2006

1. Develop a state space model for the standard three phase induction motor. State variables can be either direct-axis and quadrature-axis currents or direct-axis and quadrature-axis flux linkages or a combination of currents and flux linkages.
2. Implement the model in (1) using Simulink and simulate:
 - a. DOL start-up from rest.
 - b. Sudden application of mechanical load with the motor initially operating at steady-state speed on no-load.
3. Design and carry out physical tests to verify some of the predictions of step (2).
4. Develop a state-space model for an AC variable speed drive that consists of the induction motor model in (2), slip compensation and stator resistance voltage drop compensation.
5. Implement the model in (4) using Simulink and analyse the performance and stability of the drive.

AGREED:

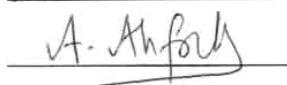
Student:



Date:

14/9/06

Supervisor:



Date:

14/9/06

Appendix B – Power Measurement for Testing

This appendix details power measurement using one instantaneous phase voltage and two instantaneous phase currents for balanced three phase conditions.

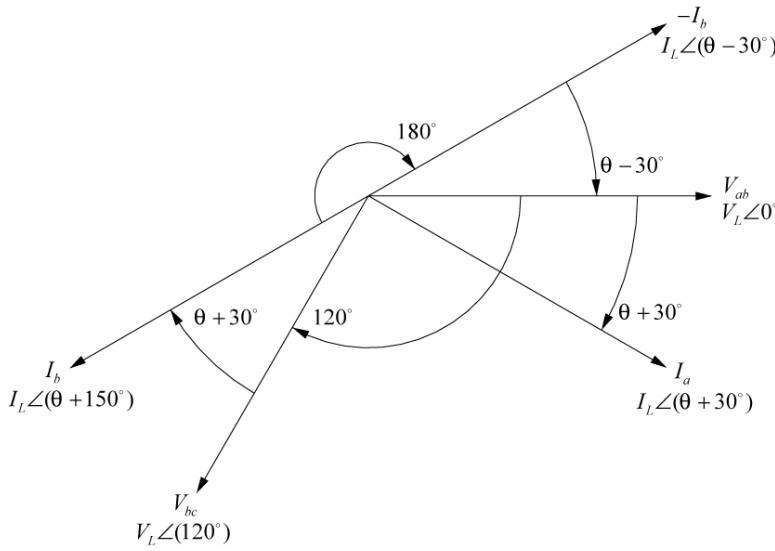


Figure B.1 Power Measurement Vector Diagram

$$\begin{aligned}
 \text{Power} &= \text{mean}(v_{ab}i_a) + \text{mean}(v_{ab}(-i_b)) \\
 &= I_L V_L \cos(30^\circ + \theta) + I_L V_L \cos(\theta - 30^\circ) \\
 &= I_L V_L \left[(\cos 30^\circ \cos \theta - \sin 30^\circ \sin \theta) + (\cos \theta \cos 30^\circ + \sin \theta \sin 30^\circ) \right] \\
 &= I_L V_L \left[2 \cos 30^\circ \cos \theta \right] \\
 &= I_L V_L \sqrt{3} \cos \theta
 \end{aligned} \tag{B.1}$$

where:

$$V_{ab} = V_L \angle 0^\circ \tag{B.2}$$

$$\begin{aligned}
 -I_b &= I_L \angle (150^\circ + \theta) \cdot 1 \angle (-180^\circ) \\
 &= I_L \angle (\theta - 30^\circ)
 \end{aligned} \tag{B.3}$$

using trigonometric identities:

$$\cos(\alpha + \beta) = \cos(\alpha)\cos(\beta) - \sin(\alpha)\sin(\beta) \quad (\text{B.4})$$

$$\cos(\alpha - \beta) = \cos(\alpha)\cos(\beta) + \sin(\alpha)\sin(\beta) \quad (\text{B.5})$$

Appendix C – Stability Analysis

Derivation of Closed Loop System Equations

The IM state space equations are represented by:

$$\dot{X} = AX + BU \quad (C.1)$$

The VSD control equations are:

$$\begin{bmatrix} u_{sx} \\ u_{sy} \end{bmatrix} = \begin{bmatrix} i_{sx} \tilde{R}_{sx} \\ i_{sy} (\tilde{R}_{sy} + \beta \omega_{ms}) + \alpha \omega_{ms} \end{bmatrix} \quad (C.2)$$

where:

$$\alpha = \frac{V_{so}}{\omega_{rated}} \quad \beta = \frac{S_{rated}}{I_{srated}} \frac{V_{so}}{\omega_{rated}}$$

To simplify analysis of the closed loop system the stator flux angular position is set to zero so that the stator and stator flux axes align. Therefore the voltages and currents in the two reference frames are equal and are:

$$\begin{bmatrix} u_{sd} \\ u_{sq} \end{bmatrix} = \begin{bmatrix} u_{sx} \\ u_{sy} \end{bmatrix} \quad (C.3)$$

$$\begin{bmatrix} i_{sd} \\ i_{sq} \end{bmatrix} = \begin{bmatrix} i_{sx} \\ i_{sy} \end{bmatrix} \quad (C.4)$$

At alignment of the two reference frames the VSD control equations are given by:

$$\begin{bmatrix} u_{sd} \\ u_{sq} \end{bmatrix} = \begin{bmatrix} i_{sx} \tilde{R}_{sx} \\ i_{sy} (\tilde{R}_{sy} + \beta \omega_{ms}) + \alpha \omega_{ms} \end{bmatrix} \quad (C.5)$$

The above can be expressed in terms of the stator currents by:

$$\begin{bmatrix} u_{sd} \\ u_{sq} \end{bmatrix} = \begin{bmatrix} \tilde{R}_{sx} & 0 \\ 0 & (\tilde{R}_{sy} + \beta\omega_{ms}) \end{bmatrix} \begin{bmatrix} i_{sd} \\ i_{sq} \end{bmatrix} + \begin{bmatrix} 0 \\ \alpha\omega_{ms} \end{bmatrix} \quad (C.6)$$

Extending the matrices above, the control equations can be expressed in terms of all the state variables such as:

$$\begin{bmatrix} u_{sd} \\ u_{sq} \end{bmatrix} = \begin{bmatrix} \tilde{R}_{sx} & 0 & 0 & 0 \\ 0 & (\tilde{R}_{sy} + \beta\omega_{ms}) & 0 & 0 \end{bmatrix} \begin{bmatrix} i_{sd} \\ i_{sq} \\ i_{rd} \\ i_{rq} \end{bmatrix} + \begin{bmatrix} 0 \\ \alpha\omega_{ms} \end{bmatrix} \quad (C.7)$$

The above control equations can be represented by the following state space system representation:

$$U = KX + U_{ref} \quad (C.8)$$

where:

$$K = \begin{bmatrix} \tilde{R}_{sx} & 0 & 0 & 0 \\ 0 & (\tilde{R}_{sy} + \beta\omega_{ms}) & 0 & 0 \end{bmatrix}$$

The complete closed loop state space model of the experimental VSD is now obtained by combining the IM and control equation state space representations such as:

$$\begin{aligned} \dot{X} &= AX + B(KX + U_{ref}) \\ &= A_c X + B_c U_{ref} \end{aligned} \quad (C.9)$$

where:

$$A_c = A + BK$$

The closed loop state matrix A_c is solved as follows:

$$\begin{aligned}
A_c &= \begin{bmatrix} -\frac{R_s}{\sigma L_s} & \frac{\omega_r L_m^2}{L_r \sigma L_s} & \frac{L_m R_r}{L_r \sigma L_s} & \frac{\omega_r L_m}{\sigma L_s} \\ -\frac{\omega_r L_m^2}{L_r \sigma L_s} & -\frac{R_s}{\sigma L_s} & -\frac{\omega_r L_m}{\sigma L_s} & \frac{L_m R_r}{L_r \sigma L_s} \\ \frac{L_m R_s}{L_r \sigma L_s} & -\frac{\omega_r L_m}{\sigma L_r} & -\frac{R_r}{\sigma L_r} & -\frac{\omega_r}{\sigma} \\ \frac{\omega_r L_m}{\sigma L_r} & \frac{L_m R_s}{L_r \sigma L_s} & \frac{\omega_r}{\sigma} & -\frac{R_r}{\sigma L_r} \end{bmatrix} + \begin{bmatrix} \frac{1}{\sigma L_s} & 0 \\ 0 & \frac{1}{\sigma L_s} \\ -\frac{L_m}{L_r \sigma L_s} & 0 \\ 0 & -\frac{L_m}{L_r \sigma L_s} \end{bmatrix} \begin{bmatrix} \tilde{R}_{sx} & 0 & 0 & 0 \\ 0 & (\tilde{R}_{sy} + \beta \omega_{ms}) & 0 & 0 \end{bmatrix} \\
&= \begin{bmatrix} -\frac{R_s}{\sigma L_s} & \frac{\omega_r L_m^2}{L_r \sigma L_s} & \frac{L_m R_r}{L_r \sigma L_s} & \frac{\omega_r L_m}{\sigma L_s} \\ -\frac{\omega_r L_m^2}{L_r \sigma L_s} & -\frac{R_s}{\sigma L_s} & -\frac{\omega_r L_m}{\sigma L_s} & \frac{L_m R_r}{L_r \sigma L_s} \\ \frac{L_m R_s}{L_r \sigma L_s} & -\frac{\omega_r L_m}{\sigma L_r} & -\frac{R_r}{\sigma L_r} & -\frac{\omega_r}{\sigma} \\ \frac{\omega_r L_m}{\sigma L_r} & \frac{L_m R_s}{L_r \sigma L_s} & \frac{\omega_r}{\sigma} & -\frac{R_r}{\sigma L_r} \end{bmatrix} + \begin{bmatrix} \frac{\tilde{R}_{sx}}{\sigma L_s} & 0 & 0 & 0 \\ 0 & \frac{(\tilde{R}_{sy} + \beta \omega_{ms})}{\sigma L_s} & 0 & 0 \\ -\frac{L_m \tilde{R}_{sx}}{L_r \sigma L_s} & 0 & 0 & 0 \\ 0 & -\frac{L_m (\tilde{R}_{sy} + \beta \omega_{ms})}{L_r \sigma L_s} & 0 & 0 \end{bmatrix} \\
&= \begin{bmatrix} \frac{\tilde{R}_{sx} - R_s}{\sigma L_s} & \frac{\omega_r L_m^2}{L_r \sigma L_s} & \frac{L_m R_r}{L_r \sigma L_s} & \frac{\omega_r L_m}{\sigma L_s} \\ -\frac{\omega_r L_m^2}{L_r \sigma L_s} & \frac{\tilde{R}_{sy} - R_s + \beta \omega_{ms}}{\sigma L_s} & -\frac{\omega_r L_m}{\sigma L_s} & \frac{L_m R_r}{L_r \sigma L_s} \\ \frac{L_m (R_s - \tilde{R}_{sx})}{L_r \sigma L_s} & -\frac{\omega_r L_m}{\sigma L_r} & -\frac{R_r}{\sigma L_r} & -\frac{\omega_r}{\sigma} \\ \frac{\omega_r L_m}{\sigma L_r} & \frac{L_m (R_s - \tilde{R}_{sy} - \beta \omega_{ms})}{L_r \sigma L_s} & \frac{\omega_r}{\sigma} & -\frac{R_r}{\sigma L_r} \end{bmatrix}
\end{aligned} \tag{C.10}$$

Derivation of Small Signal Closed Loop System Equations

The complete closed loop state space equations of the experimental VSD are obtained by combining the IM and control state space representations as performed in the previous section to obtain:

$$\begin{aligned}\dot{X} &= AX + B(KX + U_{ref}) \\ &= A_c X + B_c U_{ref}\end{aligned}\tag{C.11}$$

The above state space system can be expanded to a 5th order system to include the rotor speed as a state variable. This is achieved by using the IM torque equation (3.23) and the IM rotor speed equation (3.24) to add a 5th row to the state space equations. The state space equations then describe the electrodynamics of the VSD and IM. The new 5th row of the state space system is:

$$\frac{d\omega_r}{dt} = \frac{n_p}{J} \left(n_p L_m \frac{2}{3} (i_{sq} i_{rd} - i_{sd} i_{rq}) - f \frac{\omega_r}{n_p} - T_L \right)\tag{C.12}$$

The resultant state space equation is:

$$\frac{d}{dt} \begin{bmatrix} i_{sd} \\ i_{sq} \\ i_{rd} \\ i_{rq} \\ \omega_r \end{bmatrix} = \begin{bmatrix} \frac{\tilde{R}_{sx} - R_s}{\sigma L_s} & \frac{\omega_r L_m^2}{L_r \sigma L_s} & \frac{L_m R_r}{L_r \sigma L_s} & \frac{\omega_r L_m}{\sigma L_s} & 0 \\ -\frac{\omega_r L_m^2}{L_r \sigma L_s} & \frac{\tilde{R}_{sy} - R_s + \beta \omega_{ms}}{\sigma L_s} & -\frac{\omega_r L_m}{\sigma L_s} & \frac{L_m R_r}{L_r \sigma L_s} & 0 \\ \frac{L_m (R_s - \tilde{R}_{sx})}{L_r \sigma L_s} & -\frac{\omega_r L_m}{\sigma L_r} & -\frac{R_r}{\sigma L_r} & -\frac{\omega_r}{\sigma} & 0 \\ \frac{\omega_r L_m}{\sigma L_r} & \frac{L_m (R_s - \tilde{R}_{sy} - \beta \omega_{ms})}{L_r \sigma L_s} & \frac{\omega_r}{\sigma} & -\frac{R_r}{\sigma L_r} & 0 \\ 0 & 0 & \frac{2n_p^2 L_m i_{sq}}{3J} & -\frac{2n_p^2 L_m i_{sd}}{3J} & -\frac{f}{J} \end{bmatrix} \begin{bmatrix} i_{sd} \\ i_{sq} \\ i_{rd} \\ i_{rq} \\ \omega_r \end{bmatrix} + \begin{bmatrix} \frac{1}{\sigma L_s} & 0 & 0 \\ 0 & \frac{1}{\sigma L_s} & 0 \\ -\frac{L_m}{L_r \sigma L_s} & 0 & 0 \\ 0 & -\frac{L_m}{L_r \sigma L_s} & 0 \\ 0 & 0 & -\frac{n_p}{J} \end{bmatrix} \begin{bmatrix} 0 \\ \alpha \omega_{ms} \\ T_L \end{bmatrix}\tag{C.13}$$

The above 5th order state space equation is non-linear and the stability of the system can not be easily accessed. However the system can approximated as a linear system for small signal displacements about a steady state condition. Linear system control theory can then be applied to analyse the stability of the small signal linear approximation.

Stability of the small signal linear approximation implies a region of stability in the non-linear system.

To develop the small signal displacement system the state variables and the control inputs are formed from a fixed term and a small displacement term. The state variables and the control inputs are:

$$\begin{bmatrix} i_{sd} \\ i_{sq} \\ i_{rd} \\ i_{rq} \\ \omega_r \end{bmatrix} = \begin{bmatrix} *i_{sd} + \Delta i_{sd} \\ *i_{sq} + \Delta i_{sq} \\ *i_{rd} + \Delta i_{rd} \\ *i_{rq} + \Delta i_{rq} \\ *\omega_r + \Delta \omega_r \end{bmatrix} \quad \begin{bmatrix} \omega_{ms} \\ T_L \end{bmatrix} = \begin{bmatrix} *\omega_{ms} + \Delta \omega_{ms} \\ *T_L + \Delta T_L \end{bmatrix}$$

Application of the above state space variables and control inputs to the closed loop state space equations for the VSD produces the following:

$$\begin{aligned} \frac{d}{dt} \begin{bmatrix} *i_{sd} + \Delta i_{sd} \\ *i_{sq} + \Delta i_{sq} \\ *i_{rd} + \Delta i_{rd} \\ *i_{rq} + \Delta i_{rq} \\ *\omega_r + \Delta \omega_r \end{bmatrix} &= \begin{bmatrix} \frac{\tilde{R}_{sx} - R_s}{\sigma L_s} & \frac{(*\omega_r + \Delta \omega_r)L_m^2}{L_r \sigma L_s} & \frac{L_m R_r}{L_r \sigma L_s} & \frac{(*\omega_r + \Delta \omega_r)L_m}{\sigma L_s} & 0 \\ -\frac{(*\omega_r + \Delta \omega_r)L_m^2}{L_r \sigma L_s} & \frac{\tilde{R}_{sy} - R_s + \beta(*\omega_{ms} + \Delta \omega_{ms})}{\sigma L_s} & -\frac{(*\omega_r + \Delta \omega_r)L_m}{\sigma L_s} & \frac{L_m R_r}{L_r \sigma L_s} & 0 \\ \frac{L_m(R_s - \tilde{R}_{sx})}{L_r \sigma L_s} & -\frac{(*\omega_r + \Delta \omega_r)L_m}{\sigma L_r} & -\frac{R_r}{\sigma L_r} & -\frac{(*\omega_r + \Delta \omega_r)}{\sigma} & 0 \\ \frac{(*\omega_r + \Delta \omega_r)L_m}{\sigma L_r} & \frac{L_m(R_s - \tilde{R}_{sy} - \beta(*\omega_{ms} + \Delta \omega_{ms}))}{L_r \sigma L_s} & \frac{(*\omega_r + \Delta \omega_r)}{\sigma} & -\frac{R_r}{\sigma L_r} & 0 \\ 0 & 0 & \frac{2n_p^2 L_m (*i_{sq} + \Delta i_{sq})}{3J} & -\frac{2n_p^2 L_m (*i_{sd} + \Delta i_{sd})}{3J} & -\frac{f}{J} \end{bmatrix} \begin{bmatrix} *i_{sd} + \Delta i_{sd} \\ *i_{sq} + \Delta i_{sq} \\ *i_{rd} + \Delta i_{rd} \\ *i_{rq} + \Delta i_{rq} \\ *\omega_r + \Delta \omega_r \end{bmatrix} \\ &+ \begin{bmatrix} \frac{1}{\sigma L_s} & 0 & 0 \\ 0 & \frac{1}{\sigma L_s} & 0 \\ -\frac{L_m}{L_r \sigma L_s} & 0 & 0 \\ 0 & -\frac{L_m}{L_r \sigma L_s} & 0 \\ 0 & 0 & -\frac{n_p}{J} \end{bmatrix} \begin{bmatrix} 0 \\ \alpha(*\omega_{ms} + \Delta \omega_{ms}) \\ *T_L + \Delta T_L \end{bmatrix} \end{aligned} \quad (C.14)$$

The state variables and control inputs are present in the state matrix. Rearranging the above system to remove the variables from the state and inputs matrices allows the system to be analysed with linear system control theory.

The product of the state matrix and state variables can be expanded to:

$$\begin{aligned}
 A_c X = & \begin{bmatrix} \frac{\tilde{R}_{sx} - R_s}{\sigma L_s} & \frac{(*\omega_r + \Delta\omega_r)L_m^2}{L_r \sigma L_s} & \frac{L_m R_r}{L_r \sigma L_s} & \frac{(*\omega_r + \Delta\omega_r)L_m}{\sigma L_s} & 0 \\ -\frac{(*\omega_r + \Delta\omega_r)L_m^2}{L_r \sigma L_s} & \frac{\tilde{R}_{sy} - R_s + \beta(*\omega_{ms} + \Delta\omega_{ms})}{\sigma L_s} & -\frac{(*\omega_r + \Delta\omega_r)L_m}{\sigma L_s} & \frac{L_m R_r}{L_r \sigma L_s} & 0 \\ \frac{L_m (R_s - \tilde{R}_{sx})}{L_r \sigma L_s} & -\frac{(*\omega_r + \Delta\omega_r)L_m}{\sigma L_r} & -\frac{R_r}{\sigma L_r} & -\frac{(*\omega_r + \Delta\omega_r)}{\sigma} & 0 \\ \frac{(*\omega_r + \Delta\omega_r)L_m}{\sigma L_r} & \frac{L_m (R_s - \tilde{R}_{sy} - \beta(*\omega_{ms} + \Delta\omega_{ms}))}{L_r \sigma L_s} & \frac{(*\omega_r + \Delta\omega_r)}{\sigma} & -\frac{R_r}{\sigma L_r} & 0 \\ 0 & 0 & \frac{2n_p^2 L_m (*i_{sq} + \Delta i_{sq})}{3J} & -\frac{2n_p^2 L_m (*i_{sd} + \Delta i_{sd})}{3J} & -\frac{f}{J} \end{bmatrix} \begin{bmatrix} *i_{sd} \\ *i_{sq} \\ *i_{rd} \\ *i_{rq} \\ *\omega_r \end{bmatrix} \\
 + & \begin{bmatrix} \frac{\tilde{R}_{sx} - R_s}{\sigma L_s} & \frac{(*\omega_r + \Delta\omega_r)L_m^2}{L_r \sigma L_s} & \frac{L_m R_r}{L_r \sigma L_s} & \frac{(*\omega_r + \Delta\omega_r)L_m}{\sigma L_s} & 0 \\ -\frac{(*\omega_r + \Delta\omega_r)L_m^2}{L_r \sigma L_s} & \frac{\tilde{R}_{sy} - R_s + \beta(*\omega_{ms} + \Delta\omega_{ms})}{\sigma L_s} & -\frac{(*\omega_r + \Delta\omega_r)L_m}{\sigma L_s} & \frac{L_m R_r}{L_r \sigma L_s} & 0 \\ \frac{L_m (R_s - \tilde{R}_{sx})}{L_r \sigma L_s} & -\frac{(*\omega_r + \Delta\omega_r)L_m}{\sigma L_r} & -\frac{R_r}{\sigma L_r} & -\frac{(*\omega_r + \Delta\omega_r)}{\sigma} & 0 \\ \frac{(*\omega_r + \Delta\omega_r)L_m}{\sigma L_r} & \frac{L_m (R_s - \tilde{R}_{sy} - \beta(*\omega_{ms} + \Delta\omega_{ms}))}{L_r \sigma L_s} & \frac{(*\omega_r + \Delta\omega_r)}{\sigma} & -\frac{R_r}{\sigma L_r} & 0 \\ 0 & 0 & \frac{2n_p^2 L_m (*i_{sq} + \Delta i_{sq})}{3J} & -\frac{2n_p^2 L_m (*i_{sd} + \Delta i_{sd})}{3J} & -\frac{f}{J} \end{bmatrix} \begin{bmatrix} \Delta i_{sd} \\ \Delta i_{sq} \\ \Delta i_{rd} \\ \Delta i_{rq} \\ \Delta \omega_r \end{bmatrix}
 \end{aligned} \tag{C.15}$$

By separating the constant and small signal displacement terms and neglecting the products of the small signal displacements the above can be further expanded to produce:

$$\begin{aligned}
A_c X = & \begin{bmatrix} \frac{\tilde{R}_{sx} - R_s}{\sigma L_s} & \frac{* \omega_r L_m^2}{L_r \sigma L_s} & \frac{L_m R_r}{L_r \sigma L_s} & \frac{* \omega_r L_m}{\sigma L_s} & 0 \\ \frac{* \omega_r L_m^2}{L_r \sigma L_s} & \frac{\tilde{R}_{sy} - R_s + \beta * \omega_{ms}}{\sigma L_s} & -\frac{* \omega_r L_m}{\sigma L_s} & \frac{L_m R_r}{L_r \sigma L_s} & 0 \\ \frac{L_m (R_s - \tilde{R}_{sx})}{L_r \sigma L_s} & -\frac{* \omega_r L_m}{\sigma L_r} & -\frac{R_r}{\sigma L_r} & -\frac{* \omega_r}{\sigma} & 0 \\ \frac{* \omega_r L_m}{\sigma L_r} & \frac{L_m (R_s - \tilde{R}_{sy} - \beta * \omega_{ms})}{L_r \sigma L_s} & \frac{* \omega_r}{\sigma} & -\frac{R_r}{\sigma L_r} & 0 \\ 0 & 0 & \frac{2n_p^2 L_m * i_{sq}}{3J} & -\frac{2n_p^2 L_m * i_{sd}}{3J} & -\frac{f}{J} \end{bmatrix} \begin{bmatrix} * i_{sd} \\ * i_{sq} \\ * i_{rd} \\ * i_{rq} \\ * \omega_r \end{bmatrix} \\
+ & \begin{bmatrix} 0 & 0 & 0 & 0 & \frac{* i_{sq} L_m^2}{L_r \sigma L_s} + \frac{* i_{rq} L_m}{\sigma L_s} \\ 0 & 0 & 0 & 0 & -\frac{* i_{sd} L_m^2}{L_r \sigma L_s} - \frac{* i_{rd} L_m}{\sigma L_s} \\ 0 & 0 & 0 & 0 & -\frac{* i_{sq} L_m}{\sigma L_r} - \frac{* i_{rq}}{\sigma} \\ 0 & 0 & 0 & 0 & \frac{* i_{sd} L_m}{\sigma L_r} + \frac{* i_{rd}}{\sigma} \\ -\frac{* i_{rq} 2n_p^2 L_m}{3J} & \frac{* i_{rd} 2n_p^2 L_m}{3J} & 0 & 0 & 0 \end{bmatrix} \begin{bmatrix} \Delta i_{sd} \\ \Delta i_{sq} \\ \Delta i_{rd} \\ \Delta i_{rq} \\ \Delta \omega_r \end{bmatrix} + \begin{bmatrix} 0 \\ \frac{* i_{sq} \beta}{L_r \sigma L_s} \\ 0 \\ -\frac{* i_{sq} L_m \beta}{L_r \sigma L_s} \\ 0 \end{bmatrix} \Delta \omega_{ms} \\
+ & \begin{bmatrix} \frac{\tilde{R}_{sx} - R_s}{\sigma L_s} & \frac{* \omega_r L_m^2}{L_r \sigma L_s} & \frac{L_m R_r}{L_r \sigma L_s} & \frac{* \omega_r L_m}{\sigma L_s} & 0 \\ \frac{* \omega_r L_m^2}{L_r \sigma L_s} & \frac{\tilde{R}_{sy} - R_s + \beta * \omega_{ms}}{\sigma L_s} & -\frac{* \omega_r L_m}{\sigma L_s} & \frac{L_m R_r}{L_r \sigma L_s} & 0 \\ \frac{L_m (R_s - \tilde{R}_{sx})}{L_r \sigma L_s} & -\frac{* \omega_r L_m}{\sigma L_r} & -\frac{R_r}{\sigma L_r} & -\frac{* \omega_r}{\sigma} & 0 \\ \frac{* \omega_r L_m}{\sigma L_r} & \frac{L_m (R_s - \tilde{R}_{sy} - \beta * \omega_{ms})}{L_r \sigma L_s} & \frac{* \omega_r}{\sigma} & -\frac{R_r}{\sigma L_r} & 0 \\ 0 & 0 & \frac{2n_p^2 L_m * i_{sq}}{3J} & -\frac{2n_p^2 L_m * i_{sd}}{3J} & -\frac{f}{J} \end{bmatrix} \begin{bmatrix} \Delta i_{sd} \\ \Delta i_{sq} \\ \Delta i_{rd} \\ \Delta i_{rq} \\ \Delta \omega_r \end{bmatrix}
\end{aligned} \tag{C.16}$$

The 1st matrix in the above is a constant and the 3rd matrix is a product of the small signal control inputs. The 2nd and 4th matrices are products of the small signal state variables and are combined to form the small signal displacement state matrix.

The small signal displacement state matrix is:

$$A_{c\Delta} = \begin{bmatrix} \frac{\tilde{R}_{sx} - R_s}{\sigma L_s} & \frac{* \omega_r L_m^2}{L_r \sigma L_s} & \frac{L_m R_r}{L_r \sigma L_s} & \frac{* \omega_r L_m}{\sigma L_s} & \frac{* i_{sq} L_m^2}{L_r \sigma L_s} + \frac{* i_{rq} L_m}{\sigma L_s} \\ -\frac{* \omega_r L_m^2}{L_r \sigma L_s} & \frac{\tilde{R}_{sy} - R_s + \beta * \omega_{ms}}{\sigma L_s} & -\frac{* \omega_r L_m}{\sigma L_s} & \frac{L_m R_r}{L_r \sigma L_s} & -\frac{* i_{sd} L_m^2}{L_r \sigma L_s} - \frac{* i_{rd} L_m}{\sigma L_s} \\ \frac{L_m (R_s - \tilde{R}_{sx})}{L_r \sigma L_s} & -\frac{* \omega_r L_m}{\sigma L_r} & -\frac{R_r}{\sigma L_r} & -\frac{* \omega_r}{\sigma} & -\frac{* i_{sq} L_m}{\sigma L_r} - \frac{* i_{rq}}{\sigma} \\ \frac{* \omega_r L_m}{\sigma L_r} & \frac{L_m (R_s - \tilde{R}_{sy} - \beta * \omega_{ms})}{L_r \sigma L_s} & \frac{* \omega_r}{\sigma} & -\frac{R_r}{\sigma L_r} & \frac{* i_{sd} L_m}{\sigma L_r} + \frac{* i_{rd}}{\sigma} \\ -\frac{* i_{rq} 2n_p^2 L_m}{3J} & \frac{* i_{rd} 2n_p^2 L_m}{3J} & \frac{* i_{sq} 2n_p^2 L_m}{3J} & -\frac{* i_{sd} 2n_p^2 L_m}{3J} & -\frac{f}{J} \end{bmatrix} \quad (C.17)$$

From the closed loop system the product of the control input matrix and the control input variables is:

$$B_c U_{ref} = \begin{bmatrix} \frac{1}{\sigma L_s} & 0 & 0 \\ 0 & \frac{1}{\sigma L_s} & 0 \\ -\frac{L_m}{L_r \sigma L_s} & 0 & 0 \\ 0 & -\frac{L_m}{L_r \sigma L_s} & 0 \\ 0 & 0 & -\frac{n_p}{J} \end{bmatrix} \begin{bmatrix} 0 \\ \alpha(*\omega_{ms} + \Delta\omega_{ms}) \\ *T_L + \Delta T_L \end{bmatrix} \quad (C.18)$$

Combination of the small signal control inputs from above and from the state matrix produces the following:

$$\begin{aligned}
B_{c\Delta} U_{ref\Delta} &= \begin{bmatrix} \frac{1}{\sigma L_s} & 0 & 0 \\ 0 & \frac{1}{\sigma L_s} & 0 \\ -\frac{L_m}{L_r \sigma L_s} & 0 & 0 \\ 0 & -\frac{L_m}{L_r \sigma L_s} & 0 \\ 0 & 0 & -\frac{n_p}{J} \end{bmatrix} \begin{bmatrix} 0 \\ \alpha \Delta \omega_{ms} \\ \Delta T_L \end{bmatrix} + \begin{bmatrix} 0 \\ \frac{*i_{sq} \beta}{L_r \sigma L_s} \\ 0 \\ -\frac{*i_{sq} L_m \beta}{L_r \sigma L_s} \\ 0 \end{bmatrix} \Delta \omega_{ms} \\
&= \begin{bmatrix} 0 & 0 \\ \frac{\alpha}{\sigma L_s} + \frac{*i_{sq} \alpha}{L_r \sigma L_s} & 0 \\ 0 & 0 \\ -\frac{\alpha L_m}{L_r \sigma L_s} - \frac{*i_{sq} L_m \alpha}{L_r \sigma L_s} & 0 \\ 0 & -\frac{n_p}{J} \end{bmatrix} \begin{bmatrix} \Delta \omega_{ms} \\ \Delta T_L \end{bmatrix}
\end{aligned}
\tag{C.19}$$

To form the complete small signal state space equation all terms that are not products of small signal displacements are eliminated as they are constants and do not contribute to displacements about the steady state condition. Therefore the state variables and control inputs for the small signal displacement analysis are the small signal displacements. These small signal displacements, the small signal state matrix and the small signal input matrix form the small signal displacement state space equation which is given by:

$$\begin{aligned}
\frac{d}{dt} \begin{bmatrix} \Delta i_{sd} \\ \Delta i_{sq} \\ \Delta i_{rd} \\ \Delta i_{rq} \\ \Delta \omega_r \end{bmatrix} = & \begin{bmatrix} \frac{\tilde{R}_{sx} - R_s}{\sigma L_s} & \frac{* \omega_r L_m^2}{L_r \sigma L_s} & \frac{L_m R_r}{L_r \sigma L_s} & \frac{* \omega_r L_m}{\sigma L_s} & \frac{* i_{sq} L_m^2}{L_r \sigma L_s} + \frac{* i_{rq} L_m}{\sigma L_s} \\ -\frac{* \omega_r L_m^2}{L_r \sigma L_s} & \frac{\tilde{R}_{sy} - R_s + \beta * \omega_{ms}}{\sigma L_s} & -\frac{* \omega_r L_m}{\sigma L_s} & \frac{L_m R_r}{L_r \sigma L_s} & -\frac{* i_{sd} L_m^2}{L_r \sigma L_s} - \frac{* i_{rd} L_m}{\sigma L_s} \\ \frac{L_m (R_s - \tilde{R}_{sx})}{L_r \sigma L_s} & -\frac{* \omega_r L_m}{\sigma L_r} & -\frac{R_r}{\sigma L_r} & -\frac{* \omega_r}{\sigma} & -\frac{* i_{sq} L_m}{\sigma L_r} - \frac{* i_{rq}}{\sigma} \\ \frac{* \omega_r L_m}{\sigma L_r} & \frac{L_m (R_s - \tilde{R}_{sy} - \beta * \omega_{ms})}{L_r \sigma L_s} & \frac{* \omega_r}{\sigma} & -\frac{R_r}{\sigma L_r} & \frac{* i_{sd} L_m}{\sigma L_r} + \frac{* i_{rd}}{\sigma} \\ -\frac{* i_{rq} 2n_p^2 L_m}{3J} & \frac{* i_{rd} 2n_p^2 L_m}{3J} & \frac{* i_{sq} 2n_p^2 L_m}{3J} & -\frac{* i_{sd} 2n_p^2 L_m}{3J} & -\frac{f}{J} \end{bmatrix} \begin{bmatrix} \Delta i_{sd} \\ \Delta i_{sq} \\ \Delta i_{rd} \\ \Delta i_{rq} \\ \Delta \omega_r \end{bmatrix} \\
+ & \begin{bmatrix} 0 & 0 \\ \frac{\alpha}{\sigma L_s} + \frac{* i_{sq} \alpha}{L_r \sigma L_s} & 0 \\ 0 & 0 \\ -\frac{\alpha L_m}{L_r \sigma L_s} - \frac{* i_{sq} L_m \alpha}{L_r \sigma L_s} & 0 \\ 0 & -\frac{n_p}{J} \end{bmatrix} \begin{bmatrix} \Delta \omega_{ms} \\ \Delta T_L \end{bmatrix}
\end{aligned} \tag{C.20}$$

The above small signal displacement state space system is represented by:

$$\dot{X}_\Delta = A_{c\Delta} X_\Delta + B_{c\Delta} U_{ref\Delta} \tag{C.21}$$

The small signal rotor speed can be set as the output of a transfer function of the small signal inputs load torque and speed set point by using:

$$\Delta \omega_r = Y_\Delta = C_\Delta X_\Delta \tag{C.22}$$

$$\Delta \omega_r = Y_\Delta = C_\Delta (sI - A_{c\Delta})^{-1} B_{c\Delta} U_{ref\Delta} \tag{C.23}$$

By setting one of the small signal inputs to zero a transfer function of two variables can be achieved as given below. These equations allow the stability of the system to be analysed for changes in speed set point or load torque.

$$\frac{\Delta \omega_r}{\Delta \omega_{ms}} = C_\Delta (sI - A_{c\Delta})^{-1} B_{c\Delta} \quad \text{for: } \Delta T_L = 0 \tag{C.24}$$

$$\frac{\Delta \omega_r}{\Delta T_L} = C_\Delta (sI - A_{c\Delta})^{-1} B_{c\Delta} \quad \text{for: } \Delta \omega_{ms} = 0 \tag{C.25}$$

The stability of the small signal displacement state space system can now be analysed about a steady state condition using linear control system theory. The eigenvalue solutions for the following will be the poles of the system.

$$\det(sI - A_{c\Delta}) = 0 \tag{C.26}$$

Appendix D – Matlab[®] Function for Linear Stability Analysis

```
function proj_ss_stability(scg)
```

```
% Syntax:      <prog_ss_stability(scg)>
% Written by:   Andrew Rae for Research Project
% Description:  Function file for calculating and plotting closed system
%              poles for the experimental drive control at steady state speed.
% Inputs:       Nil
% Inputs:       scg = slip compensation gain
% Outputs:      Root locus plot of poles
% Notes:        Stator flux angular position is zero (aligns d axis)
```

```
%Induction motor parameters
Rs=1.749;      %stator resistance - ohms
Rr=1.544;      %rotor resistance - ohms
Lm=0.246;      %stator/rotor mutual inductance - henrys
Ls=0.254;      %stator leakage inductance - henrys
Lr=0.254;      %rotor leakage inductance - henrys
rho=1-Lm^2/(Lr*Ls); %leakage parameter
np=2;          %number of pole pairs
Vrated=240;    %rated phase voltage - V
Irated=8.1;     %rated current - A
RPMrated=1420; %rated speed - RPM
```

```
%Control parameters
Iso=sqrt(2)*1.5*Irated; %2 phase rated current
Vso=sqrt(2)*1.5*240-Iso*Rs; %2 phase flux voltage
wrated=RPMrated/60*2*pi; %2 phase rated speed
Srated=(1500-RPM)/1500; %rated slip
alpha=Vso/(np*wrated); %constant v/f coeff
beta=Vso/(np*wrated)*Srated/Iso %Slip compensation coeff
beta=beta*scg;
```

```
figure(3), grid, hold %Set graph for plot
j=0; %indice for Rsc calculation
for e=0.7:0.1:1.2 %for each Rs gain
    j=j+1;
    i=0; %indice for speed calculation
    for wr=10:20:380 %for rotor speeds
        i=i+1;
        A=[-Rs/(rho*Ls), wr*Lm^2/(Lr*rho*Ls), Lm*Rr/(Lr*rho*Ls), wr*Lm/(rho*Ls);...
            -wr*Lm^2/(Lr*rho*Ls), -Rs/(rho*Ls), -wr*Lm/(rho*Ls), Lm*Rr/(Lr*rho*Ls);...
            Lm*Rs/(Lr*rho*Ls), -wr*Lm/(rho*Lr), -Rr/(rho*Lr), -wr/rho;...
            wr*Lm/(rho*Lr), Lm*Rs/(Lr*rho*Ls), wr/rho, -Rr/(rho*Lr)];
        Rsy=e*Rs;
        Rsx=e*Rs;
        K=[Rsx, 0, 0, 0; 0, (Rsy+beta*wr), 0, 0];
        B=[1/(rho*Ls), 0; 0, 1/(rho*Ls); -Lm/(Lr*rho*Ls), 0; 0, -Lm/(Lr*rho*Ls)];
        Ac=A+B*K; %closed loop matrix
        ev=eig(Ac); %get poles
        poles(i,:)=ev'; %store poles in rows
    end
    poles1(:,j)=poles(:,1);
    poles2(:,j)=poles(:,2);
    poles3(:,j)=poles(:,3);
    poles4(:,j)=poles(:,4);
```

```
%plot poles
figure(3)
plot(poles1,'+', %plot(poles1)
plot(poles2,'+', %plot(poles2)
plot(poles3,'+', %plot(poles3)
plot(poles4,'+', %plot(poles4)
end
%end of file
```

Appendix E – Matlab[®] Function for Small Signal Stability Analysis

function smallsigstab

```
%Syntax:      <[speed,inertia,torque]=smallsigstab>
%Written by:  Andrew Rae for Research Project
%Description: Solving stability of experimental VSD with small signal
%             analysis
%Inputs:      nil
%Outputs:     plots of root locus and unstable pole locations
%Notes:       Stator flux angular position is zero (aligns d axis)

%define simulation constants
dt=0.0001; %simulation time step
time=4;

%***** define constants *****
% induction motor parameters
Rs=1.749; %stator resistance - ohms
Rr=1.544; %rotor resistance - ohms
Lm=0.246; %stator/rotor mutual inductance - henrys
Ls=0.254; %stator leakage inductance - henrys
Lr=0.254; %rotor leakage inductance - henrys
np=2; %number of pole pairs
Vp=240; %rated phase voltage - V
Irated=8.1; %rated current - A
RPM=1420; %rated speed - RPM
f=0.022; %friction coeff
J=0.3; %moment of inertia -kg.m^2
Trated=26; %rated torque - N.m

% control parameters for equivalent 2 phase motor
wrated=RPM/60*2*pi*np; %2 phase rated speed - rad/s
Srated=(1500/np*2-RPM)/1500;%rated slip
rho=1-Lm^2/(Lr*Ls); %leakage parameter
Iso=sqrt(2)*1.5*Irated; %2 phase rated current
Vso=sqrt(2)*1.5*Vp-Iso*Rs; %2 phase rated flux voltage

%VSD control parameters
alpha=Vso/wrated; %constant v/f coeff
beta=Vso/wrated*Srated/Iso; %slip compensation coeff
slippgain=1;
beta=beta*slippgain;

%unstable pole marks
speed=0; inertia=0; torque=0;
j=0; %unstable pole indice

i=0; %pole indice
for TI=0:2:30 %for each load torque
    %approximate intial currents
    isd=6; isq=TI/25*18; ird=isd*TI/Trated; irq=-isq*TI/Trated; %currents
    X=[isd;isq;ird;irq]; %state variables

    for wsyn=5:10:355 %for each synchronous speed

        %***** get IM steady state values *****
        Umag=sqrt(2)*1.5*Vp/wrated*wsyn; %magnitude stator voltage, cons vf source
```

```

R=floor(time*wsyn/(2*pi)); %whole revolutions
N=R*2*pi/wsyn/dt; %number of simulation steps
B=[1/(rho*Ls), 0; 0, 1/(rho*Ls); -Lm/(Lr*rho*Ls), 0; 0, -Lm/(Lr*rho*Ls)];

ps=0; %stator flux position
wr=wsyn*(1-Srated*TI/Trated); %initial rotor speed approx

%compensation terms
Rsx=Rs*0;
Rsy=Rs*0-beta*wsyn*0;
for step=1:1:N
    usx=X(1)*Rsx;
    usy=X(2)*Rsy+Umag;
    %voltage
    usd=cos(ps)*usx-sin(ps)*usy;
    usq=sin(ps)*usx+cos(ps)*usy;
    %calc currents
    A=[-Rs/(rho*Ls), wr*Lm^2/(Lr*rho*Ls), Lm*Rr/(Lr*rho*Ls), wr*Lm/(rho*Ls);...
        -wr*Lm^2/(Lr*rho*Ls), -Rs/(rho*Ls), -wr*Lm/(rho*Ls), Lm*Rr/(Lr*rho*Ls);...
        Lm*Rs/(Lr*rho*Ls), -wr*Lm/(rho*Lr), -Rr/(rho*Lr), -wr/rho;...
        wr*Lm/(rho*Lr), Lm*Rs/(Lr*rho*Ls), wr/rho, -Rr/(rho*Lr)];
    Xdot=A*X+B*[usd; usq];
    X=X+Xdot*dt;
    %calc rotor speed
    Ta=np*Lm^2/3*(X(2)*X(3)-X(1)*X(4))-TI-f*wr/np;
    wrdot=Ta/J;
    wr=wr+np*wdot*dt;
    %update values
    ps=ps+wsyn*dt;
end %end for motor simulation

%***** get IM VSD poles *****
wms=wsyn/(1+Srated*isq/Iso); %calc speed set point

%set steady state terms
isd=X(1); isq=X(2);
ird=X(3); irq=X(4);

for J=0.05:0.05:1 %for range of inertia
    Ac=[(Rsx-Rs)/(rho*Ls), wr*Lm^2/(Lr*rho*Ls), Lm*Rr/(Lr*rho*Ls), wr*Lm/(rho*Ls),
        isq*Lm^2/(Lr*rho*Ls)+irq*Lm/(rho*Ls);...
        -wr*Lm^2/(Lr*rho*Ls), (-Rs+Rsy+beta*wms)/(rho*Ls), -wr*Lm/(rho*Ls),
        Lm*Rr/(Lr*rho*Ls), -isd*Lm^2/(Lr*rho*Ls)-ird*Lm/(rho*Ls);...
        Lm*(Rs-Rsx)/(Lr*rho*Ls), -wr*Lm/(rho*Lr), -Rr/(rho*Lr), -wr/rho, -
        isq*Lm/(rho*Lr)-irq/(rho);...
        wr*Lm/(rho*Lr), Lm*(Rs-Rsy-beta*wms)/(Lr*rho*Ls), wr/rho, -Rr/(rho*Lr),
        isd*Lm/(rho*Lr)+ird/rho;...
        -irq^2*np^2*Lm/(3*J), ird^2*np^2*Lm/(3*J), isq^2*np^2*Lm/(3*J), -
        isd^2*np^2*Lm/(3*J), -f/(J)];
    ev=eig(Ac); %get poles
    i=i+1;
    poles(:,i)=ev;
    Repoles=real(ev);
    Maxpoles=max(Repoles);
    Maxpoles=max(Maxpoles);
    if Maxpoles>=0
        j=j+1;
        speed(j)=wms;
        inertia(j)=J;
        torque(j)=TI;
    end %end for unstable pole record

```

```

        end %end for J
    end %end for wsyn loop

end %end for TI

figure(1),grid
plot(poles,'b.')
xlabel('Re'), ylabel('Im')
figure(2)
plot3(speed,inertia,torque,'+'), grid
xlabel('speed set point'), ylabel('inertia'), zlabel('torque')
%end of file

```


Appendix F – Complete Experimental Drive

